SPUTTERED THIN FILM SOLID LUBRICANTS

by

Richard Cecil Leveson

A thesis submitted for the
Degree of Doctor of Philosophy
in the University of London

Department of Electrical Engineering
Imperial College of Science and Technology
July 1973

To Mei, with love and gratitude

ACKNOWLEDGEMENTS

I wish to express my deep appreciation to Professor J.C. Anderson for his continual encouragement and understanding.

I thank Dr. B.N. Chapman, who conceived and supervised the project.

Dr. Eugene Finkin, of D.A.B. Industries, Detroit, Michigan, gave much of his time in numerous stimulating discussions and for this I am extremely grateful.

I am most obliged to The Worshipful Company of Clothworkers, who generously provided a bursary.

In conclusion, I must thank Mr. Percy Robinson for constant help and advice, Miss Simone Ruddy and Mrs. Vlasta Nathoo for generous last minute assistance and all my friends in the Materials Section for countless acts of kindness.

ABSTRACT

This project is concerned with the friction and wear properties of thin solid films applied to a variety of hard substrates by sputtering.

Much consideration is given to the situation which arises if the contact between the film and the interacting surface is elastic and the role of the film in determining real area of contact is explored theoretically. The various implications upon such a theory of the pressure dependence of shear strength are examined and attention is also given to the special behaviour of very thin films where some quantitative predictions are discussed.

Attention is directed towards understanding the mechanics of hard protective coatings and to the wear of films in general.

Criteria important to sputtering system design are established and consideration given to such factors as applied magnetic field and substrate bias.

Special apparatus was constructed for this project, including a highly versatile sputtering system and both dynamic and static friction apparatus.

In the experimental work, orientation effects in the lubricative mechanism of MoS_2 were observed and strong evidence for the existence of elastic contact, predicted theroetically, has been obtained.

The wear properties of sputtered MoS_2 films have been evaluated and explained in terms of film structure.

The friction of gold films was explored and evidence for plastic behaviour is strong.

Very durable films of chromic oxide were deposited; some initial evaluation was attempted.

CONTENTS

		Page
Chapter 1 : Introduction		
1.1.	Introductory	10
1.2.	Fundamentals of Sputtering	11
1.3.	Basic Theory of Friction	13
1.4.	Contact Area Between Solid Surfaces	13
1.5.	The Effect of Films on Contact Area	16
1.6.	Frictional Energy Dissipation	17
1.7.	The Pressure Dependence of Shear Strength	19
1.8.	Thin Film Lubrication	21
1.9.	Consideration of Wear Mechanism	24
1.10.	Experimental Considerations	28
Chapter 2 : Theoretical Examination of Friction Phenomena		
2.1.	Introductory	30
2.2.	The Mechanism of Smooth Spherical and Cylindrical Contact	30
2.3.	Spherical and Cylindrical Contact with Film-Covered Surfaces	33
2.4.	Application of Cylindrical Contact Results to the Spherical Cases	36
2.5.	The Effect of the Thickness of a Film upon its Strength	40
2.6.	Examination of Rough Spherical Contact	44
2.7.	The Dependence of Shear Strength on Pressure in Friction Processes	50
2.8.	The Implication of Shear Strength-Pressure Dependence on Asperity Contacts	52

		Page
2.9.	Inclusion of Shear Strength-Pressure Dependence in a Friction Model	53
2.10.	The Increase in Friction for very Thin Films	54
2.10.1.	Film Failure	54
2.10.2.	Micro-Elastic Effects	55
2.10.3.	Micro-Plastic Effects	64
2.12.	Theoretical Examination of Hard Protective Coatings	65
2.13.	Wear Mechanisms	68
2.14.	Examination of Materials Properties	71
2.14.1.	Molybdenum Disulphide	71
2.14.2.	Soft Metals	73
2.14.3.	Chromic Oxide	74

Chapter 3 : Sputtering and Sputtered Films

3.1.	Introductory	77
3.2.	Arrival Energy of Sputtered Species	77
3.3.	Pressure Effects in Sputtering	81
3.4.	The Role of Applied Magnetic Field in Sputtering	83
3.5.	Examination of the Mechanisms Involved in Bias Sputtering	91
3.6.	Structural Properties of Sputtered Films	93
3.7.	Stoichiometry of Sputtered Films	95

Chapter 4 : Apparatus and Experimental Techniques

4.1.	Introductory	98
4.2.1.	The Design of the Sputtering System	98

		Page
4.2.2.	Details of the Target Assembly Design	103
4.2.3.	The Substrate Electrode Assembly	106
4.2.4.	The Cooling System	108
4.2.5.	The Substrate Heater	110
4.2.6.	The Design of a Matching Network for R.F. Operation	110
4.2.7.	Design Consideration for Sputter Etch and Bias Facilities	112
4.2.8.	Pressure Control and Measurement	113
4.3.	The Design of a Dynamic Friction Apparatus	113
4.4.	Static Friction Apparatus	119
4.5.	Description of the Ball and Tri-plane Friction and Wear Apparatus	121
4.6.	Target Fabrication Techniques	123
4.6.1.	Molybdenum Disulphide	123
4.6.2.	Gold	124
4.6.3.	Chromic Oxide	124
4.7.	Substrate Preparation Techniques	125
4.8.	Sputter Deposition Techniques	126
4.8.1.	The Sputtering of Molybdenum Disulphide	127
4.8.2.	The Sputtering of Gold	127
4.8.3.	The Sputtering of Chromic Oxide	128
4.9.	Techniques for Film Evaluation	128
4.9.1.	Film Thickness Determination	130
4.9.2.	Electrical Resistance of Spherical Contact with Films	130

Page

Chapter 5 : Presentation and Discussion of Results

5.1. The Dependence of Deposition Rate and other Factors upon Sputtering Parameters 131

5.1.1. The Effects of D.C. Offset Potential on Deposition Rate 131

5.1.2. The Effect of Pressure on Deposition and Diffusivity 134

5.1.3. The Effect of Bias Potential upon Deposition 138

5.2. General Observations on the Properties of Sputtered Films 138

5.2.1. Molybdenum Disulphide 138

5.2.2. Gold 140

5.2.3. Chromic Oxide 141

5.3. Electrical Resistance Measurements 143

5.4. The Measurement of Static Friction and its Dependence on Film Thickness 143

5.4.1. Static Friction of Molybdenum Disulphide 145

5.4.2. The Static Friction of Gold 147

5.5. Dynamic Friction Experiments with Molybdenum Disulphide Films 150

5.5.1. The Dependence of Friction Force on Applied Load 150

5.5.2. Analysis of Wear Tracks 153

5.6. The Wear Characteristics of Molybdenum Disulphide Films 159

5.6.1. Falex Tests on Sputtered MoS_2 films 159

5.6.2. Ball and Tri-Plane Wear Measurements 161

5.7. The Dynamic Friction of Gold Films in Sliding Contact 165

5.8. The Friction of Chromic Oxide Films 171

Page

Chapter 6 : Conclusions and Suggestions for Future Work

Appendix (1) 178

Appendix (2)

References

CHAPTER 1 --- INTRODUCTION

(1.1) When one or both of the hard surfaces of a bearing is coated with a thin film of a solid which has a low shear strength, the performance of the bearing can be greatly enhanced; both in terms of reduced friction and extended wear life. It is the study of the mechanisms by which this comes about, particularly with regard to films applied by the technique known as sputtering, that is the major preoccupation of this work.

Solid film coated bearings have been in use for many years, mainly as a complement to fluid lubricated systems in which the solid film mechanism comes into play only when the fluid film momentarily breaks down; for example in starting and under shock loading. Solid films are now finding increasing application in their own right in vacuum, at extremes of temperature and specific applications where their lifetime is sufficiently long for their use to be justified economically.

The materials normally used in this application are soft metals such as gold, lead and indium; certain polymers including P.T.F.E. and composites of inorganic solid lubricants, of which molybdenum disulphide and graphite are the commonest examples, often mixed with a polymer binder. Traditional methods of applying films employ such techniques as dipping, spraying and electroplating.

The concept of using the sputtering process to apply films has much potential, since the range of materials which can successfully be deposited is greatly increased. The durability achieved with sputtered films is probably superior to that produced in any of the traditional

processes. In the case of materials, such as molybdenum disulphide, which dissociate upon heating at normal pressures, sputtering probably offers the only effective means of applying a pure film in a highly adherent and coherent condition.

Sputtering offers a great degree of controlibility and repeatibility and so provides an excellent means of producing films for fundamental study. This was the major reason for its choice in this investigation.

(1.2) Fundamentals of Sputtering.

When a solid surface is bombarded with energetic particles, usually ions, the momentum transfer into the atoms or molecules of the solid can be sufficient for them to be ejected from the surface. This process is called sputtering. The number of atoms or molecules ejected per incident bombarding particle is known as the sputtering yield and its value can be 10 or more in favorable circumstances. If a substrate is placed in the path of the sputtered particles, these will impinge upon it and in time a continuous film can be produced. Such films have certain unique qualities and if the process can be induced with reasonable efficiency it represents a practical means of film deposition.

The simplest sputtering system consists of two plane parallel electrodes housed in a vacuum chamber. One of the electrodes is composed of the material to be deposited (the target), the other has the substrate placed upon it. If an inert gas is now admitted to the vacuum to produce a pressure of 10-20 micron Hg. and a D.C. potential of 1-4 KV. is applied across the electrodes, with the target negative, a glow discharge will be initiated. The discharge contains positive gas ions and negative electrons. The applied field accelerates the ions

which then bombard the target, sputtering off material which will form a film on the substrate. In such a system, deposition rates for metals are typically 1,000 Angstrom per minute.

In the D.C. process just described, it is only possible to sputter conductive materials. If the target were made of an insulator, the bombarding ions would accumulate their charge upon it and negate the applied field. If however a high voltage R.F. field is applied, the target and substrate electrode interchange polarity at field frequency; the insulator surface is now bombarded alternately by positive ions and electrons but because the electron mobility is much higher than that of the ions, more electrons strike the target in the positive cycle than do ions in the negative cycle. This results in a net D.C. "offset potential" accumulating on the insulator and hence, since the substrate electrode is conductive and does not retain charge, the overall effect is now that the target can be bombarded by ions and sputtering can occur.

The characteristics of an R.F. induced plasma are such that a discharge can be generated with at least an order of magnitude lower pressure than with simple D.C. This is a great advantage, as will be seen later and consequently it may also be desirable to sputter metals under R.F. power. For this to be possible, it is necessary to introduce a blocking capacitor in series with the target in order that the offset charge can be accumulated.

In a suitably designed sputtering system it is possible to apply power in such a way as to cause the substrate to be bombarded. The advantage of this is that the surface of the substrate can be very effectively cleaned, prior to deposition. Such a procedure is known as

sputter etching or back sputtering. In certain circumstances it is also desirable to feed power to the substrate, to bring it under bombardment during deposition. The advantages of this are that weakly adhering material is removed before it can become part of the film; a certain amount of 'knock-on' occurs in which the depositant is forced to imbed deeper into the substrate, improving the adhesive bond. It has also been shown that oxygen contamination is preferentially removed under these conditions. The procedure just described is termed 'bias sputtering' and the applied bias can either be D.C. (conductive substrates) or R.F. (conductive or non-conductive substrates).

(1.3) Basic Theory of Friction.

Most of the current theories of friction attribute the frictional force to the shearing of material at, or in the neighbourhood of points of real contact between the sliding surfaces. Thus frictional energy is believed dissipated in the continuous breaking of bonds.

Two fundamental considerations arise from such a theory; the determination of the real area of contact between the two surfaces and the strength of the regions at which shearing occurs. The physical principles governing these two considerations are very complex and we shall begin by examining them separately.

(1.4) Contact Area Between Solid Surfaces.

If two surfaces, which will in general be rough, come into contact, we shall expect the real area of contact to be determined by the number of asperity interactions and by the nature of each interaction. Again, in general, the real and apparent contact areas will be different. The problem of determining the real contact area must concentrate on solving

the interactive statistics of each particular situation and in view of the formidable nature of this, we must be prepared to accept some idealization.

The first attempts at solution presumed that the real contact area was so small that the stress at each contact would exceed the elastic limit of the material, resulting in plastic deformation of the contacts until the area had increased enough for the load to just be carried elastically. This theory has great intuitive appeal and explains many observed phenomena; in particular, since area must here be proportional to load, Amonton's law is upheld and apparently explained. If these ideas are applied to a friction situation, when two surfaces interact the area of true contact must be determined by the hardness of the softer of the materials, that is:

$$A = P/H \qquad (1.1)$$

where P is the load and H is the hardness (expressed as a flow pressure).

We must assume throughout this work that there is no gross plastic deformation taking place which would alter the macroscopic contour of either surface. Such events would seldom occur in real engineering mechanisms and our analysis initially excludes them. Conditions for the initiation of gross plastic yielding will be examined in the next chapter.

The next logical progression of our investigation would be to consider the case of two very smooth surfaces in contact, such as are often found in real bearings (typical roughness tolerances on a standard ball bearing are $\sim$300 Angstrom). Here the deviation of asperity heights

about the mean level is small and as surfaces are progressively pressed together, the number of contacts multiplies rapidly. The question to be asked here is; if there are a great number of interactions, can the load conceivably be carried without plastic deformation of asperities? Archard[2] was the first to attempt to quantify this problem and he modelled an interaction between two surfaces, one of which was covered with spherical asperities of equal height and the other being flat. The dependence of area upon load, assuming Hertz[3] contact for each sphere was:

$$A \propto P^{2/3} \qquad (1.2)$$

proceeding to the next stage, Archard considered each asperity to be itself covered with much smaller spherical asperities and repeating the analysis found:

$$A \propto P^{8/9} \qquad (1.3)$$

and yet again:

$$A \propto P^{26/27} \qquad (1.4)$$

Thus Archard was able to show that in the limit, the proportionality between area and load can still be achieved under purely elastic conditions, although admittedly these are extremely idealized.

More complex analyses have been undertaken by Greenwood and Williamson[4], modelling surfaces on actual experimental data for surface roughness and again showing that elastic interactions can explain the

proportionality between load and area.

It must not be assumed that the above work was aimed at discounting the existence of plastic contact; rather the extent of its applicability is reduced and it is shown that in many important engineering situations, elastic processes play a dominant role in determining contact area.

In conditions where the ratio of load to apparent contact area is high, such as might occur between a very smooth sphere and half-plane, circumstances can exist where all the asperities are pressed flat and the real and apparent contact areas approach each other. Block[5] has developed a criterion which gives an indication as to the configuration of an asperity capable of full elastic flattening:

$$h/\ell > 2H(1 - \upsilon^2)/\pi E \qquad (1.5)$$

where h and ℓ are the height and width respectively of a sinusoidal asperity, H is the material hardness, E its Young modulus and υ the Poisson ratio. Situations of this type are of great interest to the experimentalist since the real area of friction can be predicted with some confidence while at the same time such configurations have wide engineering applicability.

(1.5) The Effect of Films on Contact Area.

Let us consider the case of a flat film-coated surface, against which a spherical rider is being pressed. Let us also assume the rider and substrate to be composed of the same material, which is much harder and more rigid than that of the film. If we presume the ratio of apparent contact diameter to film thickness is large, we can expect to have a

substantial hydrostatic pressure within the film and this would effectively increase its strength; thus in favorable circumstances we might expect the film to behave elastically. This possibility is examined quantitatively in the next chapter.

From what has been said, it seems reasonable to suppose that for very thin films the elastic strain energyactually within the film is extremely small and that the bulk of this energy resides within the substrate and rider. Therefore a range of thickness exists within which the film plays a negligible role in determining contact area and we can simply apply the Hertz relationship. For thicker films a correction has to be made and we shall need to discover the nature and extent of this, since many of the thickness effects exhibited by thin film systems can be attributed to such a mechanism.

The rigorous solution to the applied mechanics problem of finding the the contact area between a sphere and a film-coated plane is extremely involved and has not been solved. The closest approach has been Finkin's modification[6] of Alexandrov, Babeshko and Kucherov's brilliant analysis of an elastic layer between a rigid sphere and half-plane[7]. This will apply in real situations where the film modulus is very much less than that of the rider and substrate and where the thickness is greater than the limit discussed above.

(1.6) Frictional Energy Dissipation.

If we consider the possible fundamental mechanisms which might be involved in dissipating the energy of friction, we are restricted to four

realistic alternatives:

(1) Energy dissipated in the breaking of cohesive bonds within one or both of the rubbing materials.

(2) Energy dissipated in the breaking of interfacial (adhesive) bonds between surfaces.

(3) Dissipation by plastic flow, either in crushing asperities or as a result of 'ploughing' action.

(4) Dissipation by elastic hysteresis, induced by the propagation of a distortion 'wave' through the materials at the speed of sliding.

Of these four possibilities, we would normally expect the first to involve the greatest dissipative energy; dissipation by plastic flow can be large but it is unlikely to be so in bearings which have been run in and hence we shall disregard this mechanism. In reality, we should expect all four mechanisms to occur in any system but the allocation of frictional energy between them would be unique to a given situation.

Bowden and Tabor[8] have proposed their now famous welding theory in which junctions are formed between asperities by a combination of high pressure and temperature. Here the bond strength is presumed to be high and also very localized work-hardening takes place on each side of the interface, resulting in a shear plane some distance away from it. The shearing is therefore characteristic of the strength of the softer of the two materials and can be stated in the form:

$$F = TA \qquad (1.6)$$

where F is the friction force, A the real contact area (assumed nearly equal to the shearing area) and T is the shear strength of the weaker material. If this result is combined with equation (1.1) we obtain an expression for the coefficient of friction, f

$$f = F/P = T/H \qquad (1.7)$$

hence the coefficient of friction now becomes a materials property, the ratio of shear strength to hardness. In continuum mechanics, for an ideal elasto-plastic material, this ratio can be shown to be equal to approximately 1/5 and this value is in the same order of magnitude as many experimental observations.

The foregoing treatment can only be expected to apply in cases where there is full plastic deformation of asperities. In the case of elastic contact, f becomes a system property because it must depend on the asperity height distributions.

For surfaces which are contaminated to the extent that strong bonding cannot occur between them or possibly for certain very hard materials, we must consider the possibility of interfacial shear. Here we see that the friction arises from the breaking of a much less energetic bond, presumably in the Van der Waals catagory and in cases where such bonding is very weak, the role of elastic hysteresis may now become significant.

(1.7) The Pressure Dependence of Shear Strength.

It is well known from the work pioneered by Bridgman[9] that all solid materials exhibit a pressure dependence of shear strength. This

Metal	Shear Strength at Atmospheric Pressure. Kg./mm.^{2}	Shear Strength at 40 Kilobars Kg./mm.^{2}
Copper	11	49
Aluminium	3	32
Nickel	25	87
Zinc	8	20

Table (1.1) Shear Strength Dependence Upon Pressure for Some Common Metals. (Data of Bridgman[9])

phenomenon has been of considerable interest to the present investigation, in view of the fact that the friction interfaces have been subjected to a wide range of real contact stress in our experimental work and this would be expected to affect the friction force. Table (1.1) gives an appreciation of the magnitude of the effect for some common engineering materials.

Where interfacial load is carried plastically (that is, at constant pressure) or when it is supported by a discrete number of elastic asperities (mean pressure is again constant because increase of the load increases the number of contacts rather than the pressure at each) we shall not expect to observe the consequences of the effect, but when we have high localized loading (see 1.4) this must be taken into account.

As an example, if we consider again the case of a sphere pressed against a flat surface, we can assume that the real contact area will depend upon the load according to the Hertz formula:

$$A \propto P^{2/3} \qquad (1.8)$$

and hence the mean contact pressure, p is given by:

$$p \propto P/A \propto P^{1/3} \qquad (1.9)$$

We should thus predict a dependence of frictional shear upon applied load.

(1.8) Thin Film Lubrication.

We have now examined sufficient material to make a preliminary survey of the thin solid film regime.

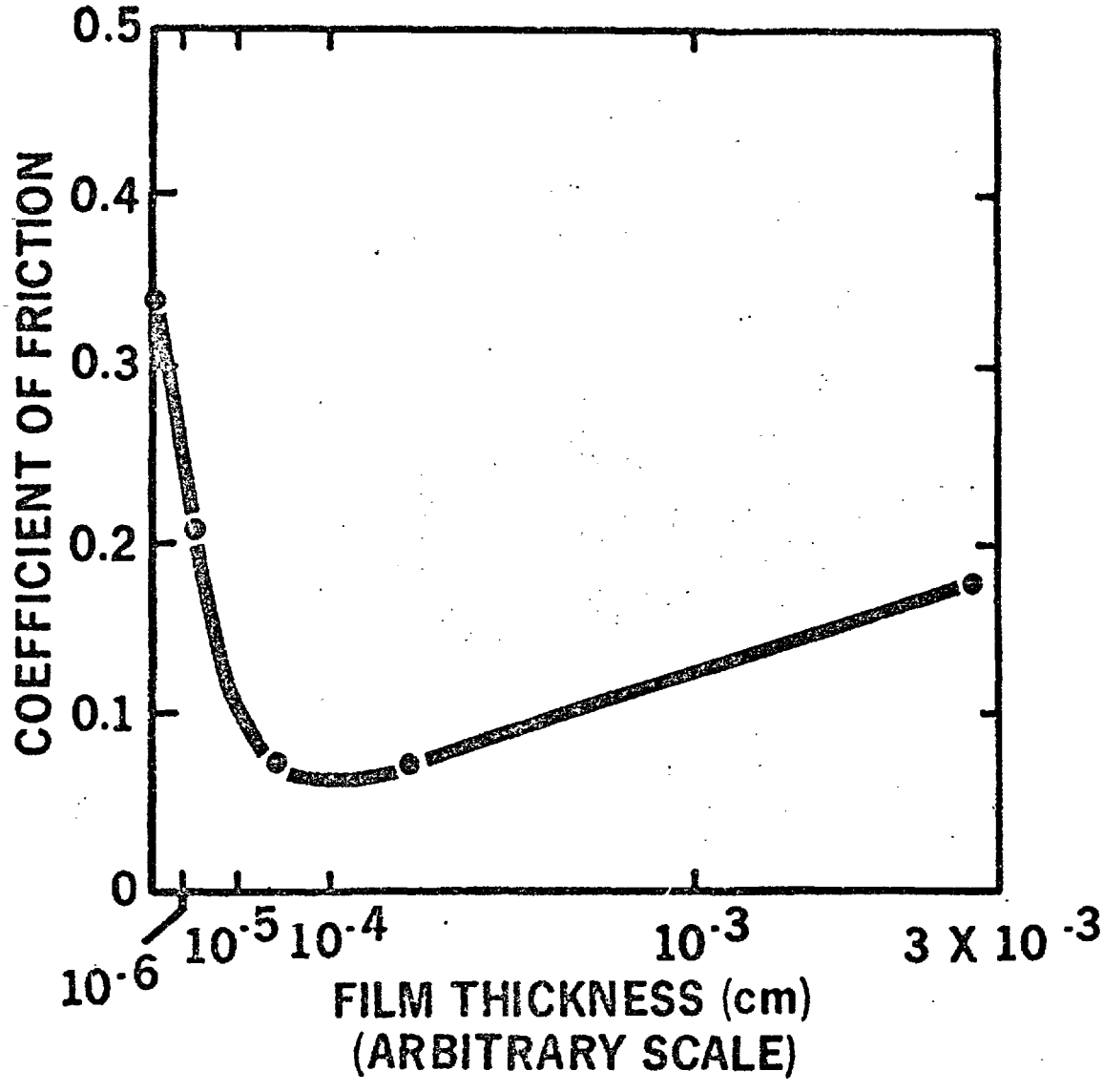

Fig. 1.1 Affect of film thickness on frictional properties of thin films of indium deposited on tool steel (from Bowden and Tabor [1])

Let us consider again the friction coefficient for a system which can be described in terms of equation (1.7). Continuum mechanics shows that the ratio shear strength/hardness is constant for an ideal isotropic material. If we require a low friction surface we must seek to minimize this ratio, which implies the use of an anisotropic material having high strength perpendicular to the friction plane and low strength in shear. In practice, bearings of this type do exist being usually composed of graphite or molybdenum disulphide in compact form. Unfortunately the load carrying properties of these materials in bulk is poor so that they are only suitable in low stress applications.

A much more attractive alternative is offered in a thin film system where the contact area is dictated by the mechanical properties of the substrate and rider but the shear strength of the interface is governed by the film. Thus provided the film strength is much lower than that of the substrate and rider, we shall expect to achieve effective anisotropy and consequently low friction.

Many workers have observed thickness effects on the friction of films. Bowden and Tabor[8], working with electroplated indium films on tool steel, obtained the results of fig.(1.1) which are qualitatively representative of those observed in many thin film systems. The reduction of friction with decreasing thickness can be attributed to the reducing effect of the film in determining contact area. A minimum is observed after which the friction increases and this increase has been the subject of considerable recent interest. The simple explanation of film breakdown[8][10] obviously satisfies some situations, but in certain others this does not appear reasonable and the possibility of a thickness

dependence of film strength, either through micro-elastic or micro-plastic mechanisms seems more feasible. Considerable attention is given to this topic in following chapters.

(1.9) Consideration of Wear Mechanisms.

In most mechanical systems subject to wear, the designer must predict the conditions under which the system will ultimately fail somewhat arbitrarily in terms of the maximum erosion of tolerances consistent with acceptable performance. In the case of thin film systems, failure is defined quite unambiguously as occuring when the film has been worn through. Thus if we are considering spherical contact, we are principally interested in the central region of the contact at which the pressure is greatest and at which failure will consequently occur.

For the purposes of the present work, we are principally concerned with only two wear mechanisms: adhesive wear and fatigue wear.

Adhesive wear is normally associated with metal contacts and is generally accepted as occuring as a result of material particles being plucked out from one of the interacting surfaces as a result of a plastic encounter between asperities. Archard[11] has produced a model in which the probability K of a plastic encounter producing a wear particle is considered and the shape of the particles is assumed to be hemispherical. The resulting expression:

$$V = \frac{KPL}{3H} \qquad (1.10)$$

in which V is the total volume of material removed in sliding a distance L

under a load P for a material of hardness H, represents a case of linear wear since the wear is in direct proportion to the sliding distance and to the load. In practice, Archard's expression would only be applied to situations of mild adhesive wear in which an intermediate film, typically of oxide, inhibits such phenomena as alloying and junction growth[8]. A severe type of adhesive wear will occur if there is no intermediate film and there is reason to suppose that sputtered metal films, operating in vacuum in sliding contact would exhibit this type of wear.

The theory of fatigue wear, to which Kragelskii[12] has made major contributions, applies to interactions between surfaces which are almost exclusively elastic. Asperities are in this case supposed to be subject to cyclic loading and become detached as a result of fatigue failure. To such situations Kragelskii has shown that linear wear can again be predicted. Sputtered films of brittle materials which can demonstrate stable elastic behaviour over long periods of operation would therefore fall into this catagory.

For the present purposes, when considering the wear of materials such as molybdenum disulphide, we shall define an expression to describe the wear in linear terms and consider the wear depth x, rather than the volume, thus:

$$x = K p L \qquad (1.11)$$

where p is the pressure of the contact and L is the sliding distance producing a wear depth of x and K is a constant of proportionality which we shall consider as our wear coefficient.

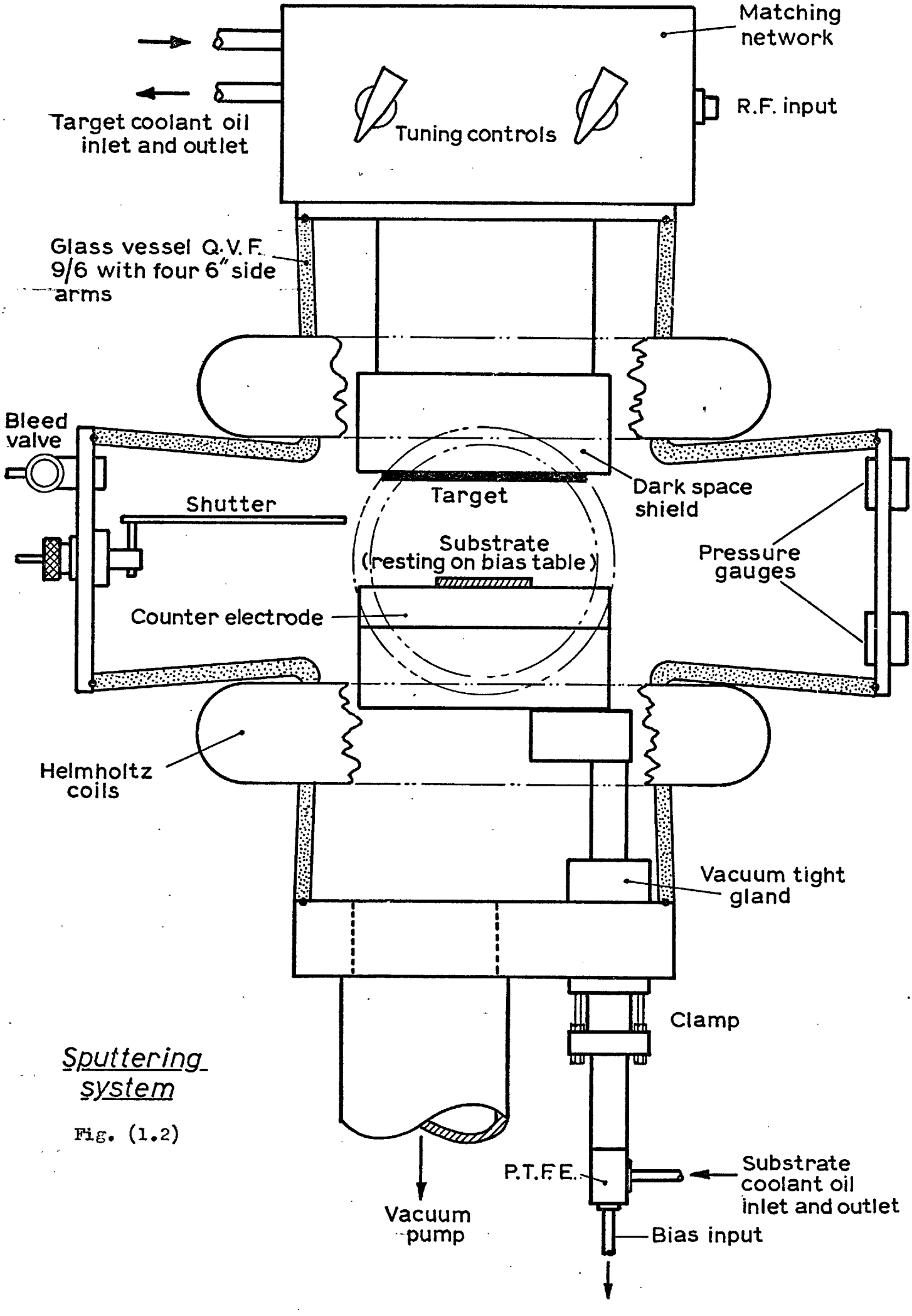

Sputtering system

Fig. (1.2)

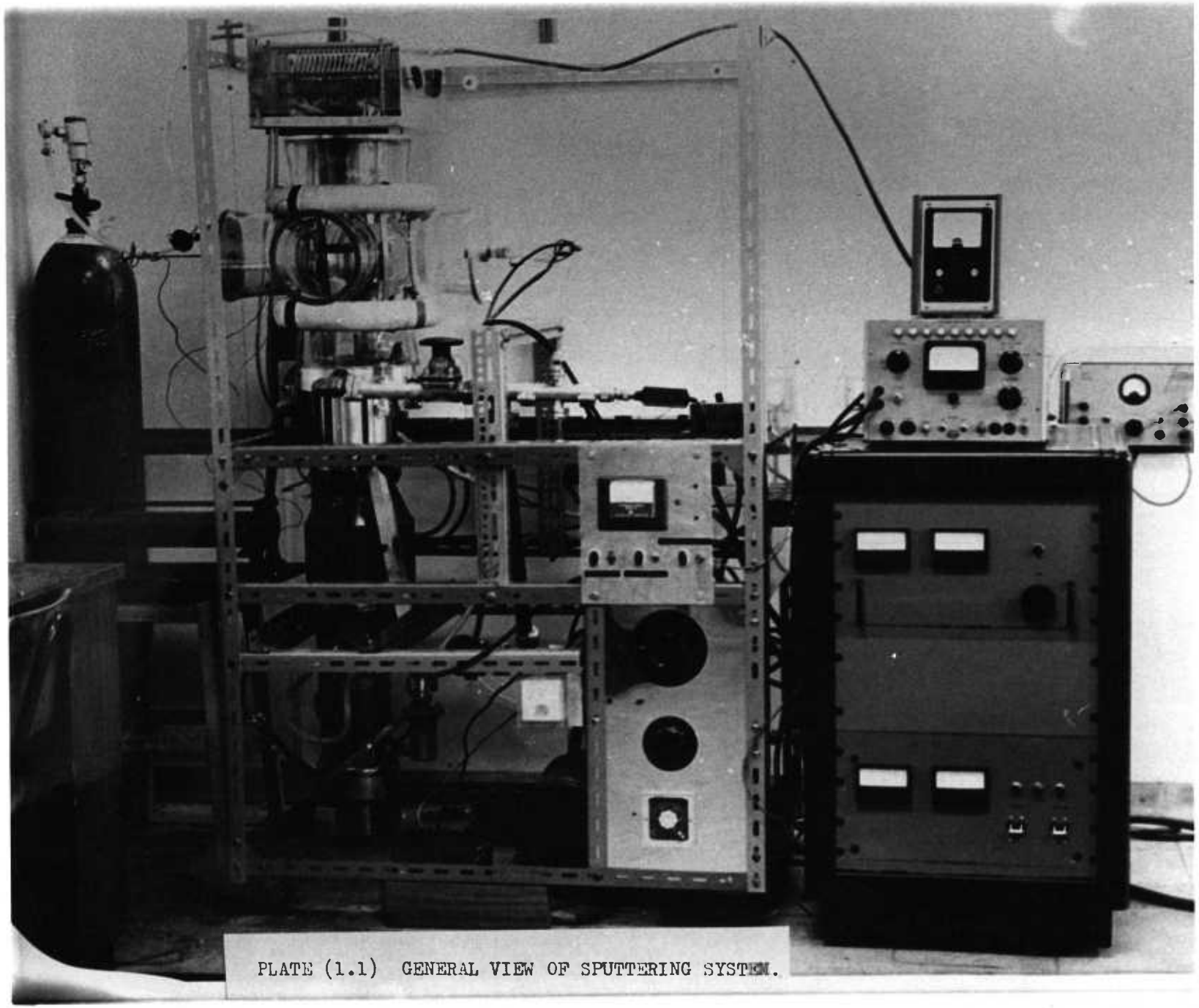

PLATE (1.1) GENERAL VIEW OF SPUTTERING SYSTEM.

(1.10) Experimental Considerations.

In order to undertake this experimental programme it was necessary to design and build a very versatile sputtering system. This had to be capable of operating in a variety of different modes in order to have enough flexibility to ensure successful production of films.

A system was built incorporating a number of novel features, see fig. (1.2) and plate (1.1), including oil cooling of both 5" target and counter-electrode. The counter-electrode consisted of a central table, to which either R.F. or D.C. bias could be applied and this was surrounded by a dark space shield, similar to the target. Access to the table for heater leads etc. could be had from beneath the assembly so that these should not introduce field distortion. The system was housed in a Pyrex chamber consisting of a wide vertical pipe-section having four orthogonal side arms. This configuration was ideal for the application of magnetic field and also allowed operation in the triode mode. Power was fed to the system from a 1.25 KW. R.F. generator through a matching network.

For the evaluation of films a dynamic friction apparatus, for operation in vacuum, was designed and built. In this, a 3/16" diameter ball could be loaded against the flat coated surface of a 2" diameter disc and the applied load and frictional force could be monitored. The speed was variable between 0 and 60 rpm.

A static friction apparatus was also built, principally to examine thickness effects. Here the substrate was placed on a table which could be introduced into the sputtering system for coating; subsequently it could be retracted, still in vacuum, and a three ball rider placed upon it.

The table was then tilted through a very accurately known angle, until slip occured. In this manner successive film thicknesses could be built up and their friction effects measured, while maintaining a vacuum throughout.

CHAPTER 2 --- THEORETICAL EXAMINATION OF FRICTION PHENOMENA

(2.1) For the reasons discussed in Chapter 1 we shall restrict ourselves to the consideration of the friction of a sphere sliding on a half-plane and in particular we shall be examining the case where the half-plane is covered with a thin solid film. In order to assist in the understanding of this problem, it will also be necessary to investigate the nature of the contact between a cylindrical rider and a half-plane; the reasons for this will later become apparent.

(2.2) The Mechanics of Smooth Spherical and Cylindrical Contact.

This idealized problem was originally solved by Hertz[3] and yields the classic results:

$$a_h = 0.909 \left[PR \left(\frac{1 - \upsilon_1^2}{E_1} + \frac{1 - \upsilon_2^2}{E_2} \right) \right]^{1/3} \qquad (2.1)$$

for spherical contact, where a_h is the contact radius, P the applied load, R the sphere radius, E and υ the Young modulus and Poisson ratio with the subscripts refering to the material of the sphere and the half-plane respectively.

For cylindrical contact:

$$a_h = 1.128 \left[\frac{PR}{\ell} \left(\frac{1 - \upsilon_1^2}{E_1} + \frac{1 - \upsilon_2^2}{E_2} \right) \right]^{1/2} \qquad (2.2)$$

here a_h represents half the contact width and ℓ is the length of the cyl-

inder.

The mean contact pressure for the above two cases is simply found by dividing the load by the contact area, thus we have:

$$p_m = P/\pi a_h^2 \qquad \text{(spherical)} \qquad (2.3)$$

$$p_m = P/2\pi \ell a_h \qquad \text{(cylindrical)} \qquad (2.4)$$

It can be shown that :

$$p_m = 2p_o/3 \qquad (2.5)$$

where p_o is the maximum pressure in the contact, whether spherical or cylindrical.

As the loading of these contacts increases, a stage must be reached when plastic yielding commences and we require a criterion to enable us to determine the circumstances under which this will occur. If our material is ideally elasto-plastic, we can expect failure to be initiated at the point of maximum shearing stress in the contact and according to Timoshenko and Goodier, the maximum shear stress is given by $\tau_o = 0.31p_o$.[13] Again, if the material is ideally elasto-plastic, the shear strength is related to the strength in tension by:

$$T = Y/3 \qquad (2.6)$$

and hence, using equation (2.5) we obtain:

Fig.(2.1)

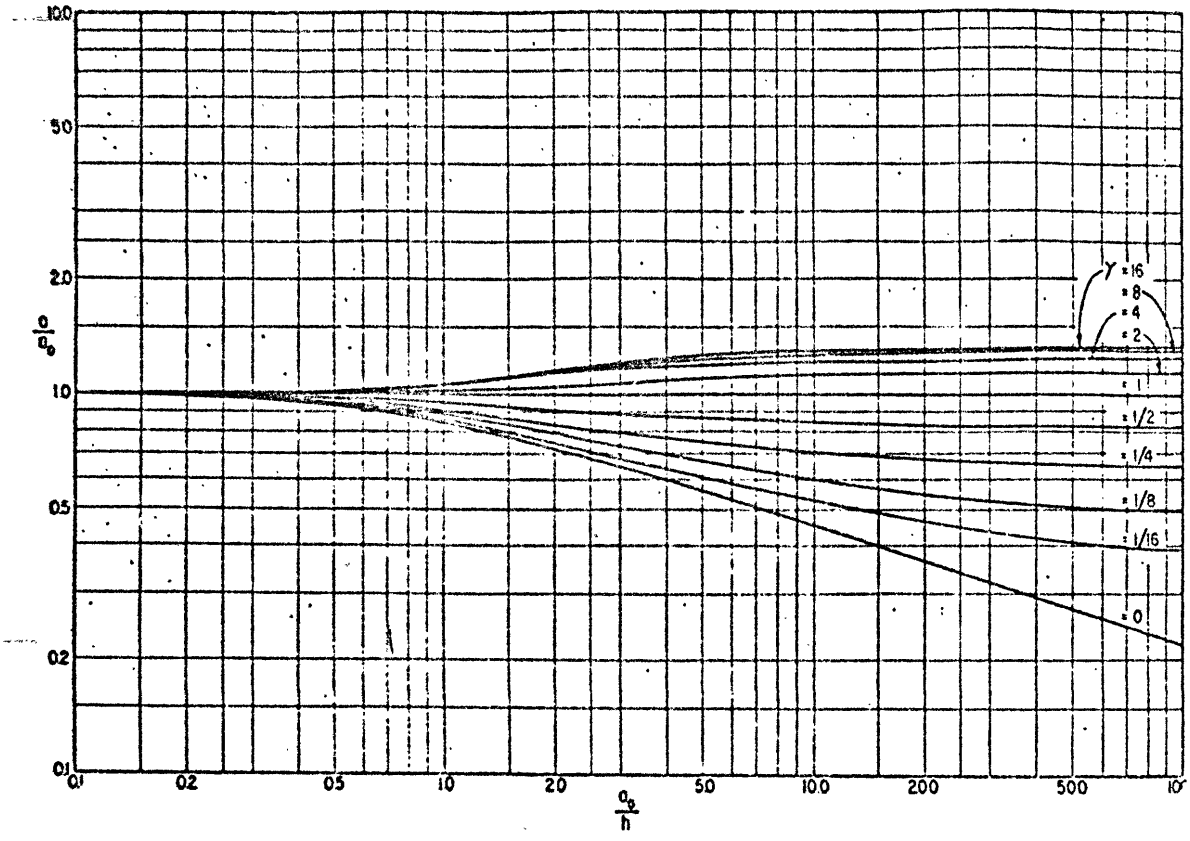

Variation of contact width for an elastic cylinder indenting an elastic layer bonded to an elastic half-space, as a function of layer thickness and relative elastic properties (with $\beta = \gamma$); from Gupta and Walowit [5]

$$p_m = 1.24\ Y \tag{2.7}$$

Thus the onset of plastic failure occurs when the mean contact stress is approximately equal to the tensile strength.

For the case of brittle materials, the criterion for failure will be determined by the maximum tensile stress occuring in the contact and again using the results of Timoshenko and Goodier, this value is given by:

$$\sigma_o = \frac{(1 - 2\upsilon)}{3} \cdot p_o \tag{2.8}$$

and thus for these materials we have the failure criterion:

$$p_m = \frac{2Y}{(1 - 2\upsilon)} \tag{2.9}$$

For simplicity we have assumed in each case that the materials of the rider and substrate are the same.

(2.3) Spherical and Cylindrical Contact with Film-Covered Surfaces.

As mentioned in (1.5) the problem of an elastic sphere indenting an elastic film-covered half-plane has not been solved. The analogous problem, with cylindrical contact, has recently been attempted by Gupta and Walowitt[14] and fig. (2.1) shows the numerical solution which they have obtained. Here the rider and substrate are of the same material and the ratio of the Young modulus for these to that of the film is $1/\gamma$. a_o is the Hertzian contact half-width for the rider indenting the bulk film material and a is the half-width of the contact for film thickness h.

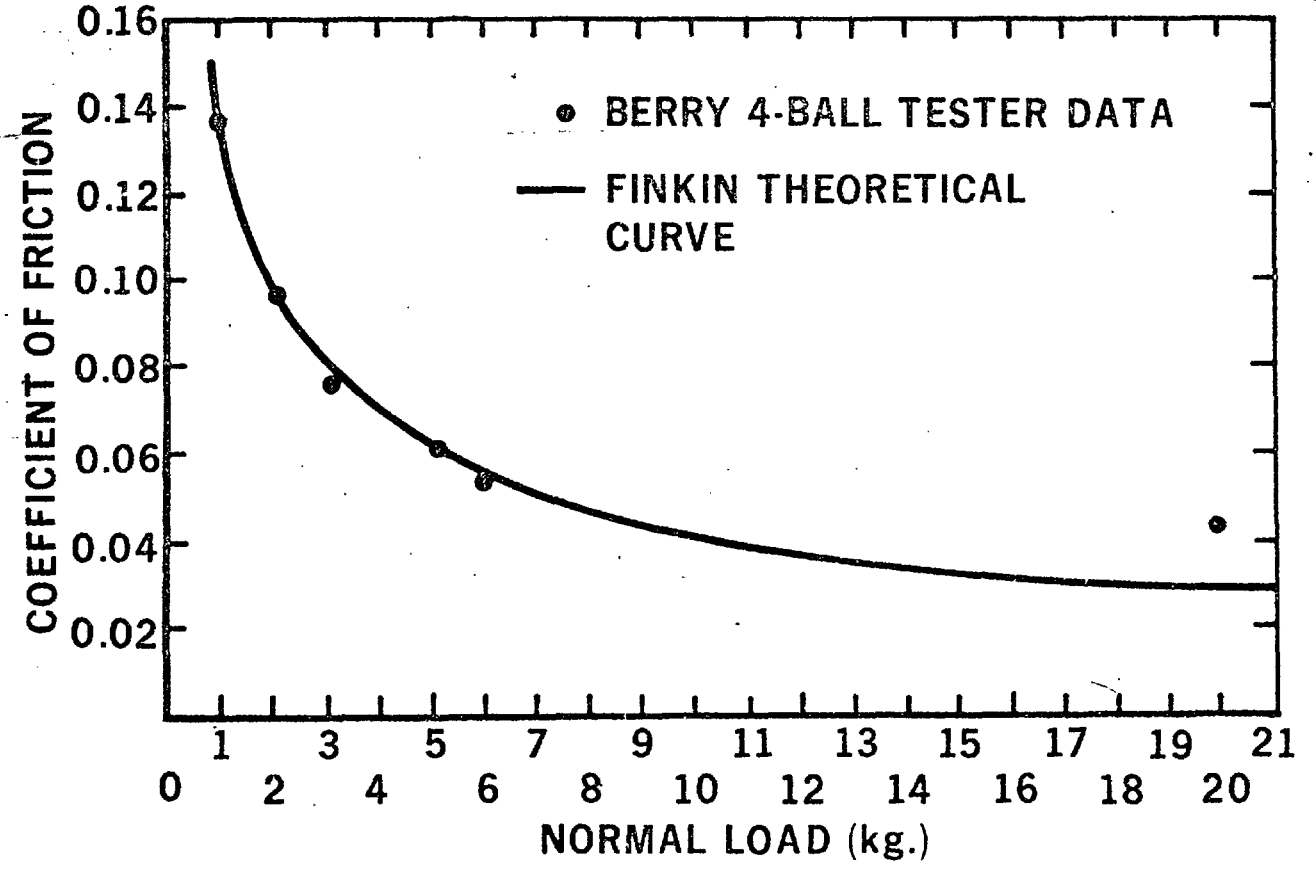

Fig. (2.2)

Friction Coefficient of Phenolic Bonded and MoS_2-1 Graphite Film as a Function of Load in a 4-Ball Tester (Data from Berry [48])

In addition to the above solution, we have solutions to the problem for the particular case in which the rider and substrate are assumed rigid and only the film is elastic (for convenience we shall refer to these as RER solutions). The RER solution for spherical contact has been obtained by Finkin[6] who modified the work of Alexandrov, Babeshko and Kucherov[7] to obtain an expression for the contact radius, a_f:

$$a_f = 0.893 \left[\frac{PRh}{G}\left(\frac{1-2\upsilon}{1-\upsilon}\right)\right]^{1/4} \qquad (2.10)$$

where h is the film thickness, G and υ the shear modulus and Poisson ratio for the film material, P is the applied load and R the sphere radius. Using additional work by Alexandrov[15] and Alexandrov and Vorovich[16], Finkin has obtained the solution for the cylindrical RER problem[17];

$$a_f = 0.909 \left[\frac{PRh}{\ell G}\left(\frac{1-2\upsilon}{1-\upsilon}\right)\right]^{1/3} \qquad (2.11)$$

in which a_f is now the contact half-width and ℓ the length of the cylinder.

RER solutions have obvious application to systems in which the film modulus is at least two orders of magnitude less than that of the rider and substrate material; thus Finkin found good agreement when applying these solutions to phenolic bonded molybdenum disulphide on steel. Fig. (2.2) gives an illustration of this and Finkin has assumed that the frictional force is proportional to the contact area in his derivation. In this present work, we are interested in such combinations as molybdenum disulphide on steel (modulus ratio 1:16) and gold on tungsten carbide (1:7). These films are also very thin, so that we cannot assume that there is no deformation

in the rider and substrate; rather we might expect to have more success in applying the Hertz formula, neglecting the film altogether, which has been routine procedure in the past (see for example Bowers and Zisman[18]). It is necessary that some attempt should be made to rationalize this problem.

(2.4) Application of Cylindrical Contact Results to the Spherical Case.

It would be of enormous value to this investigation if we could apply the results of Gupta and Walowitt to the case of spheriacl contact. The cylindrical solutions might be expected to approach the spherical ones most closely when similar stress distributions occur. Accordingly, if we put $\ell = 2a_h$ and $\ell = 2a_f$ into equations (2.2) and (2.11) respectively we have a square contact zone and these become:

$$a_h = 1.128 \left[\frac{PR}{2a_h} \left\{ \frac{1 - \nu^2}{E_1} + \frac{1 - \nu^2}{E_2} \right\} \right]^{1/2}$$

and hence:

$$a_h = 0.860 \left[PR \left\{ \frac{1 - \nu_1^2}{E_1} + \frac{1 - \nu_2^2}{E_2} \right\} \right]^{1/3} \qquad (2.12)$$

and similarly:

$$a_f = 0.909 \left[\frac{PRh}{2a_f G} \left\{ \frac{1 - 2\nu}{1 - \nu} \right\} \right]^{1/3}$$

giving:

$$a_f = 0.783 \left[\frac{PRh}{G} \left\{ \frac{1 - 2\nu}{1 - \nu} \right\} \right]^{1/4} \qquad (2.13)$$

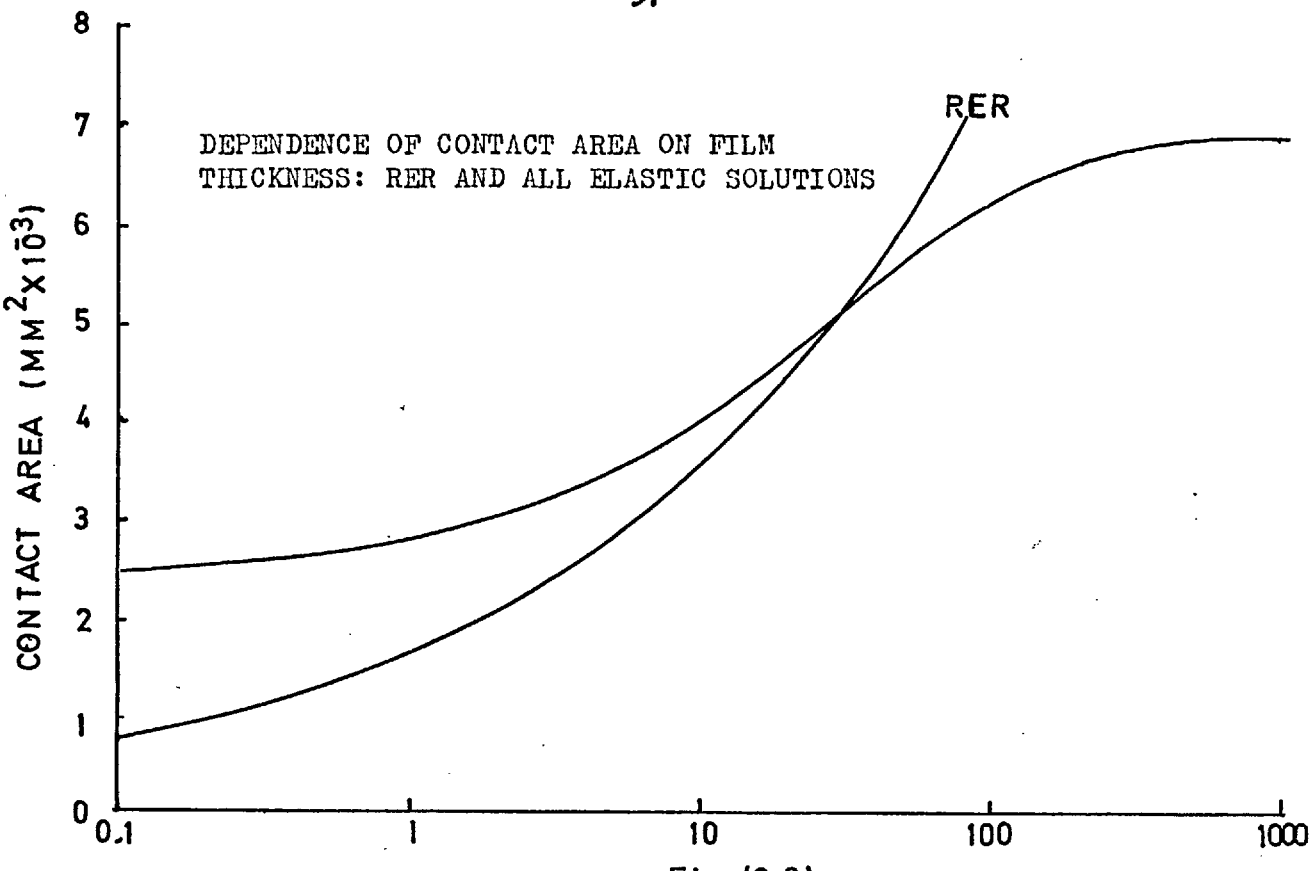
DEPENDENCE OF CONTACT AREA ON FILM THICKNESS: RER AND ALL ELASTIC SOLUTIONS
RER
CONTACT AREA ($MM^2 X 10^{-3}$)
0
1
2
3
4
5
6
7
8
0.1
1
10
100
1000
FILM THICKNESS (MICRON)

Fig. (2.3)

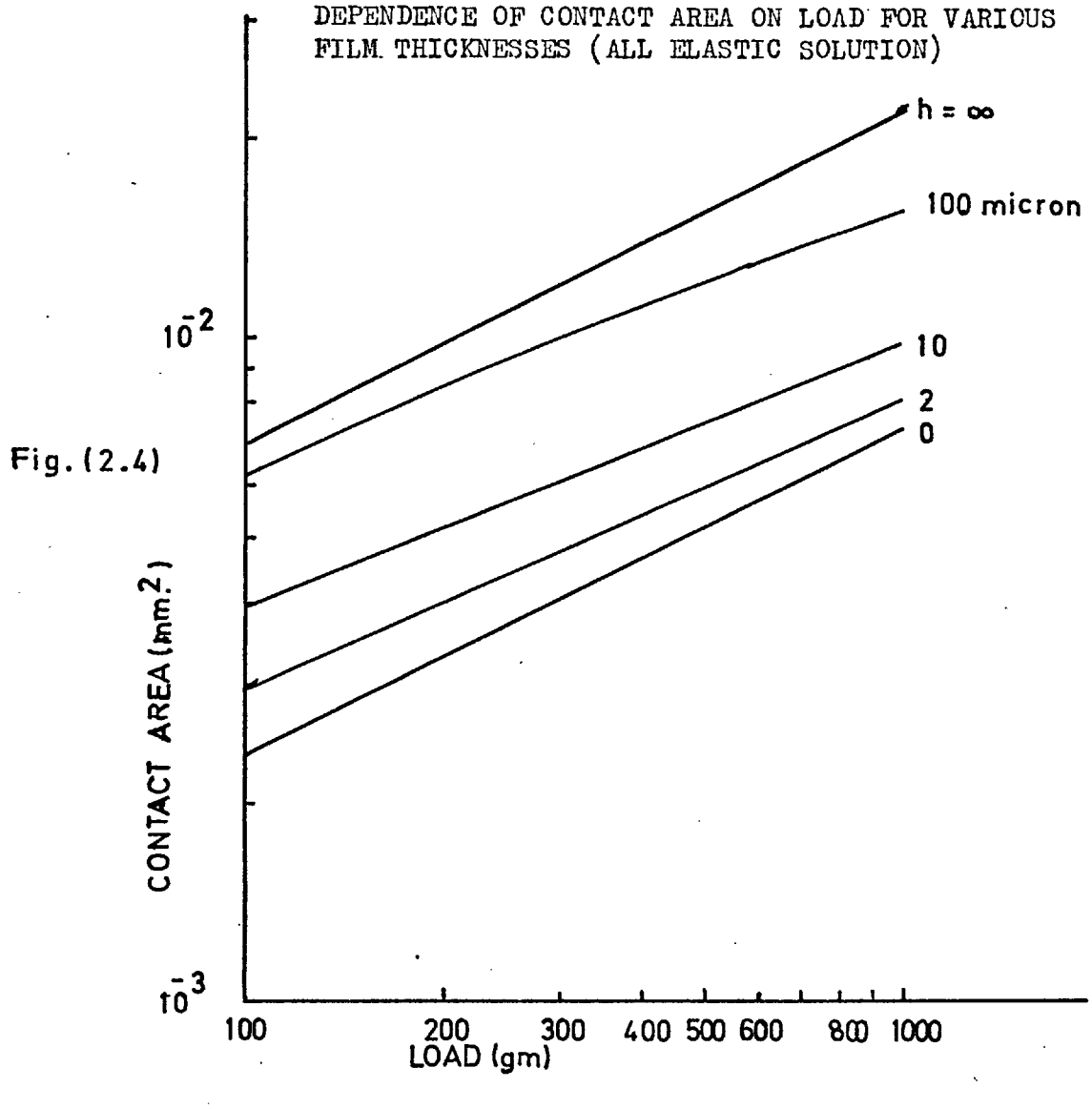
DEPENDENCE OF CONTACT AREA ON LOAD FOR VARIOUS FILM THICKNESSES (ALL ELASTIC SOLUTION)
h = ∞
100 micron
10
2
0
10^{-2}
10^{-3}
CONTACT AREA (mm.²)
100
200
300
400
500
600
800
1000
LOAD (gm)

Fig. (2.4)

We see that in each case the cylindrical equations have been transformed into new equations which are almost identical to their spherical counterparts; the only difference being in the values of the constants, which differ by 5% for the Hertz equations and 12% for the RERs. If an analytical solution for the all-elastic case existed, it would be reasonable to attempt transformation to the spherical situation using the above method. Unfortunately, the numerical solution which we have precludes our doing this but the ideas can still be applied to yield much valuable information.

In parallel with the experimental procedures of this work, we shall now examine the case of molybdenum disulphide on steel where $\gamma = 1/15$*. We choose a sphere of radius 2.381 mm. (3/32") and a load of .1 Kg. For this system we shall now investigate the dependence of contact area upon film thickness, using the information from fig. (2.1) while attempting to apply the ideas of the preceeding paragraph. Obviously we cannot maintain the condition of square contact and in fact this will only be attained for one value of thickness. We therefore choose this value to occur at some reasonable point intermediate between the two asymptotic limits** and adjust its position to give the best agreement with the two Hertzian values for spherical contact. Fig. (2.3) shows the result of choosing $\ell = 0.05$mm. (which gives square contact at h = 0.2 micron) and plotting contact area as a function of film thickness; the cylindrical RER dependence is also plotted for comparison. We see immediately that the assumption of Hertzian (steel-on-steel) contact is certainly not valid for films thicker than 1 micron and that over 75% of the area change occurs for thicknesses between 1 and 100 micron; this will consequently be the region of film thickness in which we shall expect to see significant dependence

---

*$E(MoS_2) = 1{,}250$ Kg.mm.$^{-2}$, $E(EN58) = 21{,}000$ Kg.mm.$^{-2}$

**For extremes of thickness, upper limit is the Hertz contact for steel on bulk MoS_2, lower limit is Hertz contact for steel on steel.

of friction behaviour.

Further valuable information can be extracted from fig. (2.1); in particular we can examine the load dependence of contact area and fig. (2.4) shows this dependence, plotted for a range of film thicknesses. The bounding curves are those for h = 0 and h = ∞ . It is interesting to note that the effect of the presence of the film diminishes as the load increases; this can be explained when we remember that the ratio a/h is increasing with load and hence the film beneath the rider experiences greater hydrostatic pressure. Further strain within the film is now dependent upon the bulk, rather than the axial compression and therefore more strain energy is absorbed in the rider and substrate.

Finally, fig. (2.1) shows us the effect of a film whose modulus is higher than that of the rider and substrate and we see that the effect on area is diminished. From equation (2.2) the values of the contact half-width at h = 0 and h = ∞ will be respectively:

$$a_h = C(2/\gamma E)^{1/2}$$

and

$$a_h = C((1 + 1/\gamma)/E)^{1/2}$$

where C is a constant introduced for brevity and we have assumed that the Poisson ratio is the same for the film and rider/substrate. The value of the quantity a/a_o, used in fig. (2.1), will thus vary between the extremes:

$$a/a_o = 1 \quad (\text{at } h = \infty) \text{ and } \quad a/a_o = (2\gamma/1 + \gamma)^{1/2} (\text{at } h = 0)$$

Thus, if we have a film for which $\gamma = 1/16$, the total variation in a/a_o

will be 66% while for $\gamma = 16$ (effectively reversing the materials of the film and rider/substrate) the total variation is now 37%. The transition from substrate to film dominated behaviour occurs over a much lower range of thickness when γ exceeds unity and this is of some significance to the study of hard protective coatings, a topic to which we shall return at a later point in this chapter.

(2.5) The Effect of the Thickness of a Film Upon its Strength.

In the present context the term 'strength' applied to a film refers to its ability to support loads elastically. In the analyses developed so far, we have assumed that there is no plastic flow of film material under the pressure of contact; we will now attempt to determine the extent of the validity of this assumption.

Any state of stress existing in a body can be shown to consist of two components, which are termed the spherical and the deviatoric stress fields. The spherical stress field represents the hydrostatic component of stress, which tends to bring about change in volume without change in geometric shape*; the deviatoric, on the other hand, produces only change in shape. In establishing a criterion for elasto-plastic transition, we take into account only the elastic strain energy, U, contained within unit volume of the deviatoric field (since materials can support enormous hydrostatic pressures without failure, the spherical strain energy is excluded) and state that when the value of U at any point exceeds a critical value, characteristic of the material, elasto-plastic transition occurs at this point.

In all film systems of interest to us, the film thickness is ext-

*This assumes that we are dealing with an isotropic material, since a spherical stress field will produce a change in shape for an anisotropic material.

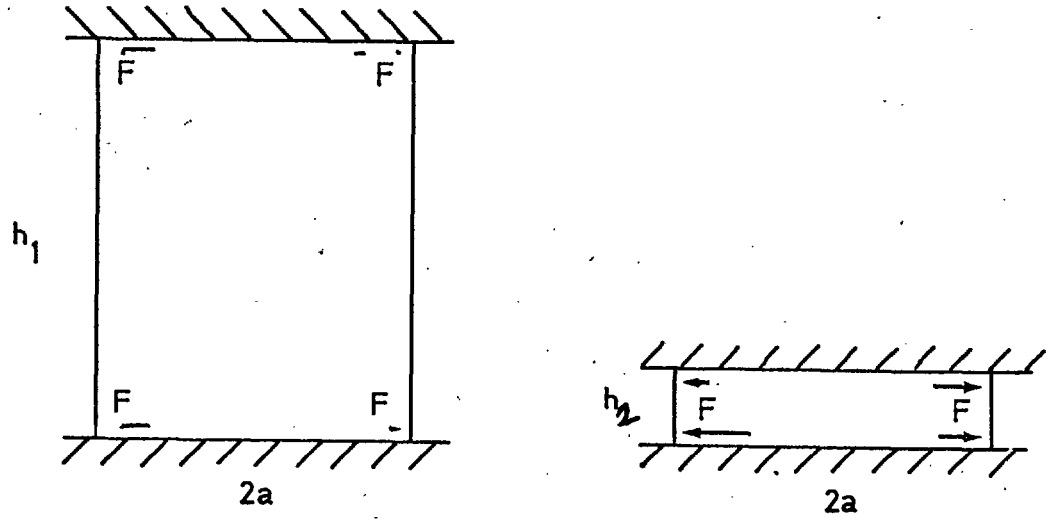

Fig. (2.5)

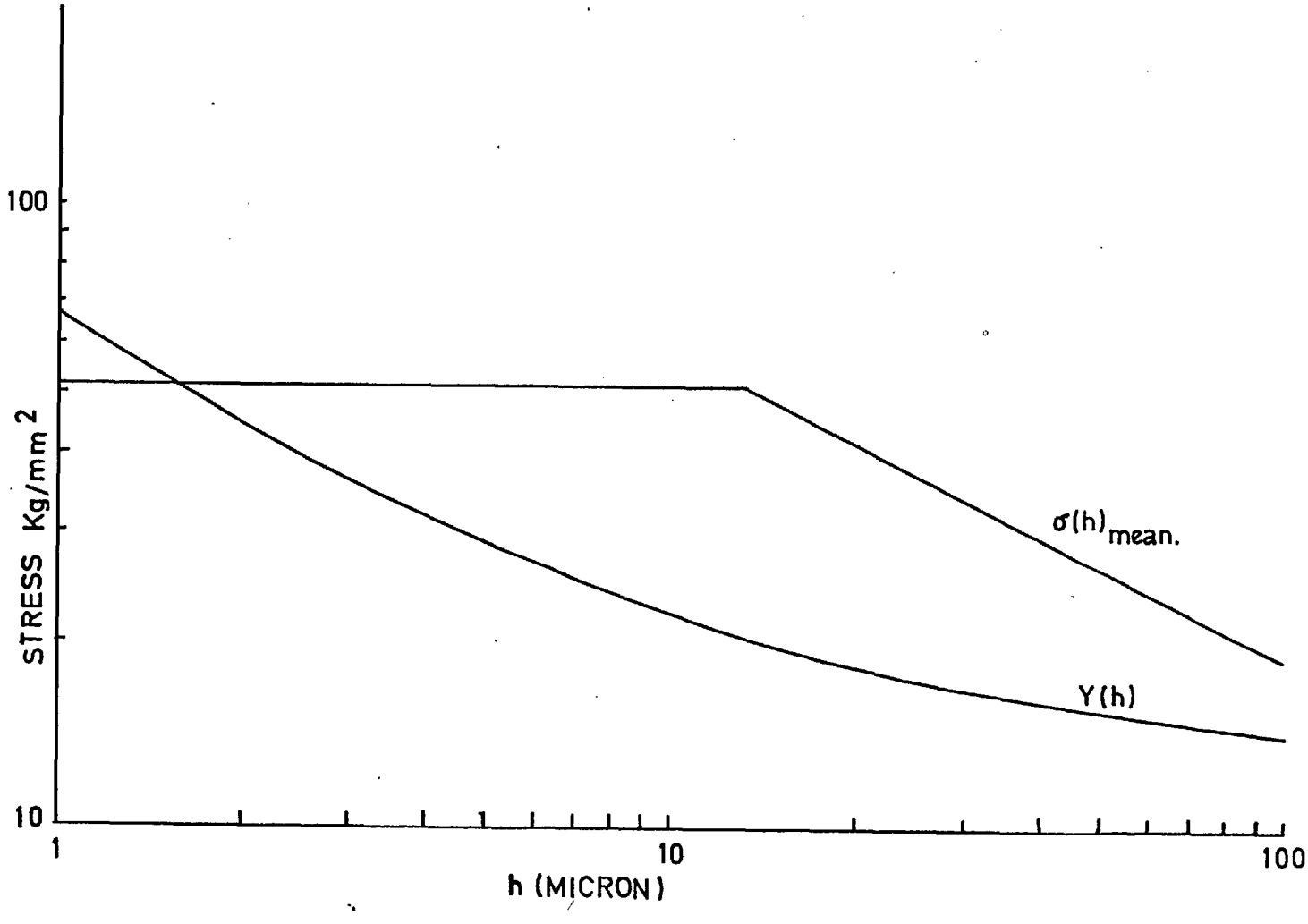

VARIATION OF CONTACT STRESS AND FILM YIELD STRESS WITH FILM THICKNESS FOR A GOLD FILM.

Fig. (2.6)

remely small compared to the radius of the indentor. We can therefore assume that the region of film under compression is effectively a cylinder, whose aspect ratio is a/h. Let us now suppose that we are performing a compression test on two cylindrical specimens, each of radius a, whose heights are h_1 and h_2 (where $h_1 > h_2$), see fig. (2.5). Our test consists of applying an increasing axial compression to each cylinder until plastic yielding commences, we assume that there is friction between the two compressing surfaces and the ends of the cylinder. Due to an interactive combination of friction and aspect ratio, we can reasonably assume that the hydrostatic component of stress will be greater in the cylinder of higher aspect ratio, for the same applied pressure; consequently the deviatoric field will contain less energy, resulting in the thinner cylinder being effectively stronger. Applying this analogy to the case of a film, it is apparent that the strength will increase as a/h increases; that is as the film becomes thinner.

We will now attempt to quantify this problem and where it becomes necessary to make simplifying assumptions, we will try to ensure that these do not exaggerate the strengthening effect but rather err on the side of pessimism because it is essential that we should have confidence in our upper limit.

Firstly we assume that all strain energy is concentrated in the film i.e. an RER solution; obviously if we permit some strain in the substrate or rider we would reduce the strain in the film and make it effectively stronger. The fact that the lower surface of the film is bonded to the substrate is disregarded and instead it is assumed that this is capable of sliding in the same manner as the upper surface with friction coefficient f.

From the work of Schröder and Webster[19] we know that[20]:

$$Y = Y_o\left[\, 1 + \frac{2f}{3}\,\frac{a}{h}\,\right] \qquad (2.14)$$

where Y_o is the yield strength in compression of the bulk film material and Y is the compressive yield strength of a cylinder of aspect ratio a/h. Restating equation (2.10):

$$a_f = 0.893\left[\frac{PRh}{G}\left\{\frac{1-2\upsilon}{1-\upsilon}\right\}\right]^{1/4}$$

substituting for a $(= a_f)$, we obtain:

$$Y = Y_o\;\; 1 \;+\; \frac{2f}{3}\;\; 0.893\left(\left[\frac{PR}{G}\left\{\frac{1-2\upsilon}{1-\upsilon}\right\}\right]^{1/4}\right)h^{-3/4} \qquad (2.15)$$

thus we have the yield strength of a film as a function of its thickness. Mean contact stress in our RER system is simply:

$$\sigma_m = P/\pi a^2 = 0.399\left(\frac{GP}{Rh}\left\{\frac{1-\upsilon}{1-2\upsilon}\right\}\right)^{1/2} \qquad (2.16)$$

but the maximum possible stress which can occur will be that for Hertz contact between the rider and substrate (discarding the RER stress when this exceeds the Hertz value) which is, from equation (2.3):

$$p_m = \sigma_m = P/\pi a_h^2$$

We are now in a position to establish the criterion of film strength,

when, for a given system:

$$\sigma_m(h) < Y(h) \qquad (2.17)$$

we have elastic contact.

Fig. (2.6) plots equations (2.15) and (2.16) on the same axes for gold on steel with P = 0.1 Kg. and R = 2.381 mm. The value of Y_o for gold is taken as 12.5 $Kg.mm.^{-2}$ and f to be 0.5*. From fig. (2.6), a value for h of 1.5 micron is obtained for the transition thickness. As we have seen, this is a highly pessimistic estimate and it would be reasonable to expect an improvement of at least an order of magnitude upon this value in practice. The transition thickness for molybdenum disulphide, as estimated by the above method, should occur at $h \simeq 6$ micron, since it will later be shown that sputtered MoS_2 probably has a compressive strength at least twice that of gold.

(2.6) Examination of Rough Spherical Contact.

So far in this chapter we have assumed that the surfaces in contact are perfectly smooth and all the results obtained apply to this situation. Since all real surfaces must have some degree of roughness, we will now examine the implications of this to our theory.

Let us imagine that we have contact between a perfectly smooth sphere and a rough half-plane (the reverse assumption is equally valid). As we begin to apply a load, a number of discrete contacts will appear and this number will increase with load until the distribution becomes approximately radial. Greenwood and Tripp[22] have analysed this situation, assuming

*A reasonable assumption for thick gold films, see for example the work of Takagi and Liu (21).

Fig.(2.7)

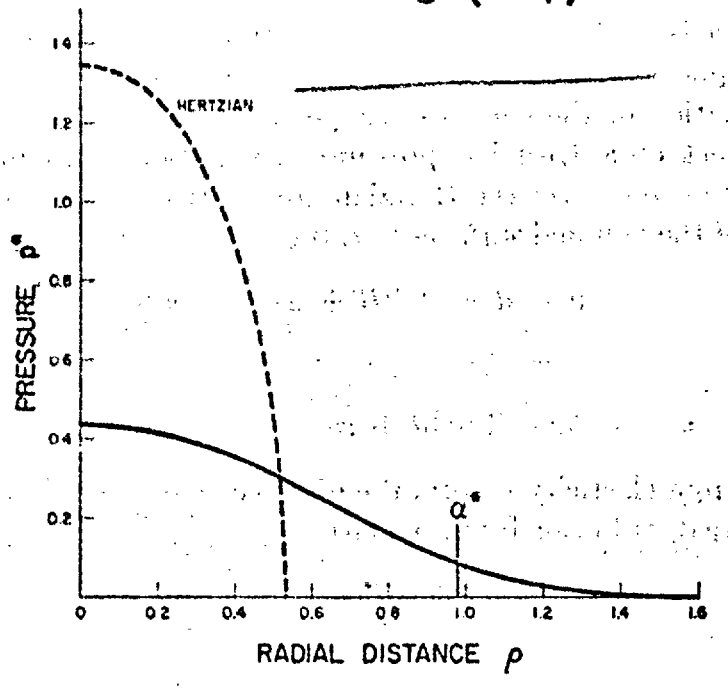

(a) At low loads pressures are much lower than Hertzian and spread over a very much larger area

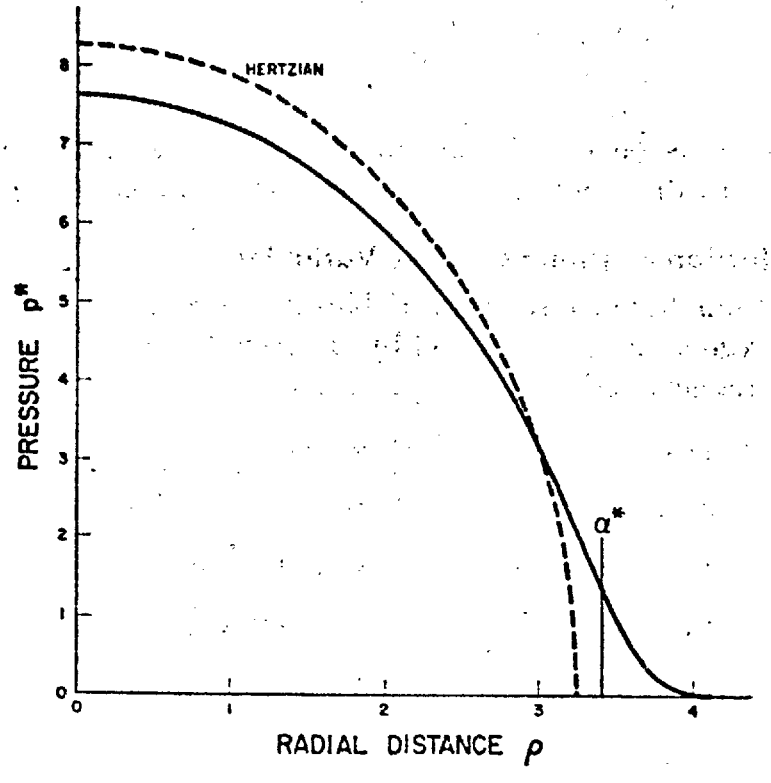

(b) At high loads calculated and Hertzian pressures agrees well

Comparison of pressure distributions with Hertzian theory. α^* is effective radius of pressure distribution.

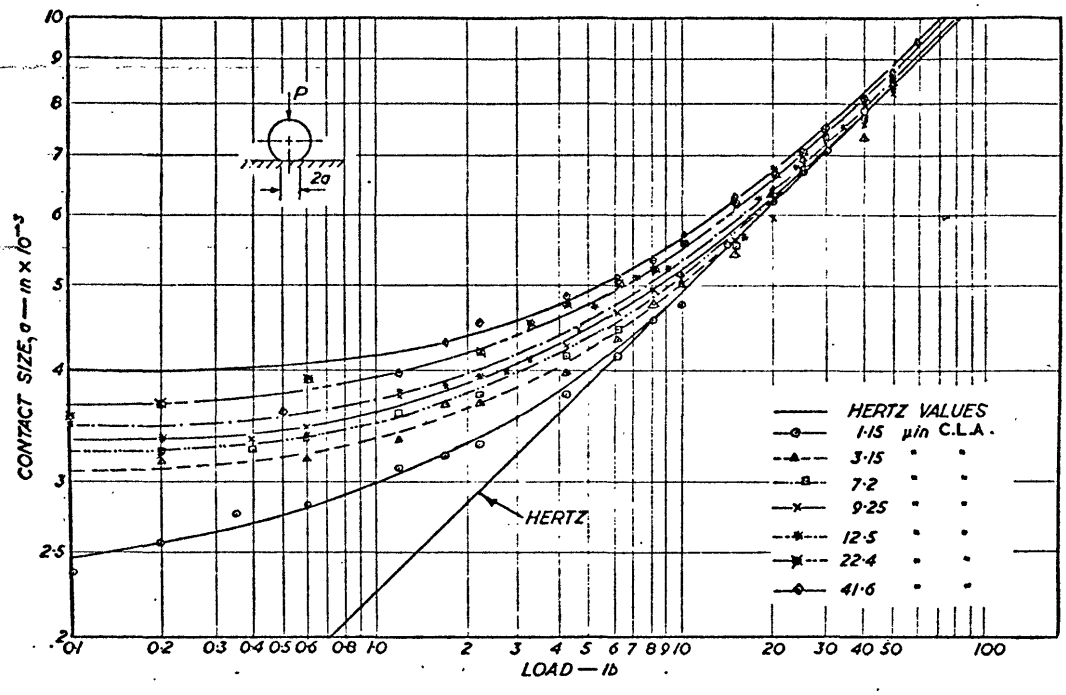

Fig.(2.8a) *Experimental results showing the effect of load and surface roughness on the track width. The corresponding values from Hertz theory are also shown*

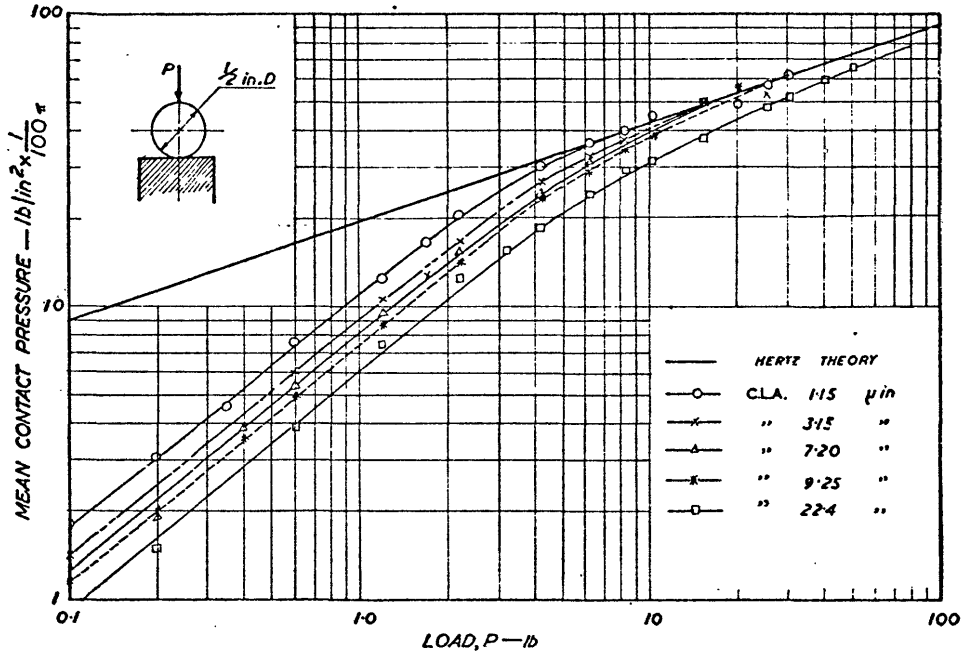

Fig.(2.8b) *Effect of load and surface roughness on the apparent contact pressure*

the distribution of asperity heights to be Gaussian and allowing for macroscopic surface deformation. The asperities are each presumed to deform elastically, according to the Hertz equation. Fig. (2.7a and b) shows two very important results of this analysis; in fig. (2.7a) the mean pressure distribution among the asperities is compared with the Hertz distribution for a lightly loaded contact and we see that the two differ profoundly. In fig. (2.7b) the same contact is shown for a much greater load and here the two distributions are very similar. Under these conditions, Greenwood and Tripp still find proportionality between load and real contact area, but it is necessary to have either a very high loading or extremely smooth surfaces before the real contact area shows a Hertzian dependence on pressure.

The work of Archard[2], confirmed by that of Greenwood and Tripp has shown that the loading of each individual contact is almost independent of the applied load, the number of contacts is the crucial factor and this is shown to increase in proportion to the load. The distribution of asperity density must therefore take the same form as the pressure distribution. Experimental work by El Refaie and Halling[23], exploring spherical contact between a variety of metals, confirms that under high load conditions the apparent contact diameter, as evidenced by the width of the track left in a very thin film of marking blue, approaches the Hertz value. Fig. (2.8a and b) show some of these results for loads between 0.1 and 60 pounds.

Archard[2] has examined the variation of contact area with load for a crossed cylinder geometry (exactly equivalent to sphere on flat) for a variety of materials. Contact area was estimated from frictional force (assuming these to be directly proportional) and it was discovered

Fig. (2.9a)

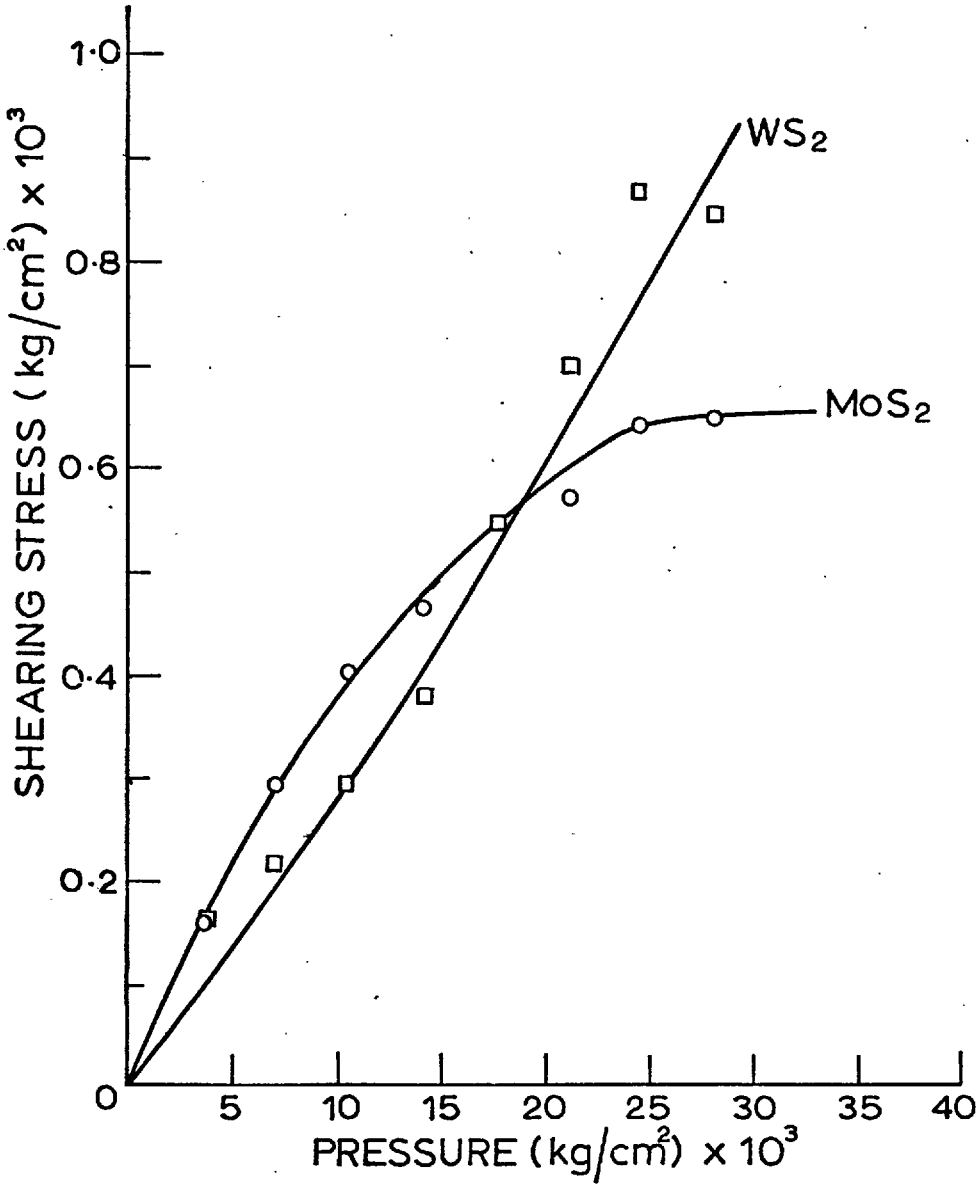

Shearing stress *vs.* Pressure (from data of Boyd and Robertson)

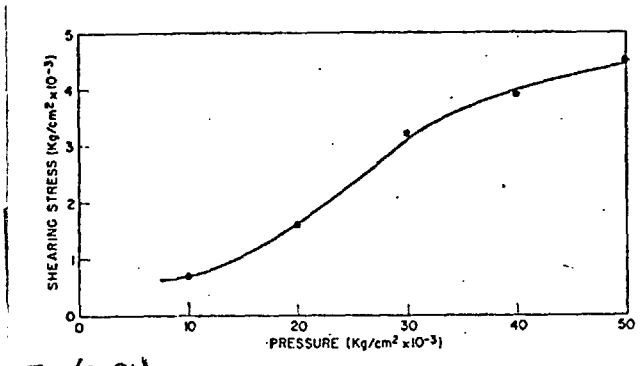

Fig. (2.9b) Shearing stress of gold as a function of pressure.

(Data of Bridgman[9])

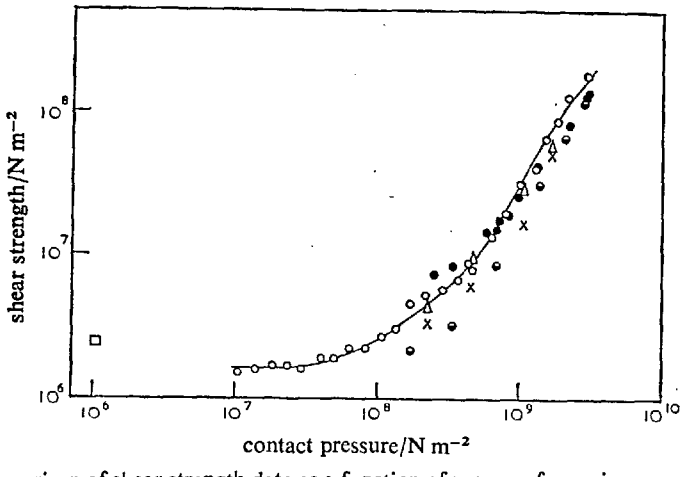

Fig. (2.9c)

Data of Briscoe and Tabor(26).

FIG. 4.—Comparison of shear strength data as a function of pressure for various paraffinic materials. It is seen that a wide range of substances of different structures and thicknesses manifest similar behaviour. ○, calcium stearate, five monolayers sheared between a glass flat and sphere [13]; □, calcium stearate+stearic acid, two monolayers sheared between mica surfaces [16]; ●, thin (*ca*, 125 nm) film of paraffin wax (m.p. 65°C) sheared between a spherical and flat surface [15]; ◒, a relatively thick initially unoriented layer of stearic acid sheared between platens [17]; ×, thick initially unoriented layer of sodium stearate sheared between platens [18] and △, thick initially unoriented layer of ferric stearate sheared between platens.[18] These data and other data [19, 20] not recorded in the figure suggest that for all these materials the shear process involves the sliding of methylene groups or chain segments over each other.

that with very smooth surfaces and high loads, the load-area dependence became Hertzian. This is consistent with asperities undergoing full elastic or plastic flattening. Archard found that with metal contact it was necessary to perform a running-in operation at high load before the contact became smooth enough to relax elastically. This of course implies a polishing effect and consequent plasticity.

From what has been said in this section, we see that the validity of the equations for smooth contact is greatly limited when roughness is considered. In our experimental work, highly polished surfaces and extremely concentrated loads have often been employed so that we have considered it reasonable to assume smooth surfaces in such cases. Quantitative justification will be attempted in a later chapter.

(2.7) The Dependence of Shear Strength on Pressure in Friction Processes.

We have shown in (1.7) that in cases where loads are carried by asperities, the real pressures of contact are almost invariant with load and thus in these cases the friction is not affected by the pressure dependence of shear strength. If this were not true, the whole basis of the elastic contact theory would founder.

Refering to Figs. (2.9a, b and c), we see the nature of the dependence for a number of interesting materials. In the case of figs. (2.9a) and (2.9b) the results were obtained by compressing samples between two flat surfaces and then rotating one of the surfaces to produce torsional shear. Due to slip between the sample and the compressing surface, bulk shearing in such a configuration does not occur consistently until pressures ~ 200 Kg.mm.$^{-2}$ are reached. We must therefore accept that these results

underestimate the effect at lower pressures but until further data are available we must make the best use of existing information. The results of fig. (2.9c) were obtained for a number of organic materials, using a method which directly measured the friction force for a known contact area; the importance of these will be seen shortly.

When real and apparent contact areas approach each other (i.e. total contact) we arrive at a situation in which the real pressure becomes a function of load. For spherical Hertzian contact, this was given in equation (1.9) as:

$$p \propto P^{1/3} \qquad (2.18)$$

In a friction situation with total contact we cannot therefore any longer assume that friction force is proportional to the real contact area. There are nevertheless a number of cases in the literature where this assumption has been made with apparent success. We have already seen an example of this in Archard's work with crossed cylinders (see 2.6); the explanation comes from careful examination of the systems that he used. In his first experiments, Archard worked with cylinders of Perspex and if we refer to Briscoe and Tabor's[26] results for various organic materials, it is seen that the dependence of shear strength on pressure is very slight for low pressures. If we assume that such results are qualitatively true for Perspex, the paradox is explained, since the low modulus of this material ensures low contact pressure. In his work with metal cylinders, Archard was obliged to use a liquid lubricant (stearic acid in cetane) to obtain smooth running, thus the shear would have tended to occur in this material.

Finkin's application (see fig. (2.2)) of an RER analysis to MoS_2-Phenolic composite films also assumes total contact. Again, the contact pressure is determined by a polymer and while the shearing may be characteristic of molybdenum disulphide, the assumption that low pressures do not greatly affect shear strength would explain the agreement. It is probably significant that the only point which deviates to any extent from Finkin's prediction is that for the highest pressure and the value for this is apparently too great. If we assume that the shear strength is now increasing, the discrepancy is explained.

Bowden and Tabor[8] report some work carried out on the friction of diamond, using a sphere on flat geometry. It was found that at high loads that the friction increased in a manner not consistent with theoretical predictions; the friction was in fact higher than anticipated. If it is remembered that the pressure dependence of shear strength may become a factor of importance at these high loads, this offers a plausible explanation for the effect.

(2.8) The Implication of Shear Strength-Pressure Dependence on Asperity Contacts.

We have seen than when asperity contact exists, the real pressure at each contact is approximately constant in both plastic and elastic situations. These pressures are nevertheless very high (up to a maximum value equal to the flow pressure) and the material in the neighbourhood of the junction will also be highly stressed. It is suggested here that this effect could have the consequence of strengthening the material in the immediate proximity of the junction, resulting in frictional shear some distance from the interface. This effect is analogous to that of work-

hardening of materials in asperity junctions, discussed in (1.6).

(2.9) Inclusion of Shear Strength-Pressure Dependence in a Friction Model.

If we examine a thin film system which has total contact, it is reasonable to suppose that the friction force will equal the shear strength of the contact and hence:

$$F = T(p)\,A\,(P) \tag{2.19}$$

and for Hertzian contact:

$$F = T(P^{1/3}/k)\,.\,k\,P^{2/3} \tag{2.20}$$

where we have simplified the Hertz expression to $A = kP^{2/3}$. Thus we may follow Bowers and Zisman[18] and insert an empirical value for T at the relevant loading. Many materials exhibit a shear-pressure dependence of a linear form:

$$T = Bp + C \tag{2.21}$$

where B and C are constants of the material. Substituting equation (2.21) into (2.20), we obtain:

$$F = BP + kCP^{2/3} \tag{2.22}$$

This expression will be compared with our experimental results at a later stage in this work.

(2.10) The Increase in Friction for Very Thin Films.

The phenomenon of increasing friction for decreasing film thickness, typified in the results of fig. (1.2), can be attributed to three basic mechanisms:

(1) Failure of the film to separate substrate and rider, resulting in increased friction, a situation which would be enhanced as the film becomes thinner.

(2) Micro-elastic stiffening of the film material, due to the proximity of the substrate (and rider). If the film becomes apparently stiffer in shear, it will be shown that its strength increases.

(3) Micro-plastic effects increasing the strength of the film as its thickness decreases.

These three mechanisms will now be examined in some detail.

(2.10.1) Film Failure.

We have seen the nature of the asperity interactions which occur when two rough surfaces come into contact. Suppose now that one of these surfaces is covered with a very thin film of solid lubricant material; how effective will this be in isolating the surfaces from each other? Dayson[10] has idealized this problem into one in which the film covered surface, presumed flat, interacts with a rough surface. In calculating contact area, Dayson implicitly assumes the rough surface to be rigid and the film and substrate to be perfectly soft. Thus by setting an arbitrary value on the equilibrium separation, Dayson calculates the contact areas of the upper surface with the film and substrate respectively. Having

made the á priori assumption that the film and indeed the substrate, offer no resistance to penetration; the analysis now admits the existence of a finite compliance by introducing asperity contact pressures for the film and for the substrate. An expression for the dependence of friction on film thickness is derived.

In (2.5) we saw how film strength can depend on contact geometry; thus for an asperity of tip radius R in contact with a film of thickness h we know that the film strength depends on the magnitude of the factor a/h, where a is the radius of contact. If we assume, following Greenwood and Tripp, an asperity radius of 0.2 mm. with a loading of 0.05 Kg. and a film thickness of 5×10^{-5} mm. (500 Angstrom), we can reasonably expect a Hertzian contact for such a thin film and hence for steel a = 0.01 mm., giving a/h = 200. Using equation (2.14), we find that $Y = 68Y_o$ and for gold, this would give a compressive strength of 850 $Kg.mm.^{-2}$ It is obvious that the steel will yield long before the gold for films of this thickness and we can expect the film to act as a very effective isolator. In dynamic shearing the position is less clear and the extent of film breakdown must depend on the wear properties of the materials involved. Certainly breakdown effects are undeniable in some systems.

(2.10.2) Micro-Elastic Effects.

As the dimensions of a material sample are reduced, we reach a point at which its physical properties are constrained by its geometry and these can become radically different from those experienced with bulk samples. Two aspects of such phenomena will be discussed in this and the following sub-section.

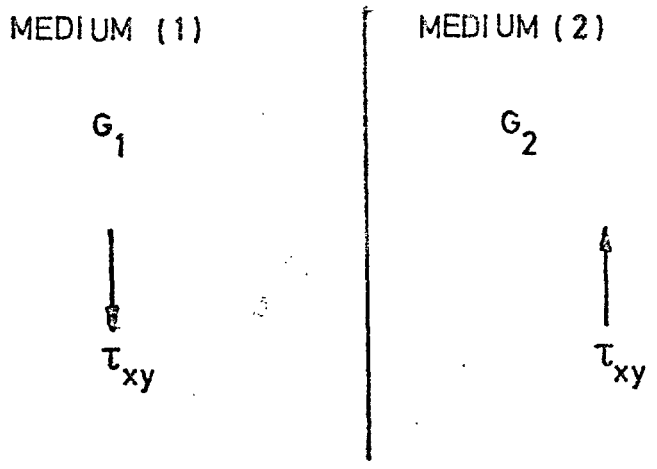

Fig.(2.10a)

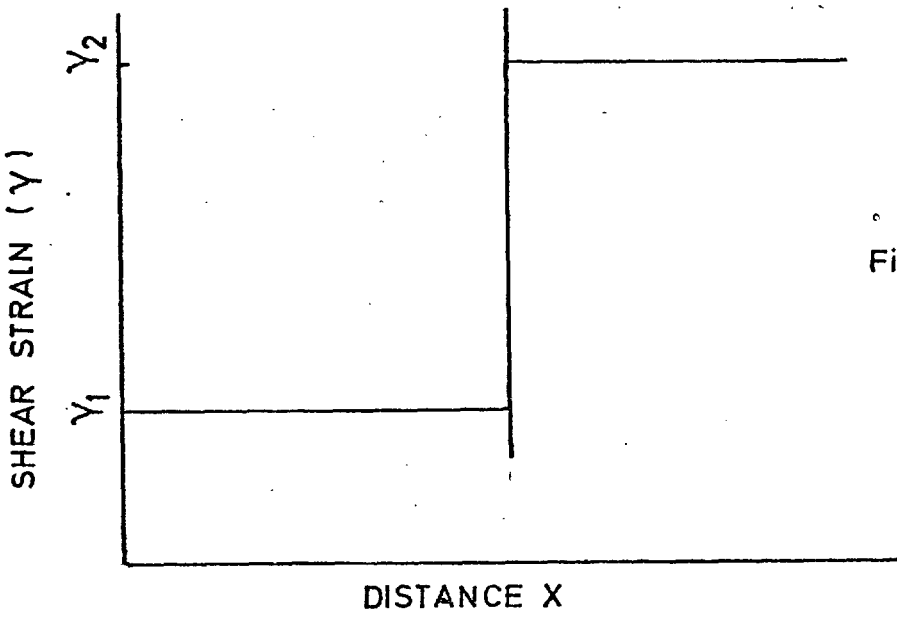

Fig.(2.10b)

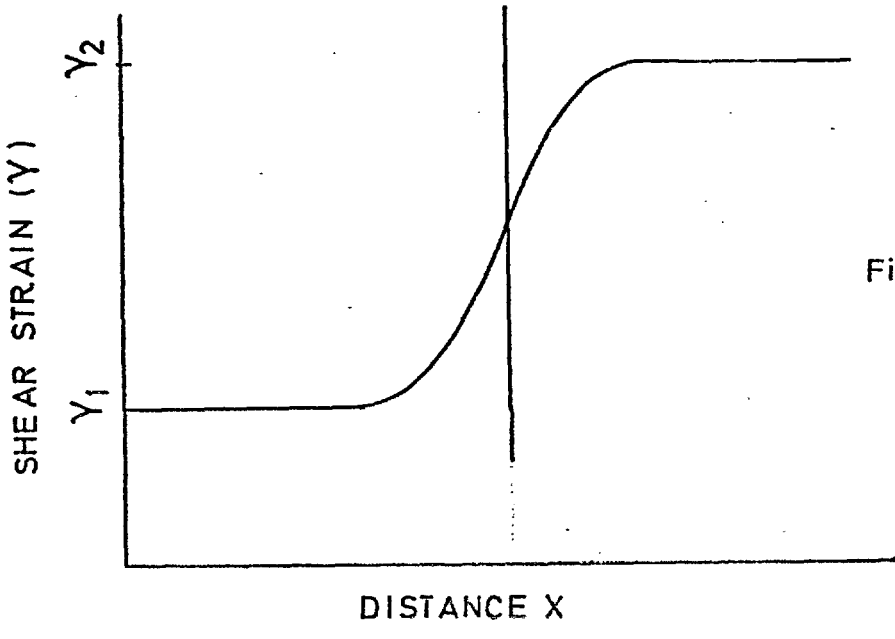

Fig.(2.10c)

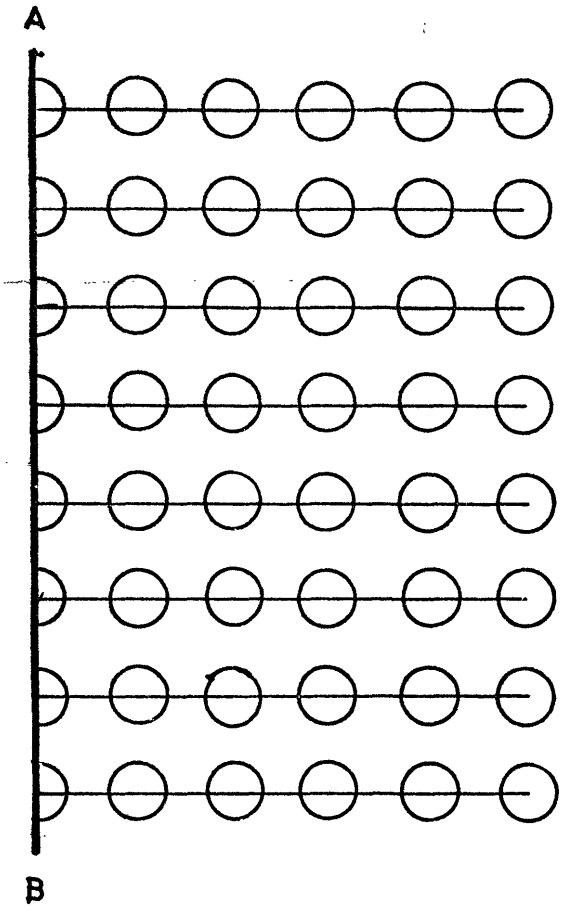

Fig. (2.11a)

ATOMISTIC MODEL DEMONSTRATING MICRO-ELASTIC EFFECT AT THE INTERFACE BETWEEN A RIGID MATERIAL AND AN ELASTIC MATERIAL

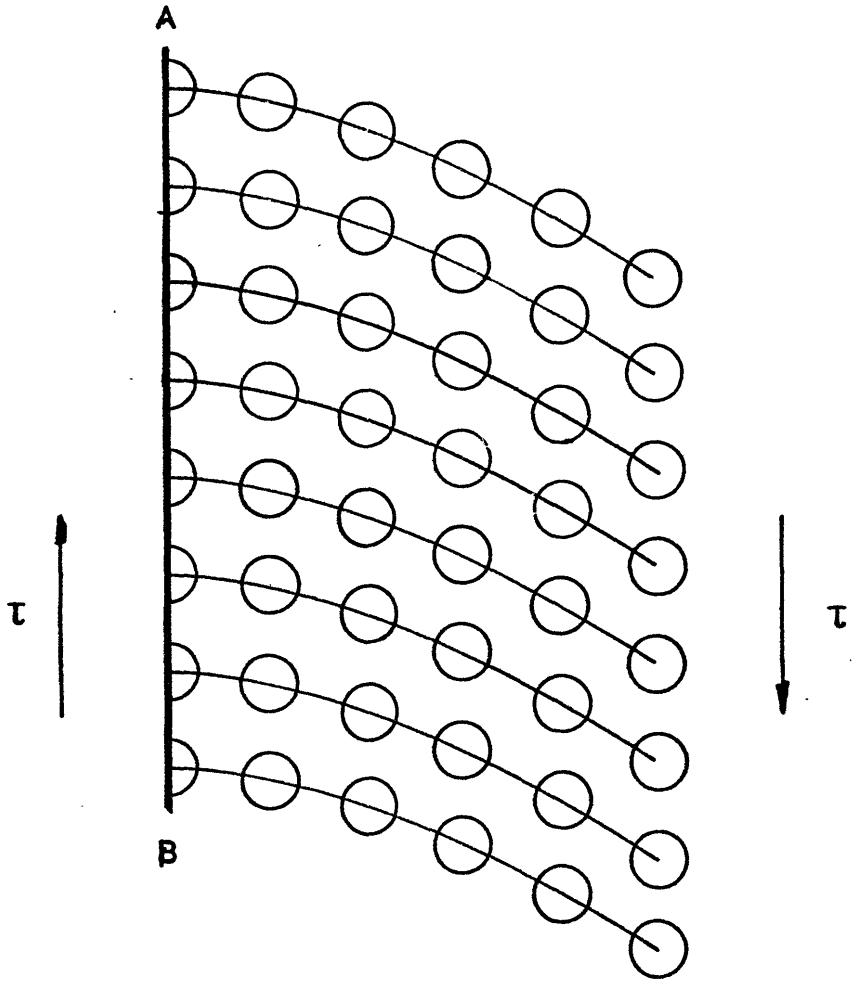

Fig. (2.11b)

Let us consider a plane interface between two materials of different elastic properties (see fig. (2.10a)). Let us imagine that we apply a shearing force across and parallel to the plane of the interface. How can we expect the resulting shear strain to behave as we move through this system? If we apply classical elasticity theory the solution is very simple: we have a strain of γ_1 in medium 1 and γ_2 in medium 2, with a discontinuity between, as in fig. (2.10b). Intuitively we know that the situation of fig. (2.10c) is more reasonable and this is justified analytically by saying that the interface cannot absorb infinite strain gradient. Thus a 'skin-effect' occurs in which material 1 has its apparent modulus reduced and material 2 has its apparent modulus increased in the vicinity of the interface (assuming $G_1 > G_2$). In fig. (2.11a and b) the phenomenon is represented by an atomistic model: a 2-dimensional lattice is rigidly constrained along the line AB and when a shear force is applied parallel to AB, the effect of the constraint is propagated for some distance into the lattice. Obviously in reality we are usually dealing with polycrystalline materials, nevertheless the effect should still occur since the strength of inter-crystallite bonds is normally as high as those within the crystal; a fact which becomes apparent when one realizes that elastic moduli of polycrystalline materials are virtually the same as their single crystal counterparts.

In classical elasticity, an state of stress within a body can be represented in tensor form, incorporating the principal stresses:

$$\begin{bmatrix} \sigma_x & \tau_{xy} & \tau_{xz} \\ \tau_{yx} & \sigma_y & \tau_{yz} \\ \tau_{zx} & \tau_{zy} & \sigma_z \end{bmatrix}$$

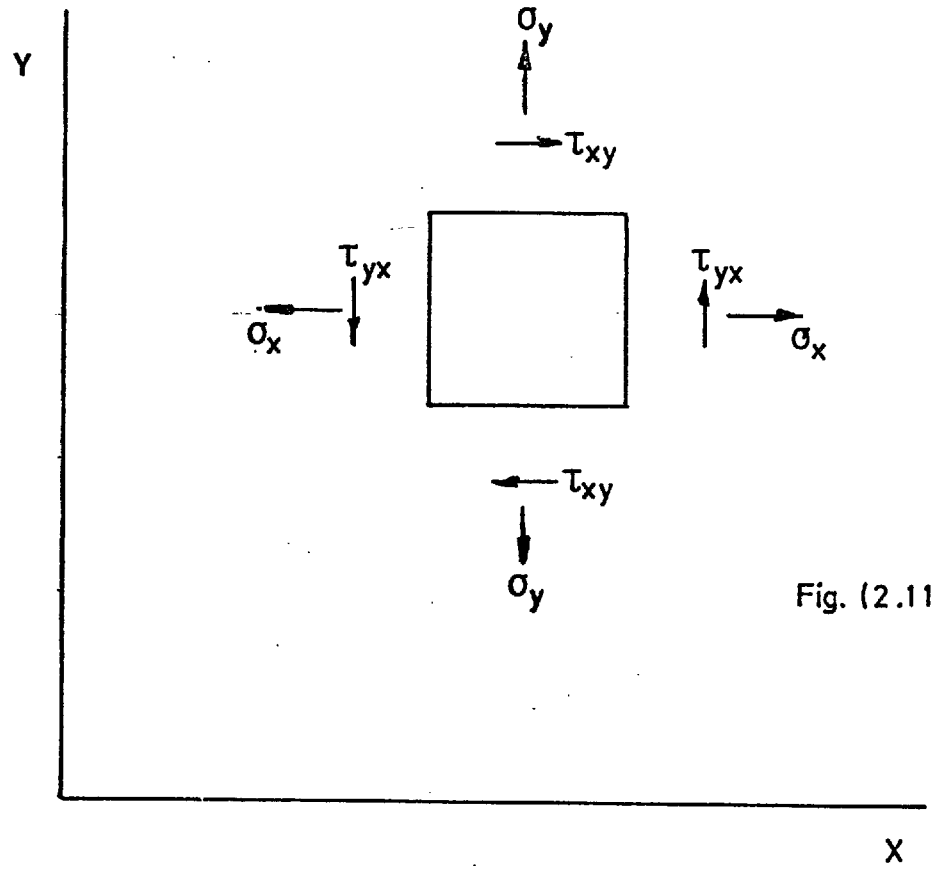

Fig. (2.11)

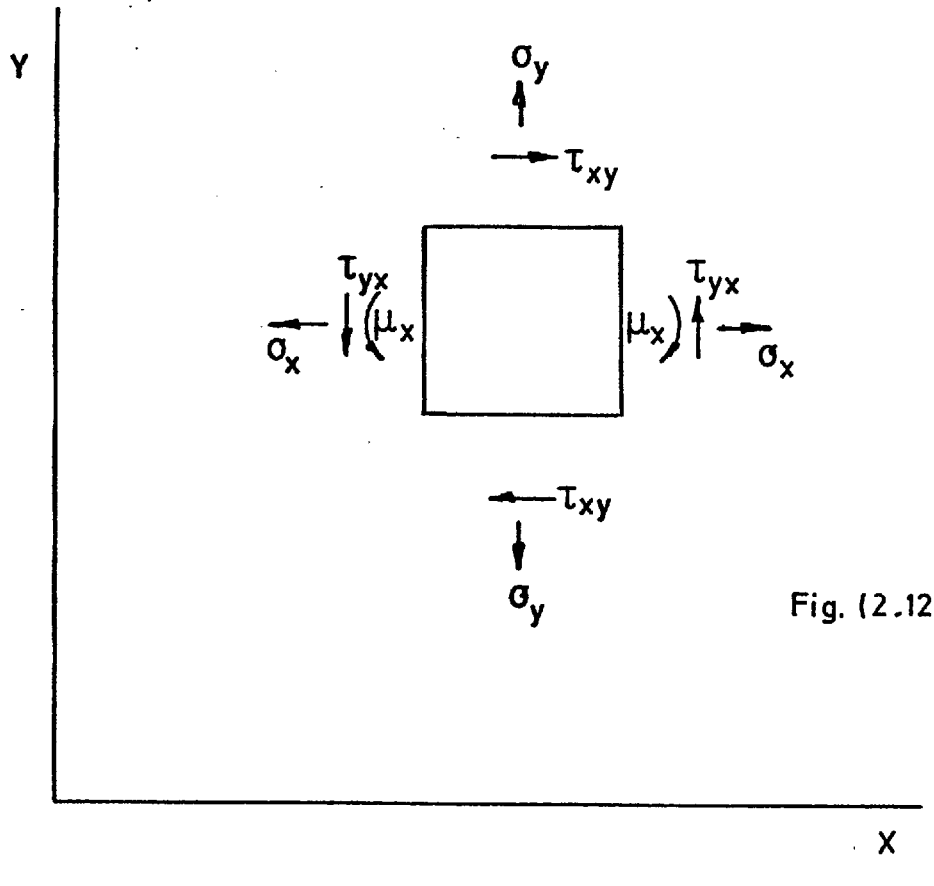

Fig. (2.12)

It is a requirement of classical theory that this tensor should be symmetric, that is, $\tau_{xy} = \tau_{yx}$, $\tau_{zx} = \tau_{xz}$ and $\tau_{yz} = \tau_{zy}$. If we examine the lattice of fig. (2.11b) we see that in the vicinity of the interface this condition is violated, because although the applied stress τ_{xy} is constant across the sample (by equilibrium); τ_{yx} varies in magnitude from zero (at the interface, which is presumed rigid) to τ_{xy} at points remote from the interface. Thus we see why classical elasticity theory cannot apply to our case.

The conventional stress elements of classical theory act upon an element of material in the manner of fig. (2.12a). This element must be in equilibrium under their action. The question is now asked: How can this situation be modified without destroying equilibrium? Clearly if we reduce one of the shear forces without simultaneously reducing another, a resultant moment will be introduced which will destroy equilibrium. The solution is found by introducing a totally new stress element, the couple-stress, to our system. This is a quantity having the dimensions of moment and producing curvature in the material upon which it acts. Thus the couple-stress μ_x acting upon opposite faces of our element in fig.(12b) does not destroy equilibrium. The couple-stress is linked to the curvature k_x by:

$$\mu_x / k_x = 4G\ell^2 \qquad (2.23)$$

where ℓ is a modulus of the new theory and G is the shear modulus.

We can now proceed to write down the equations for the equilibrium of the element for stresses which are varying with position; these are

then combined with equations relating stress to strain and equations describing the stress field result. These equations are examined in Appendix (1).

Let us now return to consideration of friction effects. We saw in the preceeding section that the aspect ratios in very thin film friction are high, thus we can follow Finkin[27] and model these as a thin film, bonded to and sandwiched between two half-planes. We shall presume for simplicity that the system is RER. Let us assume that the maximum shear strain that the film can support in bulk form is γ_o. Thus if there is an apparent increase in the film modulus to $G(h)_{app.}$, the applied stress at which shearing occurs will be increased also, according to the expression:

$$T = G(h)_{app.} \cdot \gamma_o \tag{2.24}$$

which for constant load is proportional to the friction coefficient.

Using the methods of appendix (1), the mean apparent shear modulus for a film of thickness h is shown from couple-stress theory to be:

$$G(h)_{app.} = \frac{G}{1 - (2\ell/h)\tanh(h/2\ell)} \tag{2.25}$$

and thus from equation (2.24) we have an expression for the friction coefficient as a function of h:

$$f = \frac{KG}{1 - (2\ell/h)\tanh(h/2\ell)} \tag{2.26}$$

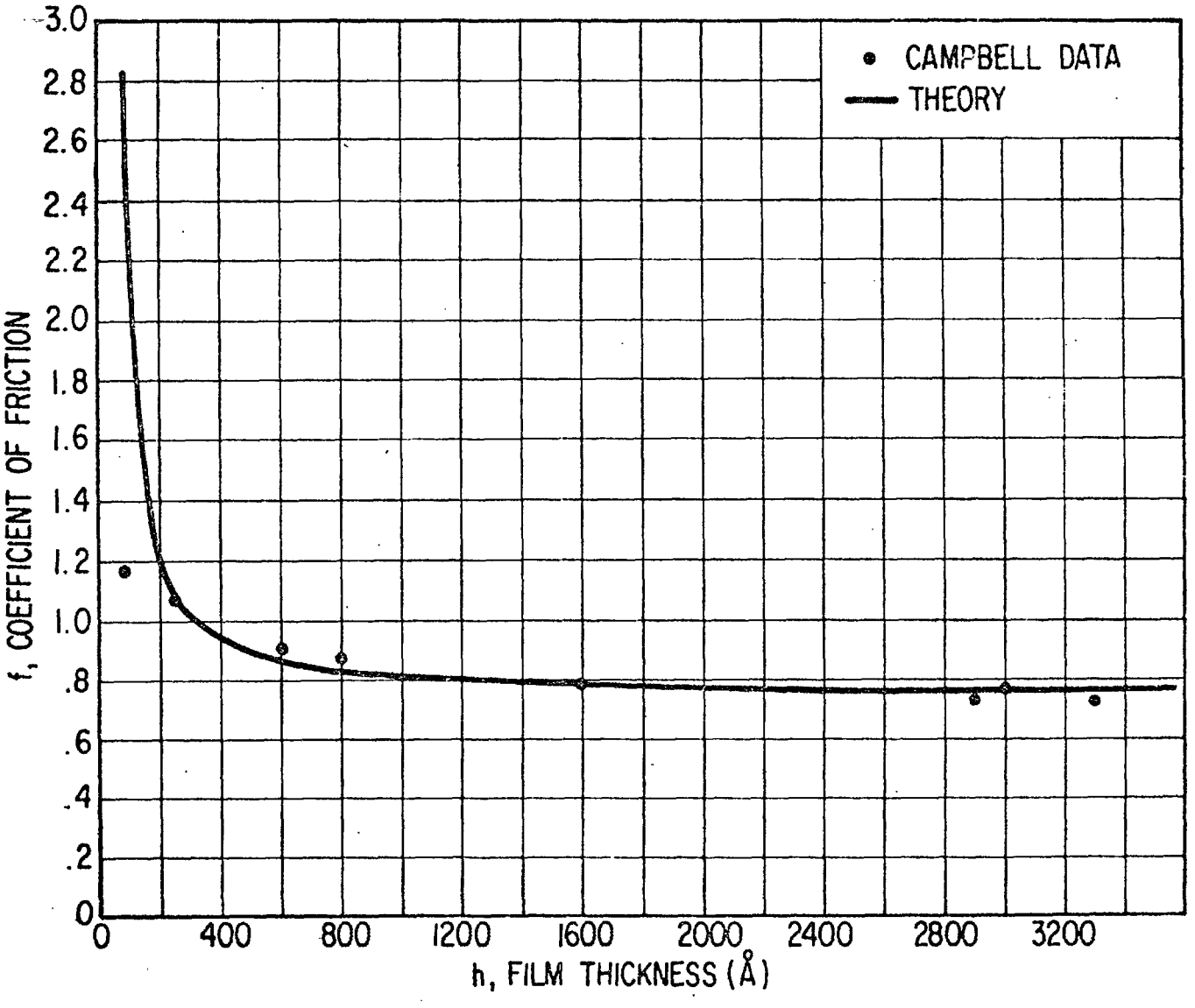

Fig. (2.13)

Theoretical Relation and Experimental Values of Static Friction Coefficient as a Function of Film Thickness for Sulfide Films on Copper (data from Campbell[28])

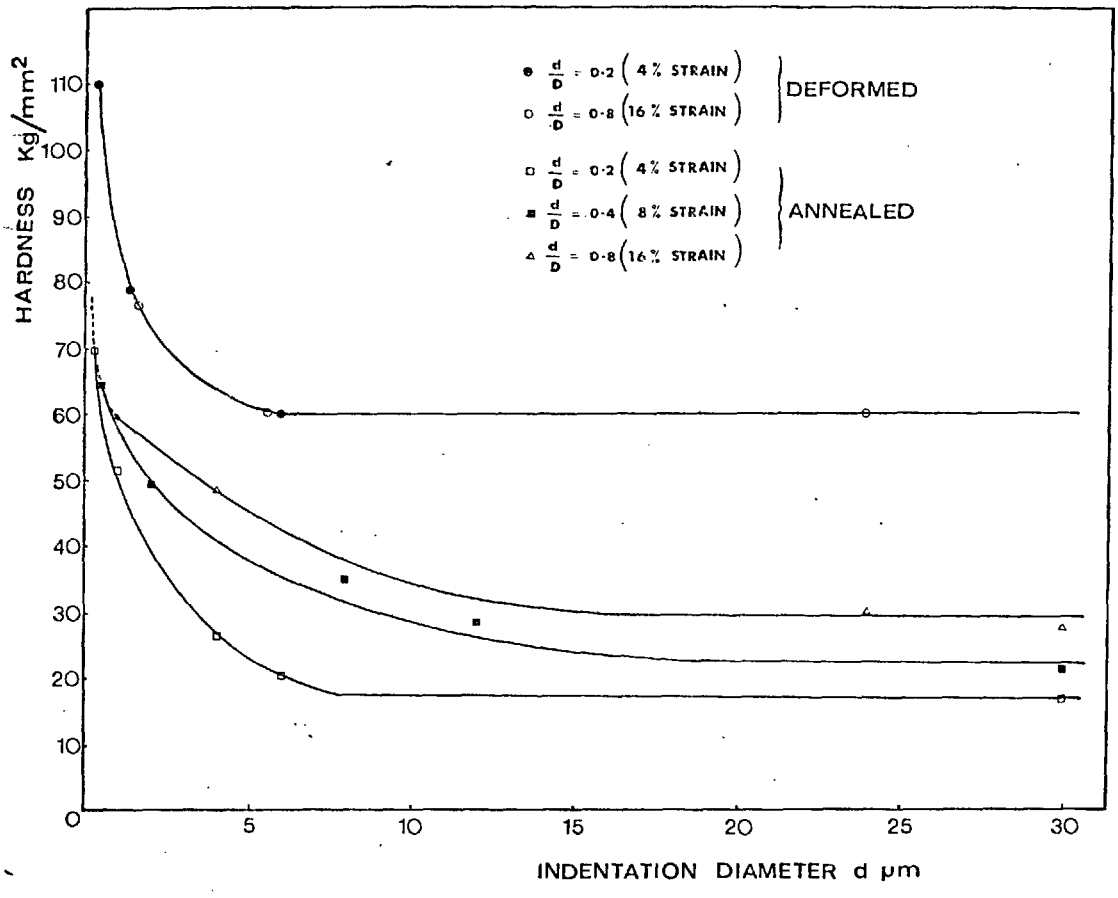

Variation of hardness with indentation size for annealed and heavily cold-worked gold. Different values of the shape factor d/D are equivalent to different amounts of strain around the indentation.

Fig. (2.14)

(Data of Gane[29])

where K is a constant of proportionality. The concept of applying micro-elasticity theory to friction phenomena was originally due to Finkin[27] who derived the above expression and applied it to some well known thin film friction results. An example is seen in fig. (2.13) for the case of copper sulphide films on copper, where the results of Campbell[28] are examined. A possible explanation for the poor agreement at very low thickness is that the RER assumption is suspect. However, extension of the theory to cover the all-elastic case would be very involved and would require more experimental data than we possess.

(2.10.3) Micro-Plastic Effects.

Since the strength of elasto-plastic materials is governed ultimately by the distribution of dislocations within them, it is reasonable to suppose that significant changes in strength might be observed in samples whose size is of the same order as the mean dislocation separation distance. Crystals whose size is in the micron range do possess strengths enormously greater than large crystals of the same material. Micro-hardness measurements, using indentors of decreasing size, exhibit pronounced enhancement of strength, as shown by the work of Gane[29], whose results for clean gold surfaces are shown in fig. (2.14). Since resistance to indentation is a strong measure of shear strength, among other parameters, these results are probably of some significance to thin film friction.

Pashley[30] and other workers have examined the strengths of a number of materials in the thin film form and have found increased strengths in tension, with elastic strains over 1% being common.

Bearing in mind the evidence above, it seems very likely that these

effects could play an important role in the dependence of friction upon film thickness.

(2.12) Theoretical Examination of Hard Protective Coatings.

The objective in applying a hard protective coating to a surface is to impart to that surface the wear resistance of the bulk hard material.

Let us denote the substrate, film and abrasive materials by the numbers 1, 2 and 3 respectively. We thus have three hardnesses H_1, H_2 and H_3 and three Young moduli E_1, E_2 and E_3.

Looking at the situation very simplistically, we can at once write down the following conditions:

(1) The unprotected surface of the substrate will be subject to wear if $H_3 > H_1$.

(2) The bulk film material will be subject to wear if $H_3 > H_2$.

(3) The beneficial effects of the film will be to provide protection from wear particles whose hardness is in the range $H_1 < H_3 < H_2$, always provided that the contact stress does not exceed that required to produce yielding in the substrate.

The final proviso of condition (3) will now be examined.

Let us assume that the wear particle makes contact with a radius R and that the load on this contact is P. If we assume that the ratio E_2/E_1 is large, we saw in (2.4) that the maximum variation in contact width due

to film thickness was given by the ratio:

$$((2\gamma/[\gamma + \gamma])^{1/2} - 1) : 1$$

which is 41% for large γ. Thus if we assume Hertzian contact with the substrate we shall not be grossly in error. The mean contact pressure can now be found from equations (2.1) and (2.3) and assuming $\nu = 0.3$ for our materials, we can apply the equations (2.7) and (2.9) to obtain the criteria for substrate yielding:

$$p_m = 1.24Y_1 \tag{2.27}$$

for elasto-plastic substrates and

$$p_m = 5Y_1 \tag{2.28}$$

for brittle substrates; Y_1 being the yield strength in tension for the substrate material. For elasto-plastic materials we know that $H = 3Y$[8] and hence we can write equation (2.27) as:

$$p_m = 0.41H_1 \tag{2.29}$$

On examination of fig. (2.1) we see that for values of $a_o/h > 1$, we have a contact which is Hertzian with respect to the <u>film</u>, this means that the stress concentration at the substrate interface will be dissipated considerably and it is not likely that yielding will occur. Thus when $a_o > h$ the condition for bulk film material is reached.

Summarizing, we can now state that a hard coating will give prot-

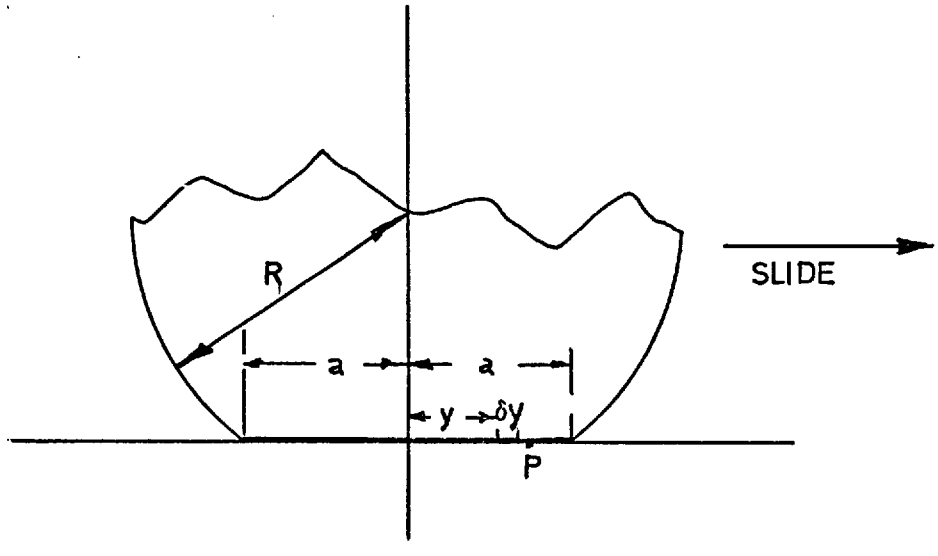

FIG.(2.15)

ection from abrasion, provided the following two conditions are valid:

(1) $H_2 > H_3$

(2) If $a_o < h$ then the mean Hertz pressure must not exceed 0.41 H_1 in the case of elasto-plastic substrates and $5Y_1$ for brittle substrates.

(2.13) Wear Mechanisms.

In (1.9) we defined an equation applying to the particular case of a thin film undergoing linear wear:

$$x = Kp\bar{L} \qquad (2.30)$$

x was the depth of film worn in sliding a distance L under a pressure p and K was the wear coefficient.

We mentioned in (1.9) that the point of major interest in spherical contact is at the centre where the pressure is highest; film penetration is most likely to occur in this region. Let us consider the situation as a spherical rider slides across a film covered surface. Fig. (2.15) shows the rider, viewed normally to the direction of sliding and we shall consider the wear of points lying on the centre of the track. The distribution of pressure beneath the rider and along the centre line is given by[13];

$$p = 3p_m(a^2 - y^2)^{1/2}/2a \qquad (2.31)$$

where p_m is the mean Hertz contact pressure, a the contact radius and y

is the distance from the centre of contact. Now let us consider a point P on the film which interacts with an element of length δy on the rider, whose distance from the centre is y. The depth of wear at P will be, from equations (2.30) and (2.31):

$$\delta x = \frac{3Kp_m}{y}.(a^2 - y^2)^{1/2}.\ \delta y \qquad (2.32)$$

Integrating between the limits y = +a and y = -a we have the wear depth for a single pass of the rider over P as:

$$x = \frac{3\pi Kap_m}{4}$$

and thus if a film of thickness h is worn through in N cycles, we have:

$$N = 4h/3\pi Kp_m a = 4ha/3KP \quad (\text{since } p_m = P/\pi a^2) \qquad (2.33)$$

Using the above expression we are able to compare the wear coefficients for similar films operating under different Hertzian contacts. An identical expression is derived for the cylindrical case, except that now $p_m = P/2a\ell$ and the expression becomes:

$$N = 8h\ell/3\pi KP \qquad (2.34)$$

We have assumed above that there has been no redistribution of contact pressure as a result of wear; since the wear is proportional to pressure we should expect the pressure to become increasingly uniform beneath the rider as wear proceeds, ultimately arriving at a situation in which the radius of the wear track conforms exactly to that of the sphere. This would

Fig.(2.16)

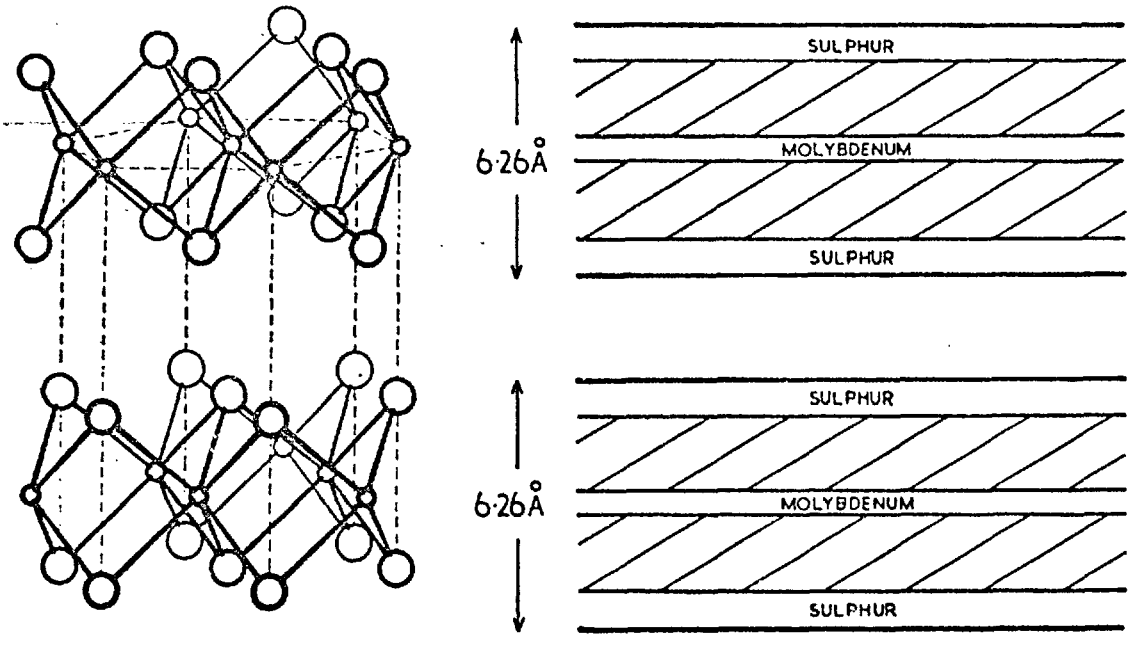

Structure of MoS_2. The individual sheets are either pure molybdenum or pure sulphur. Cleavage occurs between neighbouring planes of sulphur; these are 3·66 Å apart and the bonding between them is relatively weak.

(From Bowden and Tabor[8])

give a contact equavalent to a cylinder sliding on a plane; in practice this does not occur, since the contact radius also grows and the resulting zone is an ellipse[8].

(2.14) Examination of Materials Properties.

It is logical to divide solid lubricants into the following catagories:[31]

(1) Anisotropic solids.

(2) Soft metals.

(3) Hard ceramics.

The first group, as well as including such obvious materials as graphite and molybdenum disulphide, also includes polymers such as PTFE and Nylon which lubricate as a consequence of their anisotropy. The soft metals normally used include gold, silver, lead, copper and indium; the mechanism by which these materials operate was discussed in (1.8). Hard ceramics are normally applied to surfaces to enhance their abrasion resistance and their friction is usually high. Typical examples are silicon nitride, tungsten carbide and chromic oxide.

(2.14.1) Molybdenum Disulphide.

The crystal structure of this material is shown in fig. (2.16) and consists of a plane of molybdenum atoms sandwiched between two planes of sulphur atoms. Each molybdenum atom is covalently bonded to six sulphur atoms and each sulphur atom to three molybdenum atoms*, while the adjacent sulphur layers are bonded through Van der Waals forces. Because of this

*In fact this bonding should strictly be described as being partially satisfied covalent because trivalent bonding is abnormal for sulphur and must involve electron sharing.

weak bonding, cleaving and shearing processes can easily occur and this gives the material its excellent lubricating properties.

Due to the strength of the covalent bonding, polycrystalline aggregates of molybdenum disulphide should exhibit reasonable compressive strength since the cohesive forces will be composed of a mixture of covalent and Van der Waals bonding.

It has been established that anisotropic materials lubricate by forming complementary oriented films on the rubbing surfaces; this orientation either occurs as a result of crystallites being rotated to give minimum interaction energy during sliding, or because unfavorably oriented crystallites are plucked out from the surface and removed from the system as wear particles. If a dense compact of graphite or molybdenum disulphide is made to form one of the components of a bearing, the surface layer will become oriented while the relatively strong compacted material beneath will support the bearing load; we saw in (1.8) that such bearings are only suitable for use at light loadings.

Spalvins[32] has been one of the few workers to investigate the wear properties of sputtered molybdenum disulphide films and using ultra high vacuum friction apparatus he was able to achieve wear lives of over a million cycles (at Hertz contact pressures ~ 70 Kg.mm.$^{-2}$). This work was primarily concerned with applications and there was apparently little enquiry into the mechanics involved. It was found however that the grain size of the polycrystalline films was extremely small; implying that the material should be approaching its optimum compressive strength in the sputtered condition.

(2.14.2) Soft Metals.

In practical engineering applications, thin soft metal films are applied exclusively to bearings which are to operate in the rolling rather than the sliding mode; nevertheless, information as to the performance of these films under sliding conditions is of considerable importance.

Soft metal films are found to be extremely reliable for lubrication in vacuum and lead films used in bearings fitted to space vehicles have operated continuously for over seven years. Gold is also a material of particular interest, since although it is soft, it has a relatively high melting point and is not chemically reactive.

We have seen that under conditions of sliding friction, metallic contacts are likely to exhibit severe adhesive wear and this is compounded if such systems operate in vacuum. Sliding contacts are liable to generate temperatures which can be high enough to assist in an alloying process between the film and rider materials. Once material transfer occurs, the contact becomes considerably roughened and plastic contact between asperities may occur, resulting in a combination of further alloying and junction growth.

In rolling contact the friction dissipation is usually very small, being mainly due to elastic hysteresis in the region of deformation. The low friction, combined with the fact that the contact zone moves across both surfaces, ensures low temperature operation, which discourages any alloying effects. The results obtained from sliding friction experiments are important because relative slip, while not contributing significantly to rolling friction, must be responsible for the major part of the wear

occuring here; consequently if we discover the optimum thickness for minimum wear in sliding contact it would be reasonable to apply this to the rolling situation.

The elastic hysteresis loss is usually high for soft materials; thus if a film is applied to a rolling component which is thick enough to contain a significant proportion of the elastic strain energy, the friction due to hysteresis in the film may become important. Thickness effects of this kind offer a very interesting field for investigation.

(2.14.3) Chromic Oxide.

The requirements of a hard ceramic film are that its hardness should be greater than any of the abrasive particles that it is likely to encounter and that the film thickness should be sufficient to ensure that high stress* contacts are Hertzian with respect to the film (see (2.12)).

Chromic oxide has an excellent industrial record as a coating material, both in anti-abrasive situations and those where the material runs against itself. Unfortunately, being both hard and isotropic, the material gives high friction and its use in continuously running bearings is limited. As a surface coating for air bearings, in which the material would only be called upon to operate under load in exceptional circumstances and in which its resistance to the abrasive effect of high pressure gas is most desirable, chromic oxide offers considerable potential.

(2.14.4) Substrate Materials.

The 2" discs used in conjunction with the dynamic friction investigation were made from EN 58A (AISI 302) stainless steel. This has an Austenitic

*'High stress' in this context implies that if the same stress contact were applied to the substrate, the latter would yield plastically.

structure and contains 18% chrome and 8% nickel. The Vickers (and Brinell) hardness is approximately 300 $Kg.mm.^{-2}$

The 3/16" balls, used as riders in the dynamic friction work were made from 440C stainless steel. The structure is martensitic and the steel contains 16 - 18% chromium with no nickel. The Vickers hardness is 920 $Kg.mm.^{-2}$ (700 $Kg.mm.^{-2}$ Brinell).

In the wear evaluation tests for molybdenum disulphide films, the 1" steel balls and flat-ended pins were made from EN 31 steel (1% carbon, 1% chromium).

Tungsten carbide balls (3/16" diameter) and plane discs were made from commercial grade tungsten carbide, containing a few per cent of cobalt as a binder during sintering. The elastic modulus of this material is approximately 56,000 $Kg.mm.^{-2}$

CHAPTER 3 --- SPUTTERING AND SPUTTERED FILMS

(3.1) While it is not the intention of this work to undertake fundamental studies related to the sputtering process, it is necessary to have some understanding of the mechanisms involved in order to appreciate fully the advantages that this deposition method holds over the other available processes, particularly thermal evaporation.

As often occurs with newly developed technologies, much of the work being done is of a proprietary nature and the published literature is several years behind the real state of the art. This situation inevitably results in an unconsolidated mass of information, very often incorporating conflictions.

It is therefore the intention here to rationalize the information relating to those aspects of the process which have specific relevance to this work.

(3.2) Arrival Energy of Sputtered Species.

Stuart and Wehner[33] have studied the energy distribution of material sputtered from a variety of targets, using velocity selector techniques. Fig. (3.1) shows the velocity distribution function, $dN(v)/dv$, for sputtered copper, for bombardment energies between 150 and 600 eV. These results were for atoms ejected normally from the surface. For bombardment energies of 150 and 200 eV, the distributions were found to be very nearly Maxwellian, with temperatures corresponding to 18,500 and 26,000^{o}K respectively. For the higher bombardment energies, the distributions follow the Maxwell form

Fig.(3.1)

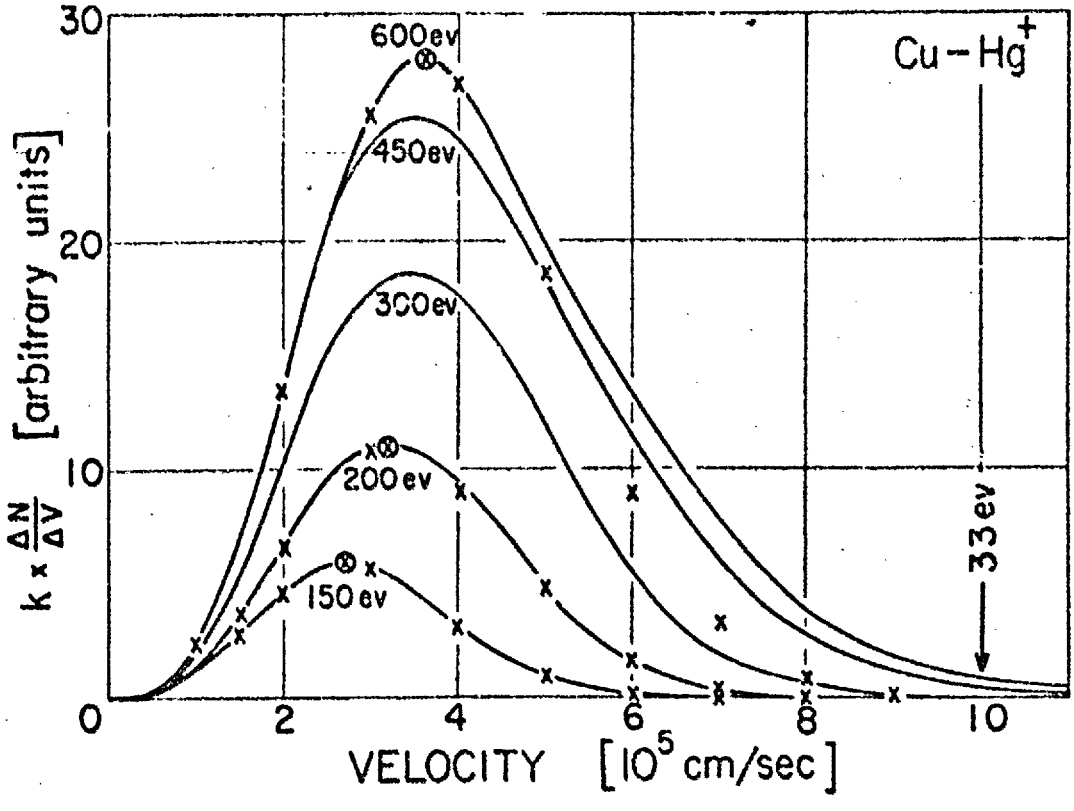

Velocity distributions of sputtered atoms ejected at 0° from a polycrystalline copper target. Points calculated from $dN/dv = av^3 \exp(-bv^2)$ are plotted as x's.

FIG. (3_2)

Comparison of velocity distributions for:

(E) Evaporated silver at 1,800°C.

(S) Sputtered silver at 3 KV. (Data from Layton and Campbell.[34])

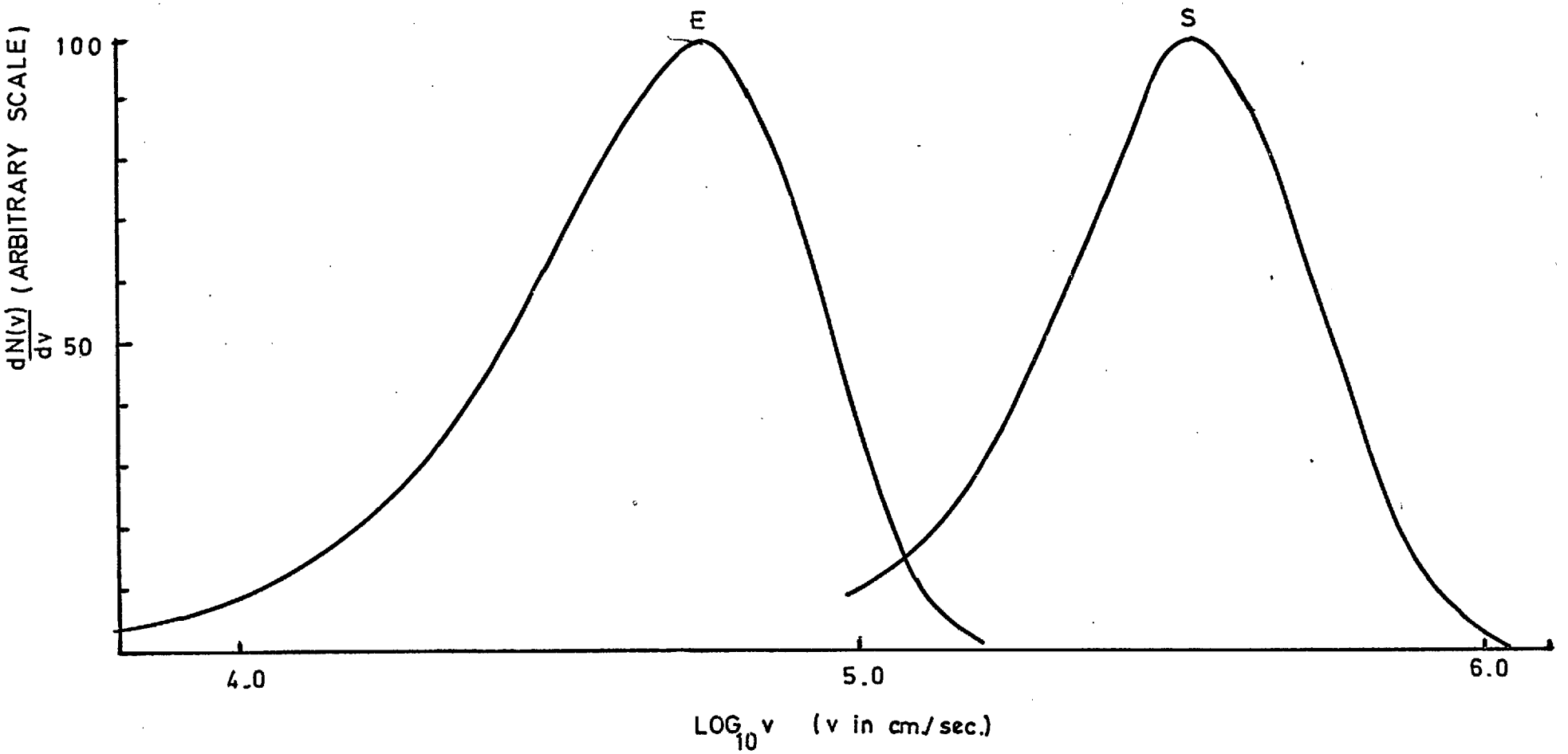

for lower velocities but depart from this at higher values to give a greater number of high energy electrons than predicted. This high energy 'tail' is probably of significance in the formation of sputtered films, as will be seen later. Of great interest is the fact that the peak values in the distributions of fig. (3.1) become less sensitive to bombardment energy as this is increased.

In the case of thermal evaporation from a melt, it can be shown that in most cases the local pressure in the region immediately above the source is sufficiently high ($\sim$0.1 mm. Hg.) for the evaporated atoms to achieve equilibrium with the surface. This will result in the evaporant having an approximately Maxwellian energy distribution and the temperature of the source. Thus using the expression:

$$\frac{dN(v)}{dv} \propto v^2 \exp(-mv^2/2kT) \qquad (3.1)$$

we can calculate the form of the distribution. Fig. (3.2) compares this distribution for silver at 1,800°C with some results due to Layton and Campbell[34] for sputtered silver. The peak for the evaporated distribution occurs at 56,000 cm./sec. (0.1 eV) while for the sputtered distribution it is 350,000 cm./sec. (4.0 eV), giving an energy approximately 40 times greater in the sputtered case.

So far we have only considered the energy of the sputtered species immediately after ejection. In a practical system, the atoms will need to traverse the space between the electrodes and may in the process collide with atoms of the sputtering gas, resulting in a loss of energy and a different energy distribution at the substrate. Layton and Campbell have

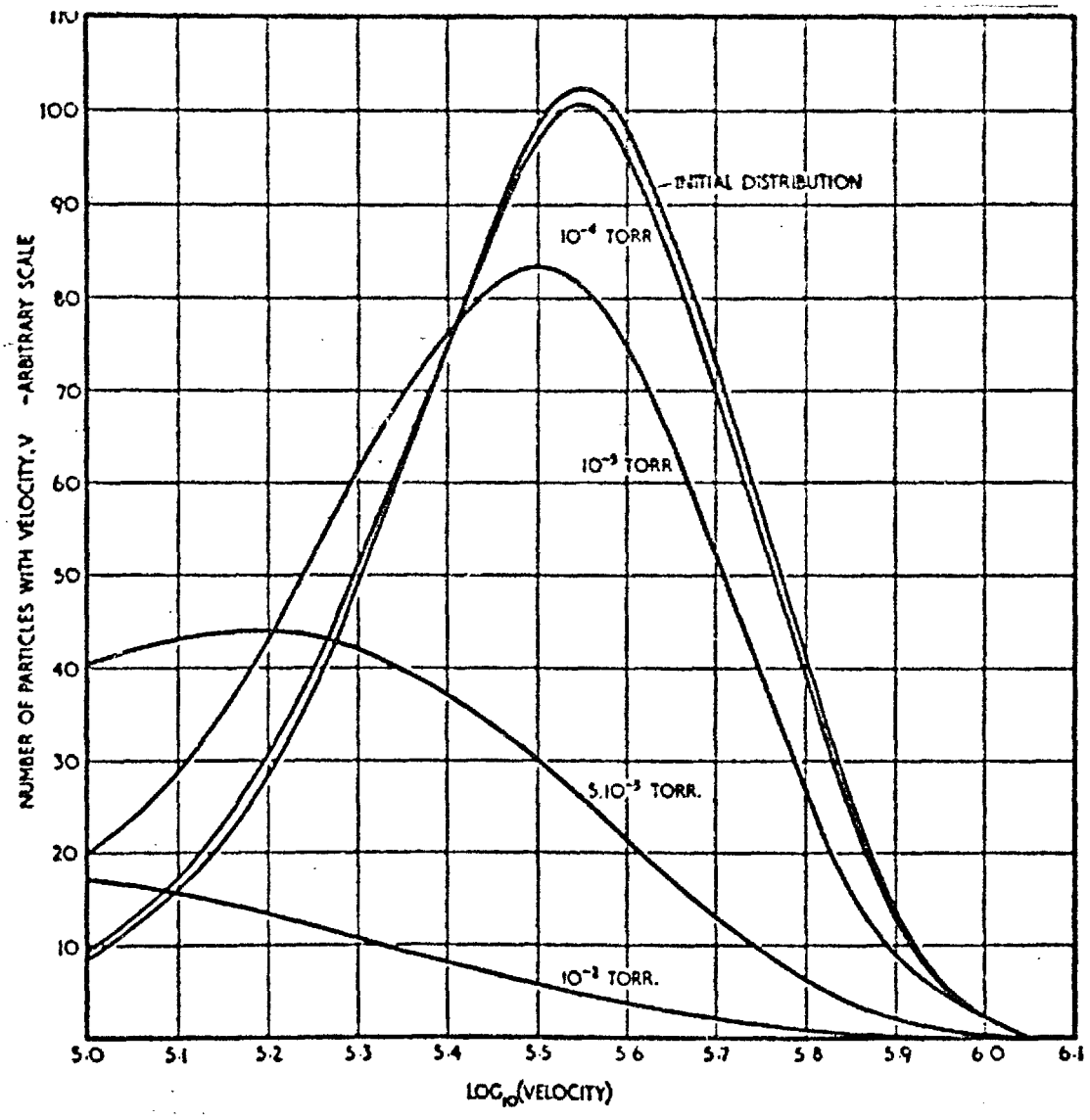

Fig.(3.3) **Calculated velocity distribution of silver atoms arriving at the substrate for various argon gas pressures (10 cm cathode-substrate spacing).**

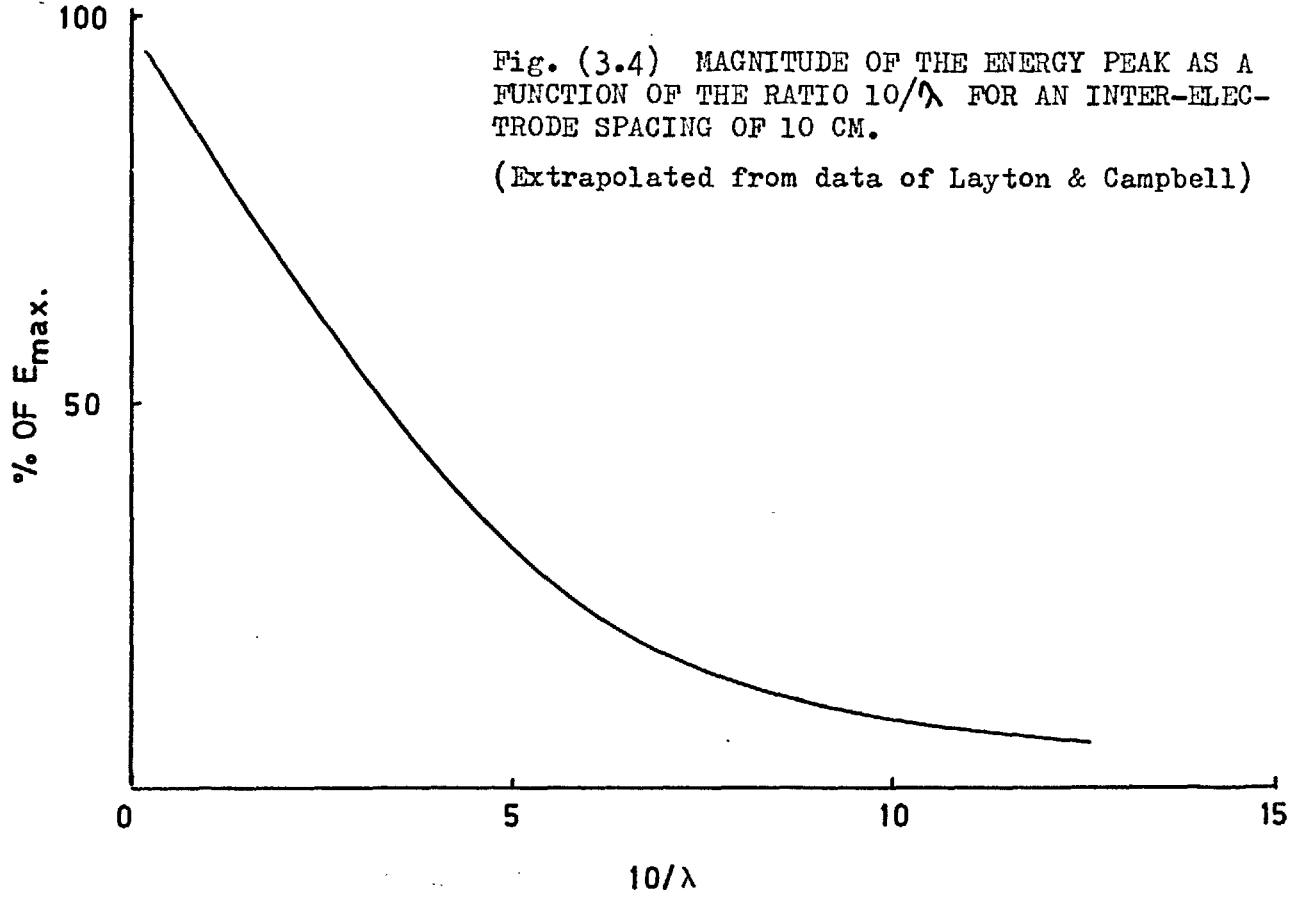

Fig. (3.4) MAGNITUDE OF THE ENERGY PEAK AS A FUNCTION OF THE RATIO 10/λ FOR AN INTER-ELECTRODE SPACING OF 10 CM.

(Extrapolated from data of Layton & Campbell)

carried out a theoretical examination of this situation and fig. (3.3) shows their results for silver, sputtered with argon at pressures between 10^{-4} and 10^{-2} Torr., the inter-electrode spacing being 10 cm. in this case. We see from these results that a radical reduction and spreading of the distribution occurs with increasing pressure. As an illustration of this, a pressure increase from 1×10^{-3} to 5×10^{-3} Torr. brings about a reduction in pesk energy of 75%. As this is the pressure range commonly utilized in R.F. sputtering, this result is of considerable interest.

(3.3) Pressure Effects in Sputtering.

The normal limits of plasma (as distinct from ion-beam) sputtering are between 5×10^{-4} and 2×10^{-2} Torr. and special systems are required for operation outside this range. The upper limit is set mainly by the pumping systems commonly used, which cannot normally handle gasses at these pressures at the required stability; furthermore, the high energy advantage would be lost at pressures of this order. The lower limit is set mainly by the fact that a stable discharge cannot be maintained below a certain pressure. Methods of overcoming this will be considered in the next section of this chapter.

The rate of deposition of material onto the substrate is dependent upon the pressure in the manner indicated in fig. (5.2), where it is seen that a reduction of 68% in the deposition rate occure as the pressure falls from 15 to 1×10^{-3} Torr. Thus in establishing the pressure of operation it is necessary to find a compromise between deposition rate and arrival energy. The scattering effect of the sputtering gas can itself be utilized to advantage in special circumstances where we may have a substrate which

is of a complex geometric shape in which certain areas cannot be coated by rectilinear transfer from the target, the scattering mechanism will ensure that some coating does occur. Some results obtained in this programme are shown in fig. (5.3) where the angular distribution of sputtered molybdenum disulphide on the surface of a 1" diameter cylindrical substrate is shown for various pressures.

The results of fig. (3.3) were obtained for an inter-electrode spacing of 10 cm. Assuming the mean free path of the sputtered atoms in the sputtering gas to be given by:

$$\lambda = 1/\sqrt{2}\,\pi d^2 N \qquad (3.2)$$

where λ is the mean free path, d the mean diameter of the two colliding atoms and N the number of gas atoms per unit volume; the values for λ corresponding to the pressures used in fig. (3.3) are shown in table (3.1).

p (Torr.)	1×10^{-4}	1×10^{-3}	5×10^{-3}	1×10^{-2}
λ (cm.)	75	7.5	1.5	0.8

Table (3.1)

Considering fig. (3.3) in the light of table (3.1), we can speculate that if the inter-electrode spacing is less than the mean free path for the particular pressure chosen, the reduction in the arrival energy is not great. When the spacing is 7λ, the energy peak is reduced by 75%.

From the above data we see that to obtain the maximum possible arrival energy we require the minimum possible electrode spacing. In practice we cannot reduce this below a value approximately twice the length of the

Crooke's dark space*, i.e. about 2-3 cm. for a pressure of 5×10^{-3} Torr., which is about 2λ. Since the width of the dark space is, like the mean free path, inversely proportional to pressure (see for example Loeb[35]) we cannot improve this situation any further by reducing pressure. Fig. (3.4) shows the peak energy (taken from fig. (3.3)) plotted against the ratio of the inter-electrode spacing to the mean free path. From this we can see that for our spacing of 2λ, the reduction in the energy peak will be approximately 30% from the theoretical maximum.

(3.4) The Role of Applied Magnetic Field in Sputtering.

We have mentioned that there are means by which sputtering systems can be made to operate at pressures below those discussed in the preceeding section. One method of doing this involves applying a magnetic field to the plasma region; there are two basic mechanisms by which the field can enhance the sputtering process:

(1) A field applied parallel to the sputtering axis can have a containment function, in that electrons which are ejected from the plasma region and would normally be lost are returned to it by the action of the field.

(2) A field perpendicular to the sputtering axis increases the electronic collision probability due to the curved path that the electrons must now assume. Since the number of collisions is increased, discharges can be maintained at lower pressures.

---

*This represents the minimum spacing consistent with a stable discharge under R.F. conditions.

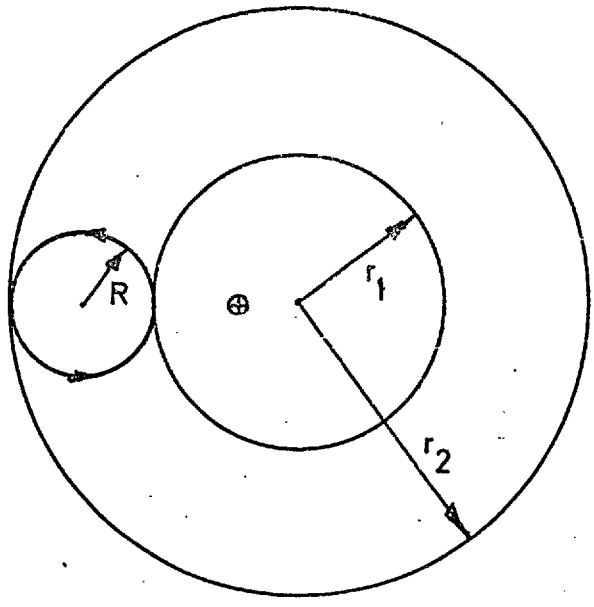

Fig. (3.5) An electron is ejected from the plasma region (radius r_1) and is returned by the magnetic field along a circular path (radius R), just avoiding the containing wall.

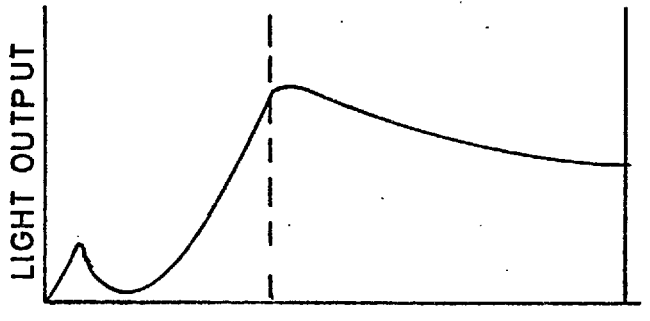

Fig, (3.6a)
Light output in a sputtering discharge.

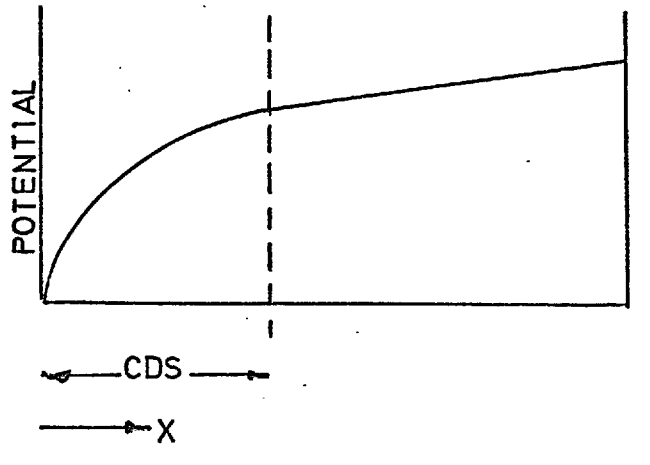

Fig. (3.6b)
Potential distribution across a sputtering discharge.

Fig. (3.5) demonstrates the mechanism (1) where an electron has been ejected from the plasma region (inner circle) and must describe a circle whose radius is sufficiently small to avoid impact with the containing wall. The required value for this radius is just:

$$R = (r_2 - r_1)/2 \qquad (3.3)$$

and hence we can write, from the Lorentz equation:

$$B = (2mV/e)^{1/2}/R \qquad (3.4)$$

where m and e are the electronic mass and charge, V the sputtering voltage and B is the magnetic flux density. For the system used in this programme, R was 3 cm. and V approximately 3KV., which requires a flux density of 0.0061 Tesla (61 Gauss); the value used in practice was 0.018 Tesla which was more than adequate for containment purposes.

Before proceeding to discuss the application of transverse magnetic field to sputtering systems, it is advisable to remind ourselves of the basic principles of operation of the D.C. glow discharge. Refering to fig. (3.6a) we see the type of discharge normally encountered in sputtering, presented in terms of light output along the axis between cathode and anode. We see that immediately adjacent to the cathode is a dark region (the Aston dark space) followed by a very shallow region of luminosity (the cathode glow) we now have another dark region (the Crooke's dark space) whose width, we have already observed, is inversely proportional to pressure. The Crooke's dark space terminates very abruptly at the negative glow and this highly luminous region extends (in the case of

sputtering configurations) right across to the anode. Fig. (3.6b) shows the axial potential distribution between the electrodes and we can simplify this for the present purpose by assuming that virtually all the applied potential is dropped across the Crooke's dark space. We are now in a position to explore the operative mechanisms of the discharge.

Let us assume that a positive ion originates at some point in the Crooke's dark space (CDS). This ion will be accelerated by the high field we have observed in the CDS and impinge upon the cathode. As well as causing sputter-ejection of cathode material, there is a high probability that a secondary electron will be emitted*; this will have a low initial energy but will be rapidly accelerated by the applied field, away from the cathode, until it reaches an energy at which it can cause excitation of neutral gas atoms with which it collides. This excitation explains the cathode glow and the Aston dark space behind it. The cathode glow terminates once the secondary electrons have acquired too much energy to take any further part in excitation reactions; from this stage on; ionization commences and the extra electrons generated produce further ionization. Thus we have an avalanche process as we proceed across the dark space. We now ask the question: What mechanism limits the avalanche process? For each ionization that occurs, the electron produced is rapidly removed due to its high mobility; while the much less mobile ions remain in the vicinity of the cathode for a far greater time. This means that a net positive space-charge will exist close to the cathode and when sufficient ions have been created to neutralize the charge on the cathode, there will be no significant fall in potential beyond this region, which has almost the potential of the anode. The consequence of this is that

---

*The probability of this occuring, per incident ion is denoted by γ, the secondary electron coefficient.

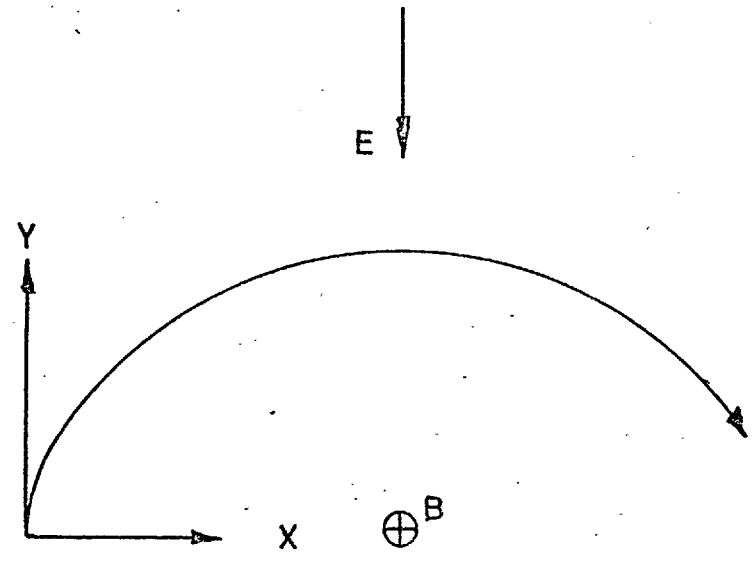

Fig. (3.7) Coordinate system of equations (3.6a & b).

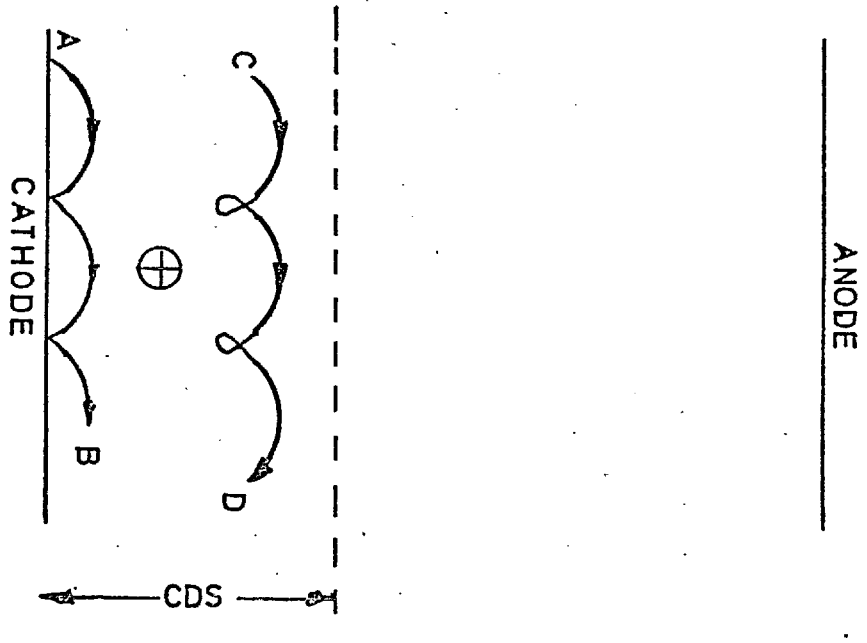

Fig. (3.8) Paths of electrons in the CDS for transverse magnetic field.

the avalanche is stopped and electrons injected into the field-free region can rapidly loose energy, initially by further ionization and finally by exciting neutral atoms; which results in the negative glow. The ultimate fate of these low energy electrons is recombination, which again contributes to the negative glow. A sizeable proportion of the injected electrons mentioned above can have energies which are too great to favour ionizing collisions and these may travel considerable distances into the negative glow region, making only elastic collisions on the way; these result in the well known electron bombardment of sputtering anodes and their attendant heating effect.

We have seen that the majority of the ions in the glow discharge are produced in the latter half of the CDS and we shall now determine how this process can be assisted in order to maintain the discharge at lower pressures; since obviously, if the production of ions is inadequate, the discharge will be extinguished. Remembering that the CDS is a region of high electric field, a magnetic field applied perpendicular to it will cause the electrons present to describe cycloidal* paths according to the equations:

$$y = \frac{eV}{dm\omega^2}(1 - \cos\omega t) \qquad (3.6a)$$

$$x = \frac{Vt}{B}\left(1 - \frac{\sin\omega t}{t}\right) \qquad (3.6b)$$

where V/d is the field in the CDS (assumed uniform), e/m is the electronic charge to mass ratio and $\omega = eB/m$; x and y are coordinates whose sense is indicated in fig. (3.7) and t is the time.

---

*This is in fact a simplification as the path is in general trochoidal, the cycloid being the special case obtained by assuming that t = 0 when y = 0.

The situation we desire is that of fig. (3.8), where electrons produced at the cathode describe paths AB, while the electrons resulting from ionization of gas atoms make paths (generally trochoidal) such as CD. The height of the cycloid is easily found from eqs. (3.6a and b) to be:

$$H = 2Vm / deB^2 \qquad (3.7a)$$

while the range is given by:

$$r = 2\pi Vm / deB^2 \qquad (3.7b)$$

We must choose a value for B which will cause H to be small enough to allow a large proportion of the electrons produced in the CDS to execute complete cycloidal paths. At the same time, we must not make this value too small, otherwise the electrons will not obtain sufficient energy to ionize effectively. The maximum energy in a cycloidal path is:

$$U_m = m(\dot{x}^2 + \dot{y}^2) / 2$$

and using equations (3.6a and b):

$$U_m = 2mV^2 / d^2B^2 \qquad (4.8)$$

We can now establish the limiting criteria upon the magnetic flux density. Let U_o be the optimum electron energy for ionization of the gas; we therefore set the upper limit on B as:

$$B < \frac{V}{d}(2m/U_o)^{1/2} \qquad (4.9)$$

Fig. (3.9) TYPICAL BIASABLE COUNTER-ELECTRODE

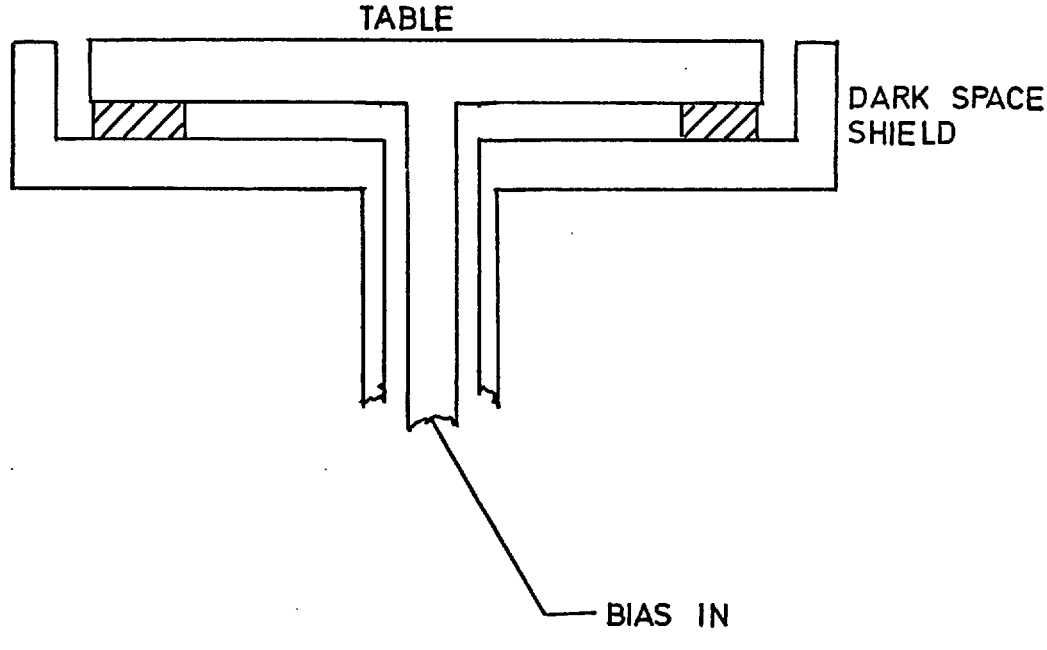

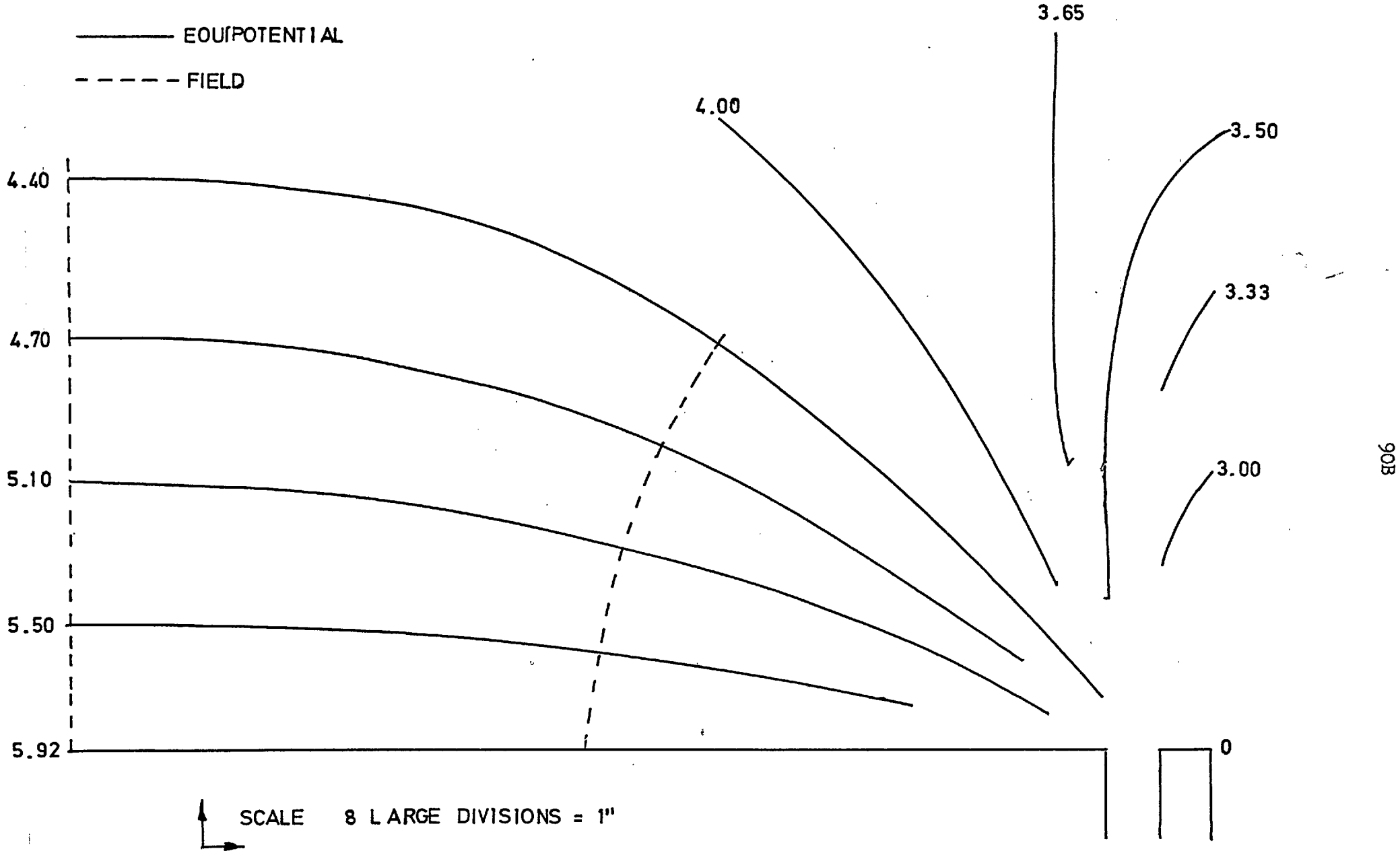

Fig. (3.10) THE ELECTROSTATIC FIELD IN THE NEIGHBOURHOOD OF THE BIASED COUNTER-ELECTRODE

while the lower limit might be set as $H < d/2$, thus:

$$\frac{V}{d}(2m/U_o)^{1/2} > B > \frac{2}{d}(Vm/e)^{1/2} \qquad (3.10)$$

The arguments developed in this section have been highly simplistic, having made assumptions as to uniformity of electric field, simple cycloidal paths etc. Thus in a real system, the establishment of a criterion such as eq. (3.10) would be an extremely complex process; however we can now see the qualitative basis of the problem and eq. (3.10) gives us a logical starting point from which to commence an empirical investigation. For the system used in this programme, eq. (3.10) sets the value of B between 0.018 and 0.071 Tesla.

(3.5) Examination of the Mechanisms Involved in Bias Sputtering.

We saw in 1.2 that application of a negative potential to the substrate with respect to the anode, during sputter deposition could have beneficial effects upon the film produced. In this section we shall explore the technique by which this is accomplished.

Fig. (3.9) shows a standard electrode configuration employed for the application of bias potential. This configuration is in fact almost identical to that used for the target (cathode), consisting of a central circular 'table' surrounded by a cylindrical guard ring, with a constant spacing between the two. In the system used for this work, the table was 5" in diameter while the guard ring had an internal diameter of 5 1/2 " and an external diameter of 6". Fig. (3.10) demonstrates the field dist-

ribution in the space above this electrode, which is assumed to be free of any field due to the potential applied at the target (that is, the negative glow region). Ions extracted from the negative glow region are accelerated normally to the equipotentials until they impinge upon the central table. If we now assume that the length of the field free region is 1" then the only ions striking the table will be those extracted from this region (those beyond will be captured by the cathode). From fig. (3.10), assuming an applied bias of -59.2 volt, the maximum energy of ions arriving at the centre of the table will be approximately 12eV, while at a point 1-1/4" from the centre, this energy will have increased to approximately 15eV. Outside this region, the energy increases rapidly, approaching a maximum of 59.2eV at the edge. It is also worth noting that ions drawn to the central region of the table are taken from the centre of the negative glow whereas those arriving at the outer areas of the table must have been drawn from the fringes of the negative glow and consequently will be fewer in number. Thus many low energy ions impinge on the table center, while a small number of high energy ions arrive at the edge.

We have attempted here to relate the arrival energy of bias species to electrode geometry; the results of fig. (3.10) were obtained by field plotting techniques and are considered reliable. It is hoped that these will now enable more accurate assessments of the effect of bias to be made.

In concluding this section we should note that if the substrate has a complex geometry, it will be necessary to re-solve the field distribution problem and that, in particular, if the substrate has sharp edges, local field distortions may result in higher impingement energies at such points.

(3.6) Structural Properties of Sputtered Films.

In (3.2) and (3.3), much emphasis was placed on the arrival energy of sputtered species and its maximization; the reasons for this will now be made apparent.

We have demonstrated that the energy distribution of sputtered species has a peak value at, typically, 10eV and that a very significant number of species (in the high energy 'tail') have energies of the order 100eV. When such particles impinge upon a substrate, four basic and distinct mechanisms can operate to enhance the adhesion:

(1) The normal component of impingement energy can readily be converted after impact into a transverse component whose energy is of the same order of magnitude[36]. Such an energetic particle can then only be captured by a very strong surface bond (potential well) and thus good adhesion is assured.

(2) It is quite possible for particles whose energy is $\sim$ 100eV to become implanted into the surface, which allows the interface to become more diffuse, again enhancing adhesion.

(3) Arriving particles can operate a 'knock-on' mechanism in which atoms adhering to the surface are forced to imbed into it.

(4) Any weakly adhering particles will be back-sputtered by momentum transfer from arriving species.

Once a viable coating has appeared on the substrate, these same four mechanisms continue to operate, ensuring high cohesive strength of the film.

Layton and Campbell[34] have explored the structural properties of sputtered films of silver, deposited onto single crystal rock salt and in particular they examined the variation of structure with thickness. Orientation in these films was found to vary strongly with thickness; at a nominal value of 7 Angstrom, films were seen to be randomly oriented polycrystalline but symmetry began to appear at 25 Angstrom and full orientation was reached by 220 Angstrom. Layton and Campbell speculate that, after an initial period during which the sputtered atoms nucleate on the substrate with random orientation, there is an enhanced growth rate for those crystallites intimately associated with the substrate, i.e. those growing epitaxially. For films grown upon polycrystalline substrates, such an effect could still be expected to occur, particularly for values of film thickness less than the grain size of the substrate, although in this case epitaxy would be microscopic rather than macroscopic.

It appears therefore that if we examine the structural profile of a sputtered film, we can expect an increase in crystallite size with thickness. This would indicate that the strength of sputtered films increases with decreasing thickness and this is a well documented fact[30]. In terms of friction and wear phenomena, this could lead to a shear strength which depends inversely upon thickness; and a wear coefficient which decreases with thickness. Both of these phenomena have been observed in this programme.

Sputtered films are known to contain high residual stress, a significant component of which must be due to the differential expansion rate between substrate and film. We can speculate that thin films are sufficiently strong to withstand such stresses but thicker films, being weaker, can be broken up by them; this sets a gross upper limit on the practical thickness of a sputtered film and the effect is frequently encountered.

(3.7) Stoichiometry of Sputtered Films.

Implicit in our discussion to this point has been the assumption that sputtered species were atomic in nature, emanating from a target composed of a single element. In many cases, targets of chemical compounds are employed and the question as to whether the sputtered film has the same composition as the target must be considered.

Much of the research into the fundamental sputtering process has involved elemental targets and progress has been extensive; while compounds are frequently sputtered successfully, little has been published regarding the nature of the process and in particular regarding the nature of the sputtered species. While it appears possible that single molecules can be removed intact, these are inevitably accompanied by dissociated fragments and the removal of certain fragments may well be preferential, making it unlikely that the resulting film will be stoichiometric.

As an illustration we can consider the work of Croset, Rigo and Amsel[37] who have employed nuclear microanalysis techniques to study the composition of sputtered silicon nitride films. When sputtered in pure

Fig.(3.11)

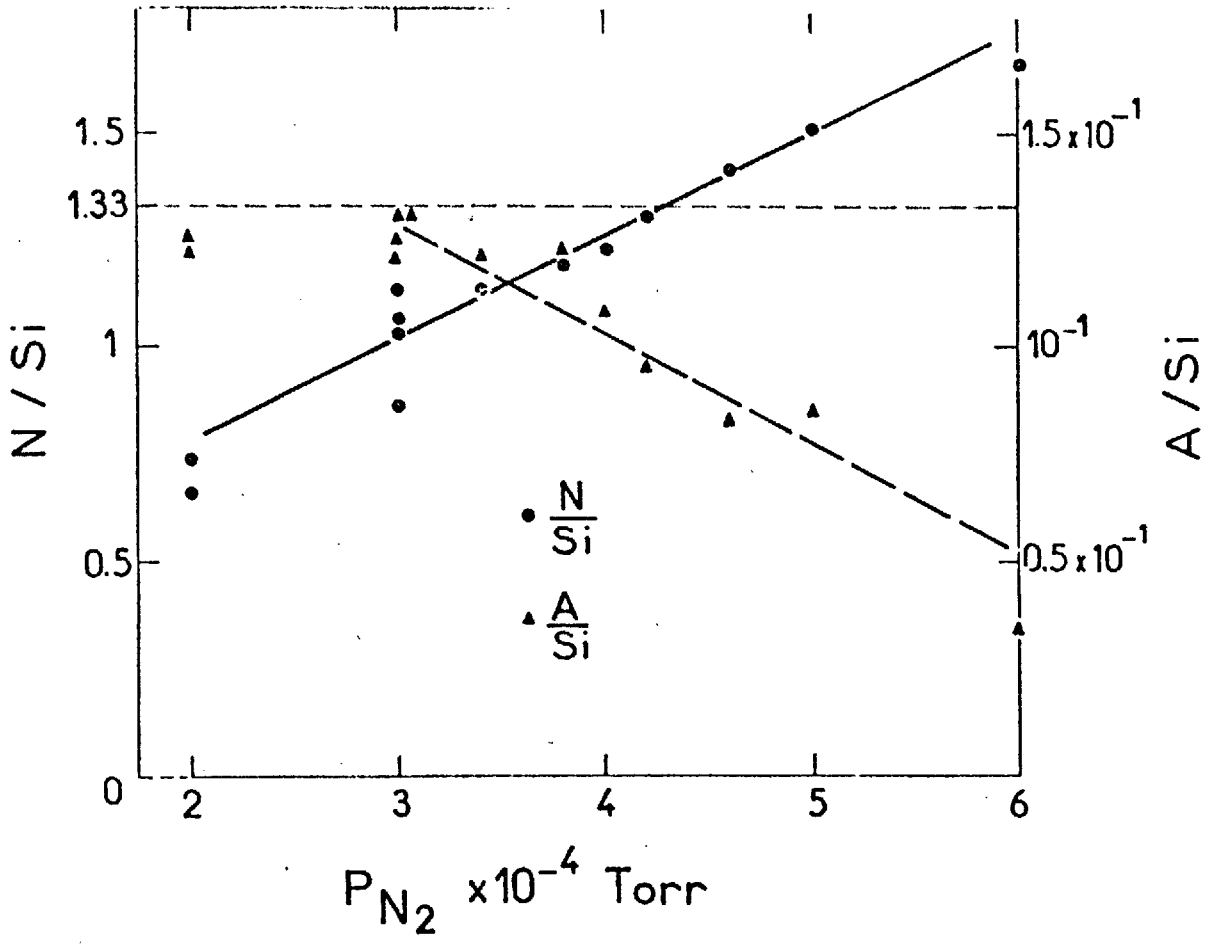

N/Si (●) and Ar/Si (▲) ratios (in atoms) for sputt red silicon nitride films as a function of the partial nitrogen pressure P_{N_2} at an argon pressure $P_{Ar} = 10^{-2}$ Torr.

argon at 10^{-2} Torr. the ratio of N:Si could be extrapolated as approximately 0.5, very different from the stoichiometric value of 1.33 (Si_3N_4). These workers found that the addition of nitrogen to the sputtering gas at a partial pressure of about 4.2×10^{-4} Torr. produced the required stoichiometry. Fig. (3.11) shows some of the results; including information relating to the argon content of such films, which we shall not discuss here.

Spalvins[32] has analysed the composition of MoS_2, sputtered in pure argon by a number of techniques and has determined that the films are approximately stoichiometric. This has been confirmed in the present work.

CHAPTER 4 --- APPARATUS AND EXPERIMENTAL TECHNIQUES

(4.1) In the first part of this chapter we shall discuss the construction of the apparatus which was built specifically for this programme, as well as giving some account of existing equipment which was also utilized. In the second part we shall examine the experimental techniques which have been employed in the operation of this apparatus and in the evaluation of the films.

(4.2.1) The Design of the Sputtering System.

We have already mentioned* that a highly versatile sputtering system was required in order to carry out the objectives of the programme and we shall consider here the necessary specification.

Since the programme required the investigation of the feasibility of various sputtered materials, it was reasonable to assume that a wide variety of different substrates would have to be used, some of which could be engineering components of quite large size. Consequently it was decided that the sputtering system should employ a target size consistent with most forseeable needs; a target diameter of 5" was chosen and this size gave the additional advantage of being interchangable with existing equipment. Having chosen this target size, the power requirements were now specified automatically as being between 100 and 1,000 Watt. Both D.C. and R.F. supplies were available, the D.C. supply was a Wareham model C085, having a continuously variable output voltage from 0 to 10 KV. and a maximum current output of 500 mA. The R.F. power was provided by

---

*This system is depicted in fig. (1.3) and plate (1.1).

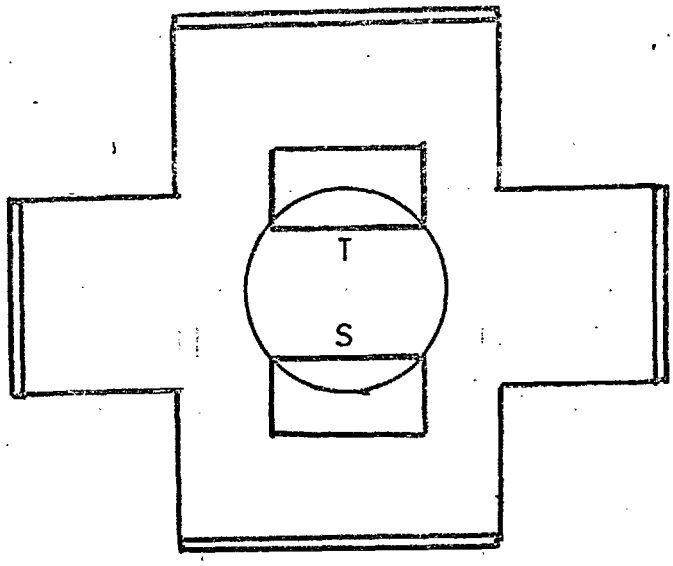

Fig. (4.1a)
Simple diode

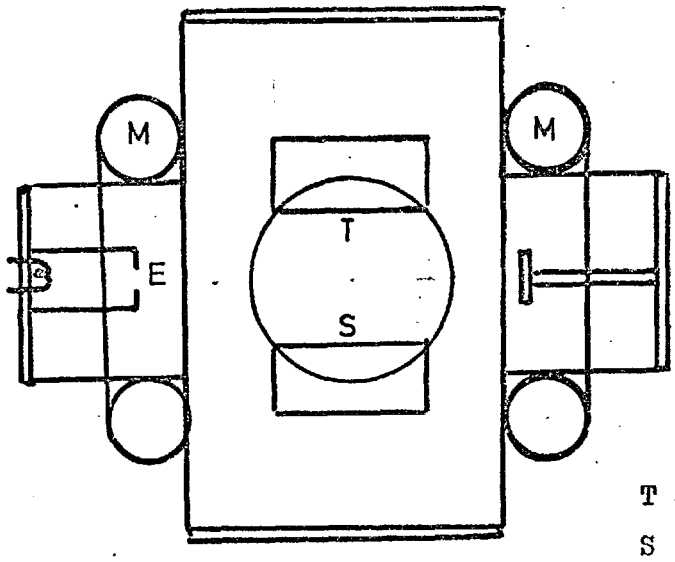

Fig. (4.1b)
Triode-magnetron

T = Target

S = Substrate table

E = Electron gun

M = Magnetic coil

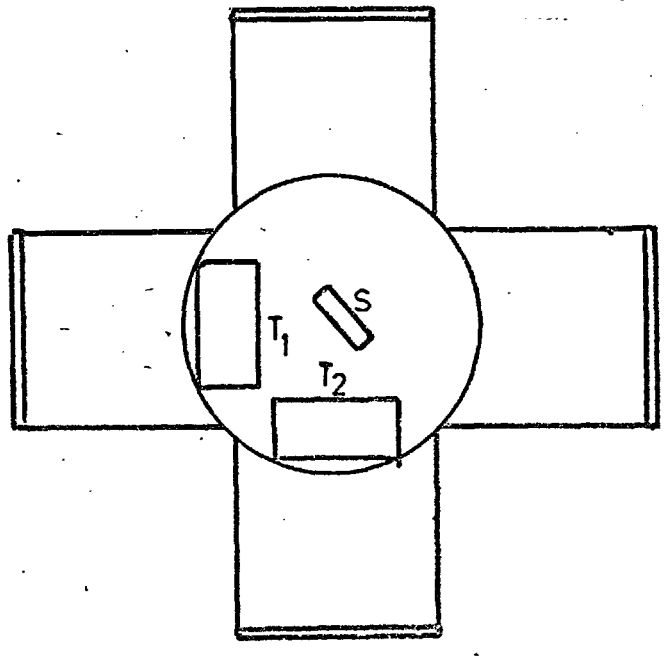

Fig. (4.1c)
Dual target system for sequential and simultaneous deposition.

an M.R.C. model S3007 generator, with voltage controlled power output continuously variable between 0 and 1.25 KW.; this supply employs a protection system which ensures that the level of reflected power does not exceed a predetermined limit.

To accomodate all possible future requirements, it was decided that the system should be capable of easy modification to operation in the triode mode and that simultaneous and sequential sputtering from two targets should also be possible. Consequently, the vessel used to house the system was a Q.V.F. 6/9 Pyrex chamber, which consisted of a 9" internal diameter pipe section with two pairs of 6" side-arms projecting orthogonally. This geometry enables an electron gun and target to be fitted for triode operation and also allows orthogonal Helmholtz coils to be mounted. Where two targets must be employed, these can be mounted in two side-arms so that their planes are perpendicular. Fig. (4.1a,b,c) shows the use of the system in three of the possible configurations.

In order to contain the plasma, the target was to be surrounded with a dark space shield (a type of guard-ring) which would be at earth potential. The substrate electrode chosen was of the type discussed in chapter 3 and was similar in appearance to the target; this allowed for sputter etching and bias operation. Both target and substrate electrode were oil-cooled in order to elliminate corrosion problems and to ensure insulation between certain components and for this purpose a heat exchanger and pump were required.

A substrate heater was required and it was decided that this should be designed in such a way as to avoid distortion of the field between

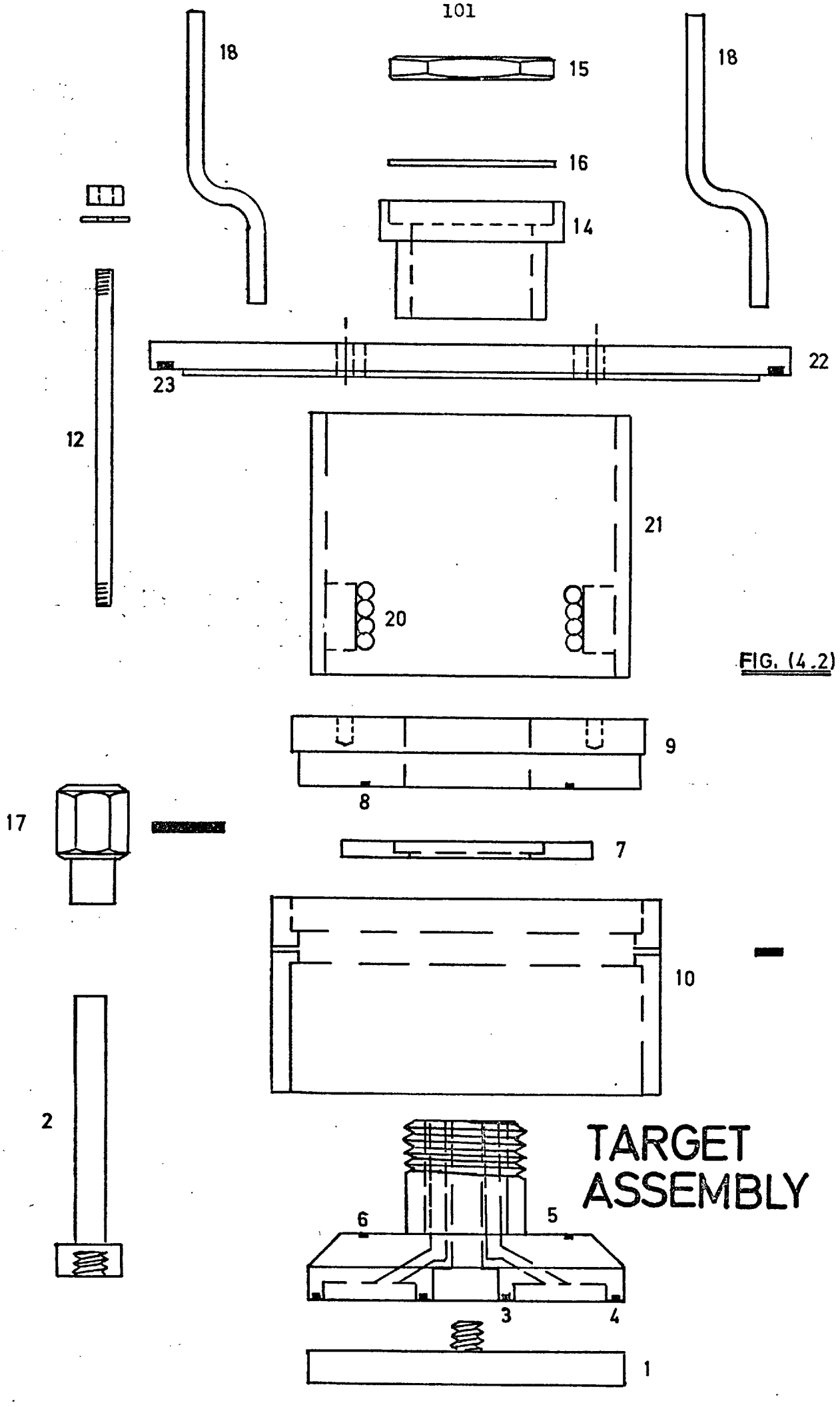

FIG. (4.2)

PARTS LIST (1.1) Target Assembly

1. Target
2. Target draw bar
3. Seal
4. Seal
5. Target holder
6. Seal
7. Insulator ring
8. Seal
9. Target holder backing plate
10. Dark space shield
11.
12. Tie rod (six)
13.
14. Support collar
15. Nut
16. Washer
17.
18. Tube (two)
19.
20. Cooling coil
21. Extension collar
22. Top plate
23. Seal

target and substrate, this was achieved by introducing the necessary leads from beneath the substrate electrode.

Other areas in which special design considerations were required were in the provision of a matching network for R.F. operation, the fitting of a suitable shutter for use in pre-sputter (target cleaning) and sputter etch operation and in the correct choice of gas admittance and vacuum gauging equipment.

The vacuum system used throughout consisted of an Edwards ES 200 rotary pump, backing an F 403 diffusion pump (4"). A cold trap was also fitted and this was filled with liquid nitrogen.

(4.2.2) Details of the Target Assembly Design.

The assembly is detailed in fig. (4.2). The target (1) consists of a Dural backing plate, with a threaded boss, to which the target material is bonded with conductive epoxy. The target is attached to the target holder (5) by screwing the boss into the end of the target draw-bar (2) and this can be tightened from above via nut (17). Coolant circulates behind the target and this is sealed in by o-rings (3,4), the coolant enters and leaves the target holder through two tubes (18) which are cemented in place with epoxy. The target holder is insulated from the target holder backing plate (9) using a PTFE. ring (7) and a support collar (14), also of PTFE.; these components are held together by a nut and washer (15,16), which apply compression to seals (6,8). The dark space shield (10) is fitted over the target holder backing plate and secured with two screws. The target holder backing plate is mounted

FIG. (4.3)

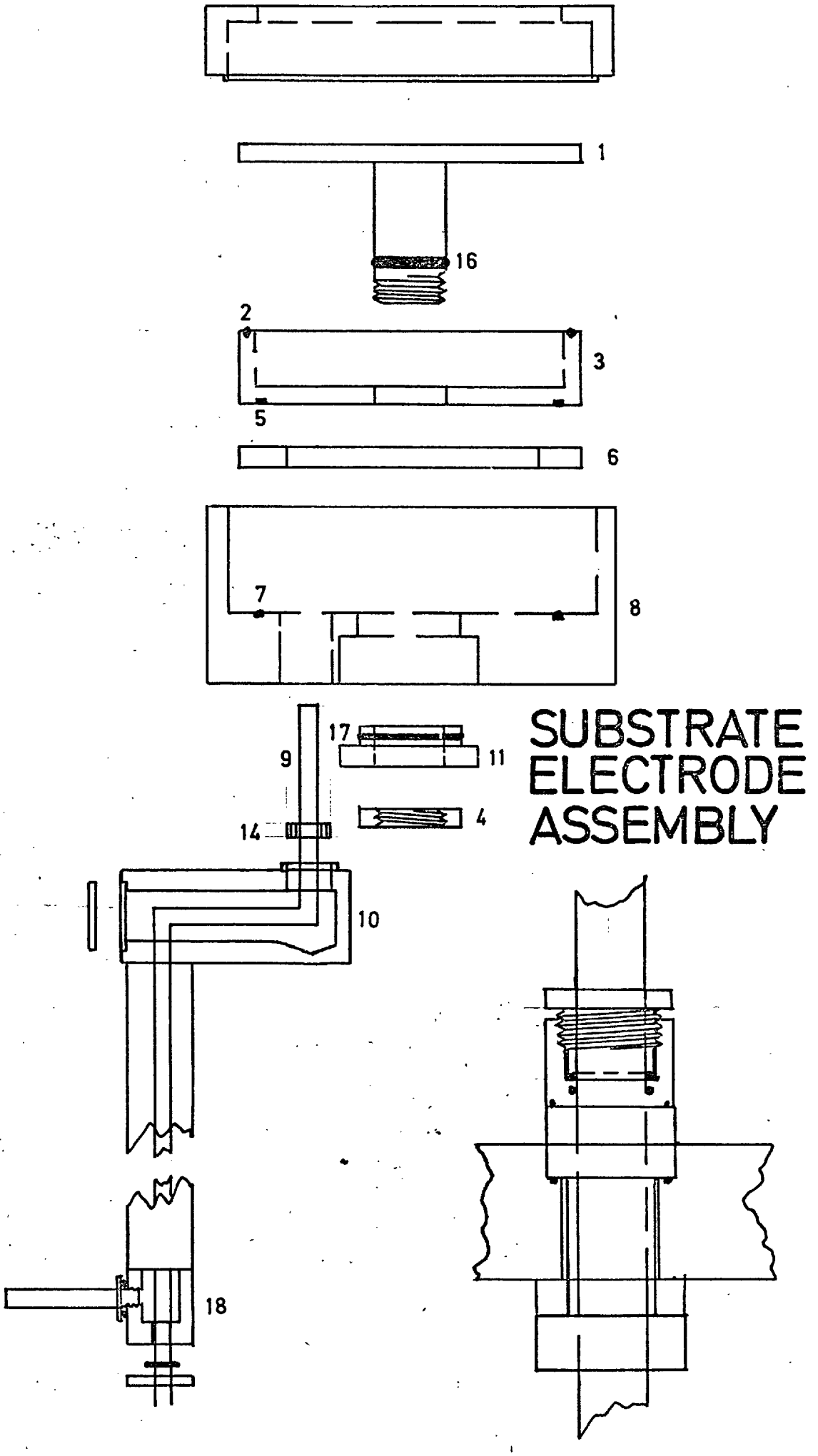

PARTS LIST: (1.2) Substrate Electrode Assembly

1. Substrate table
2. Seal
3. Table cup
4. Nut
5. Seal
6. Insulator ring
7. Seal
8. Substrate electrode housing
9. Tube
10. Positioning block
11. Insulator collar
12.
13.
14. Spacer (four)
15.
16. Seal
17. Seal
18. Insulator plug

the top plate (22) via an extension collar (21) which positions the target correctly with respect to the vacuum chamber. Indium seals are used on the upper and lower ends of the extension collar and these are compressed by a circle of six tie-rods (12). The extension collar is fitted with cooling coils (20) in order to protect the indium seals from heat, these coils are in series with the main target cooling flow.

The whole target assembly is mounted on top of the vacuum vessel and sealed by o-ring (23).

(4.2.3) The Substrate Electrode Assembly.

This was designed to incorporate the following features and is seen schematically in fig. (4.3):

(1) Biasable centre table, surrounded by a dark space shield.

(2) Oil cooling of centre table and internal insulation via the oil.

(3) Provision for raising and lowering the whole assembly with ease, thereby enabling the target to substrate distance to be continuously variable between 0 and 12 cm.

(4) Access to the table top by way of a hole passing through its centre, this enables the heater leads etc. to be brought through without disturbing the symmetry of the electric field above the table.

Fig. (4.3), in conjunction with parts list (2) shows the construction. The substrate table (1) is supported on the table cup (3) and this rests

FIG. (4.4)

COOLING SYSTEM

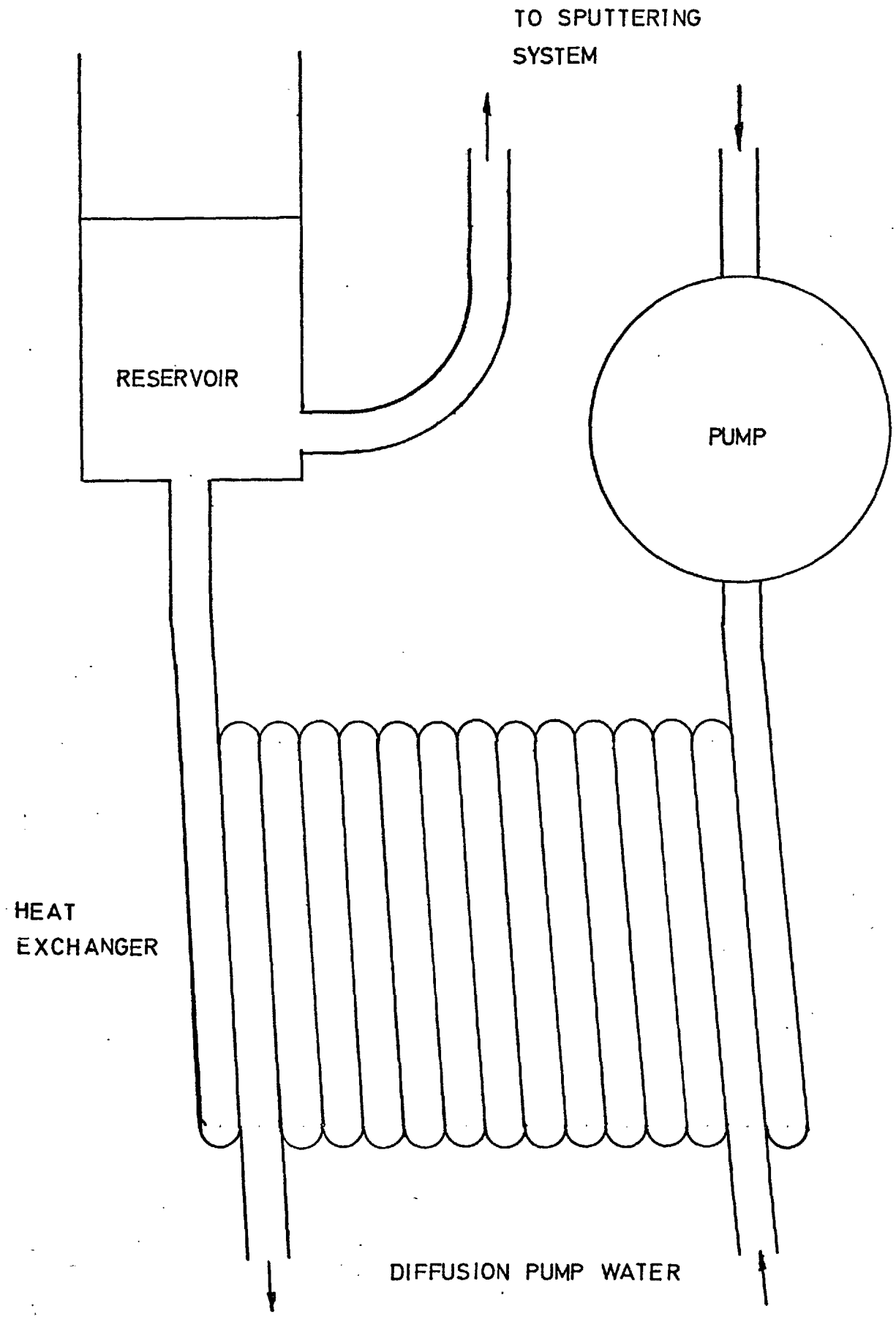

on top of a PTFE (formerly Pyrex) insulator ring (6). These components are enclosed in the substrate electrode housing (8) and the stalk of the substrate table passes through a hole in the bottom of the housing, where it is further insulated by the insulator collar (11). The table is secured in its housing by a special nut (4) and this also applies compression to the various seals (2,5,7). Two further o-rings (16,17) complete the sealing of the substrate table assembly. Coolant and electrical power enter the housing via the positioning block (10) and this is secured to the housing by two screws, which also compress an indium seal between the two. The coolant leaves the system through a copper tube (9) which also serves as a conductor for the electric power; this is kept from touching the surrounding metal by PTFE. spacers (14). The copper tube passes down through a 15/16" external diameter steel rod which is brazed at its upper end to the positioning block. This rod is drilled to an internal diameter of 3/4" so that coolant (and electrical power) can flow in and out coaxially. The rod is terminated outside the vacuum by a PTFE. insulator plug (18) and the coolant inlet and outlet tubes protrude from this. The rod passes through a vacuum gland assembly having a double o-ring seal and this allows the electrode assembly to be raised and lowered.

(4.2.4) The Cooling System.

This consists of a pump, heat exchanger and reservoir; fig. (4.4) gives a schematic picture of the system. The pump is a Jabsco AT 1/4-204 and this utilizes a rubber rotor and is consequently very quiet in operation; drive for the pump comes from an 0.25 HP. 900RPM sqirrel cage motor. The heat exchanger is formed by soldering together two lengths of 5/16" bore copper tube and then winding them into a cylinder and solder-

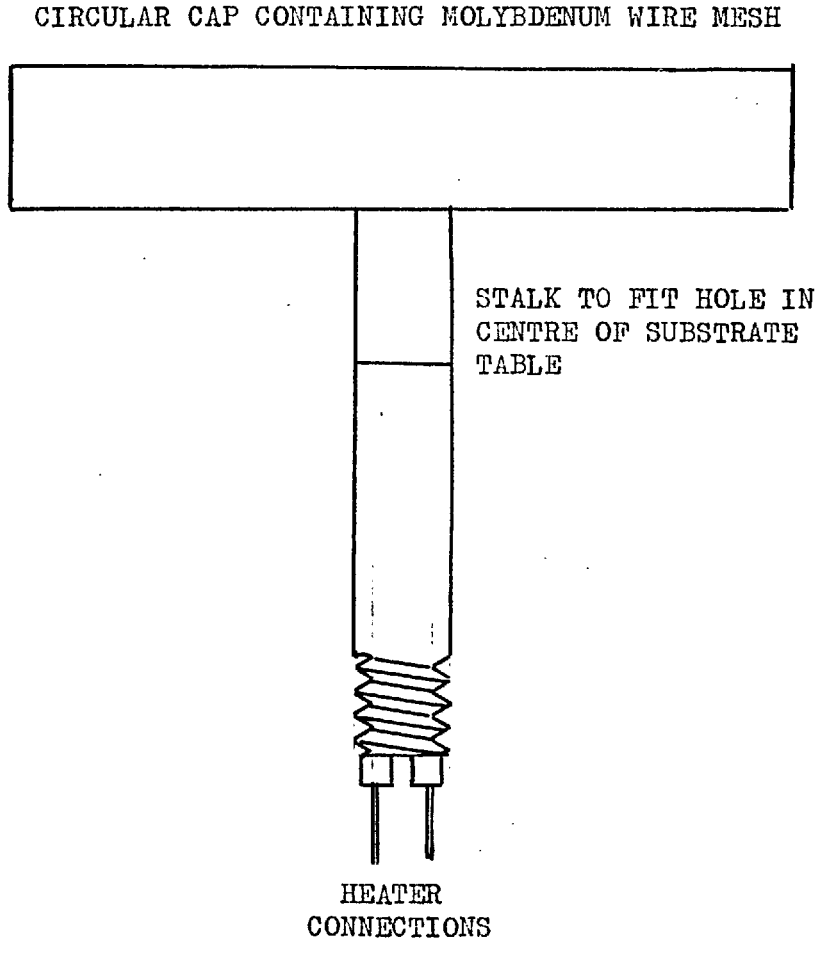

Fig. (4.5) SUBSTRATE HEATER

ing again. One of the tubes is connected in series with the water supply to the diffusion pump, the other carries the oil. The reservoir is designed to aid bleeding of the oil circuit and is also the point at which oil is poured into the system.

The cooling system is connected in series with the target, the extension collar cooling coils and the substrate electrode; the flow rate is approximately 900 cc. per minute.

(4.2.5) The Substrate Heater.

The problem in designing a heater for operation on a biasable electrode is to avoid interaction (i.e. discharge) between the heater wires, which are effectively at earth potential, and the substrate table which is at bias potential. Fig. (4.5) shows the configuration employed, with a grid of molybdenum wire placed upon the substrate table and enclosed by a protective metal cover. The arrangement is such that the spacing between the wires and the substrate table are always smaller than the dark space width so that a discharge cannot be initiated. This heater is capable of raising the substrate to at least $300^{o}C$.

(4.2.6) The Design of a Matching Network for R.F. Operation.

The requirements of matching between two R.F. systems are:

(1) The impedance of one shall be the conjugate of the other.

(2) The standing wave ratio must be unity.

These conditions are normally met in practice by arranging for the out-

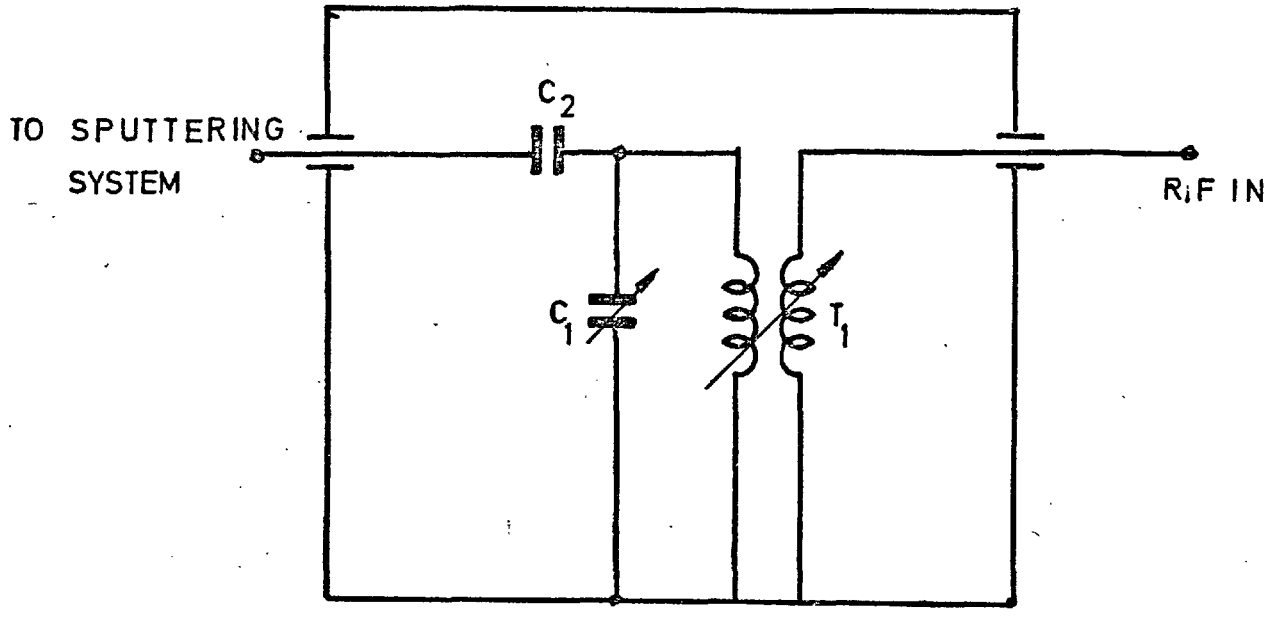

FIG.(4.6) MATCHING NETWORK

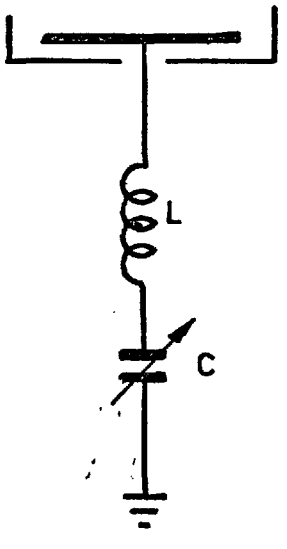

FIG.(4.7) R.F. BIAS SYSTEM

put from the generator to be purely resistive, which is achieved by connecting the generator to a resistive load and adjusting the standing wave ratio to be unity; the generator is now connected to the desired load and the reactive components of this are adjusted until the standing wave ratio is again unity. This condition coincides with the resonance condition for the load and if this is a parallel resonant circuit, we shall have voltage amplification; an ideal situation for our sputtering system.

Fig. (4.6) shows the circuit employed in the present system. The transformer T_1 couples the generator to the network and variable capacitor C_1 acts in conjunction with the secondary of T_1 to give a parallel resonant circuit; C_1 should have a voltage rating of 10 KV and a capacitance of 0 to 500 pF. A blocking capacitor (10 KV at 500 pF, fixed) is inserted in series with the target. The lower limit upon the value of the blocking capacitor is that its impedance should be small compared to that of the sputtering system, otherwise too much voltage will be lost across it. The upper limit is set by the fact that the time constant should not be so high that the target cannot follow the driving frequency, which in our system is 13.56 MHz.

(4.2.7) Design Considerations for Sputter Etch and Bias Facilities.

For conductive substrates both sputter etch and bias can effectively be carried out with an applied D.C. potential and if the bias operation is performed with R.F. target drive, the substrate table must be connected to earth through a decoupling capacitor. With insulating substrates it is necessary to feed a fraction of the R.F. power to the substrate table and fig. (4.7) shows a typical system for doing this. Reactive components in series with the substrate table result in a potential difference app-

earing between the table and earth, due to the current through the reactance. The capacitance C ensures that the offset potential generated does not leak away. For sputter etching it would be necessary to apply the full R.F. output to the substrate table and furthe matching elements would be required.

For sputter etch and pre-sputter operations it is necessary to have a shutter, in the first instance to shield the target from back-sputtered contamination and in the second to shield the substrate while contamination is removed from the target. The shutter in the present system was in the form of a rectangular blade which could be retracted into one of the side-arms of the vacuum vessel when not in use. The shutter must at all times be securely earthed.

(4.2.8) Pressure Control and Measurement.

The sputtering gas used throughout this programme has been argon, and this is admitted to the system through a vernier needle valve. The pressure at entry to the needle valve is regulated at 5 psi. Measurement of argon pressure within the chamber is made using
Pirani head in conjunction with an Edwards model 8/2 control box; this measures pressure in the range 1×10^{-4} Torr. to atmospheric. Pressures below this are measured using an ion gauge.

(4.3) The Design of a Dynamic Friction Apparatus.

A system was required which could evaluate the friction properties of the sputtered films in spherical sliding contact under various environmental conditions, including vacuum at 10^{-6} Torr. The apparatus designed

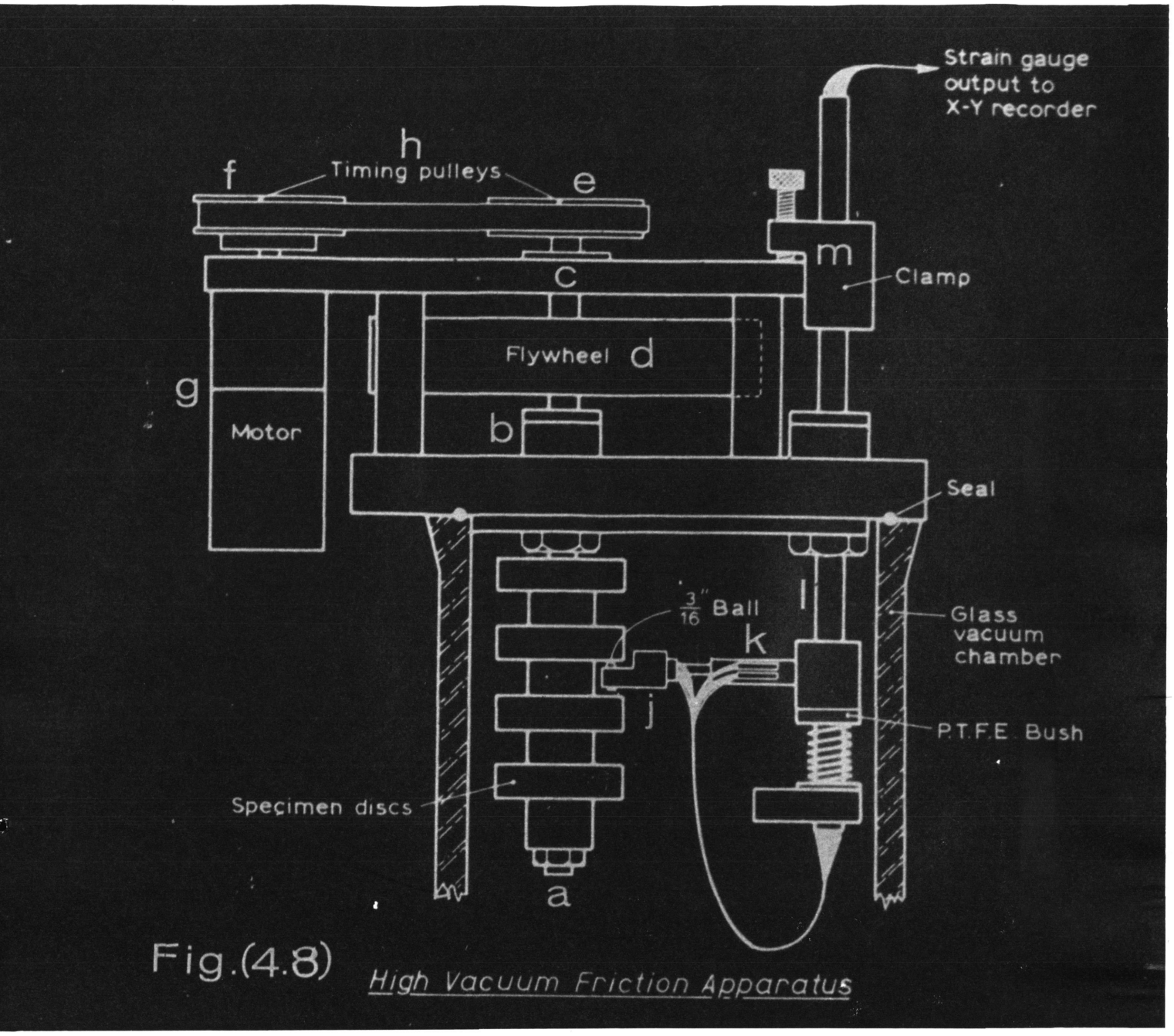

Fig.(4.8) *High Vacuum Friction Apparatus*

PLATE (4.1) DYNAMIC FRICTION APPARATUS

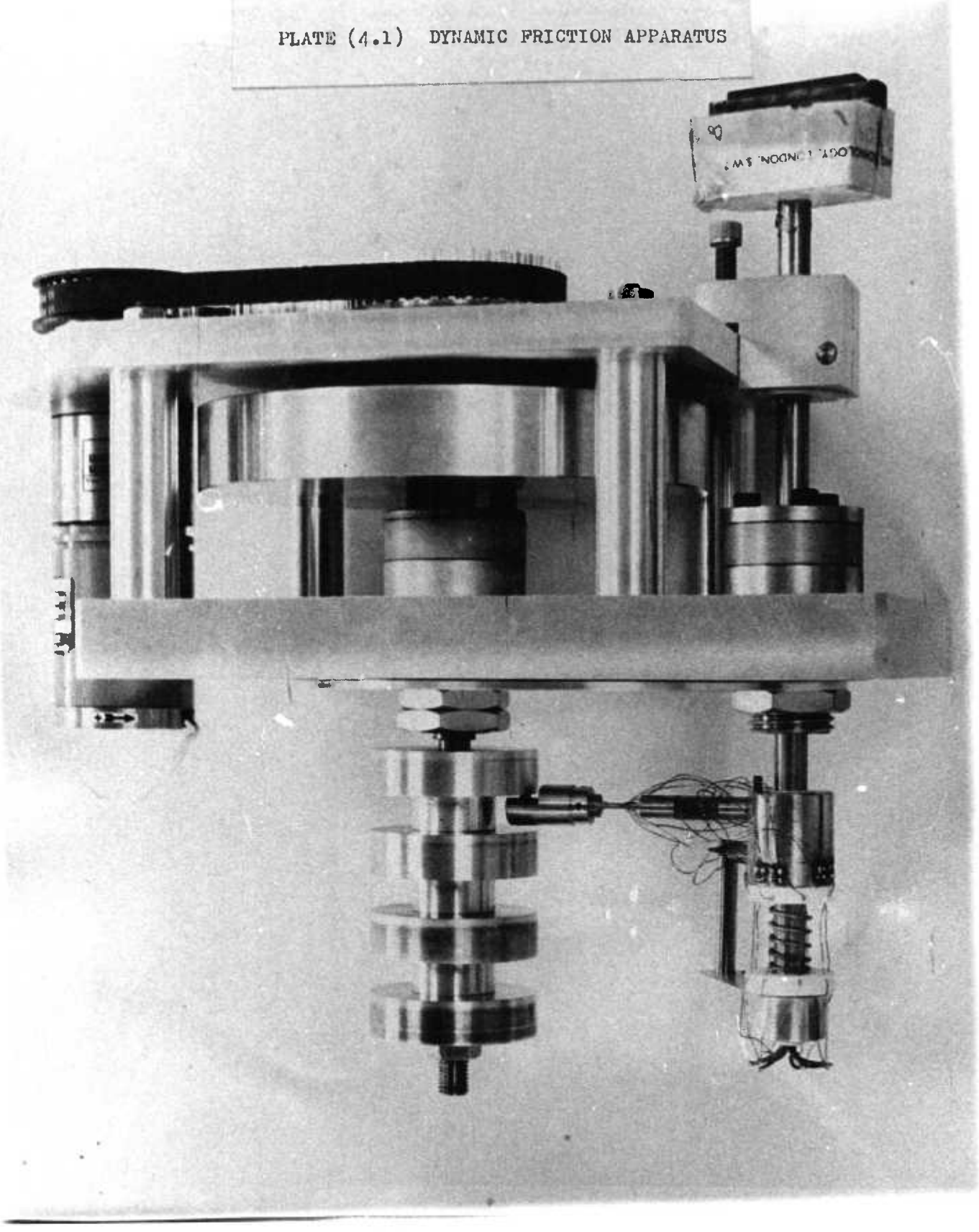

and built for this programme is seen in plate (4.1) and schematically in fig. (4.8). The substrate discs used with this apparatus were 2" in diameter and 1/2" thick; EN58 stainless steel was the material chosen, and one of the flat surfaces was highly polished prior to deposition. Once coated, the discs were mounted on a shaft A, which passes through a rotary seal B and is supported at its upper end by a bearing C. The shaft also carries a flywheel D, to assist smooth running and a timing pulley E is fitted to it between B and C. The timing pulley is connected through a timing belt to a second pulley F, which is fixed to the shaft of a D.C. motor and gearbox unit G. An idler pulley H maintains tension in the belt.

Contact with the coated surface is made through a 3/16" diameter 440C stainless steel ball, which is held in a special clamping head J; the ball may simply be replaced when necessary. The head J is mounted at the end of an arm K, which is fitted with two four element strain gauge cells and these monitor the normal and tangential components of the force acting on the ball, i.e. the load and the friction force. The arm is mounted on a vertical shaft L which can be raised or lowered in order to vary the loading on the ball. L passes through a vacuum seal and is clamped at its upper end by the clamp M, which is fitted with a screw with which the shaft assembly is raised or lowered. The output from the strain gauge cells is brought out through the hollow centre of L and this is sealed with epoxy. The strain gauges are operated from a 6V power supply and the two strains may then be displayed on an X-Y plotter which shows F as a function of P.

It is never possible to balance a resistance strain gauge bridge

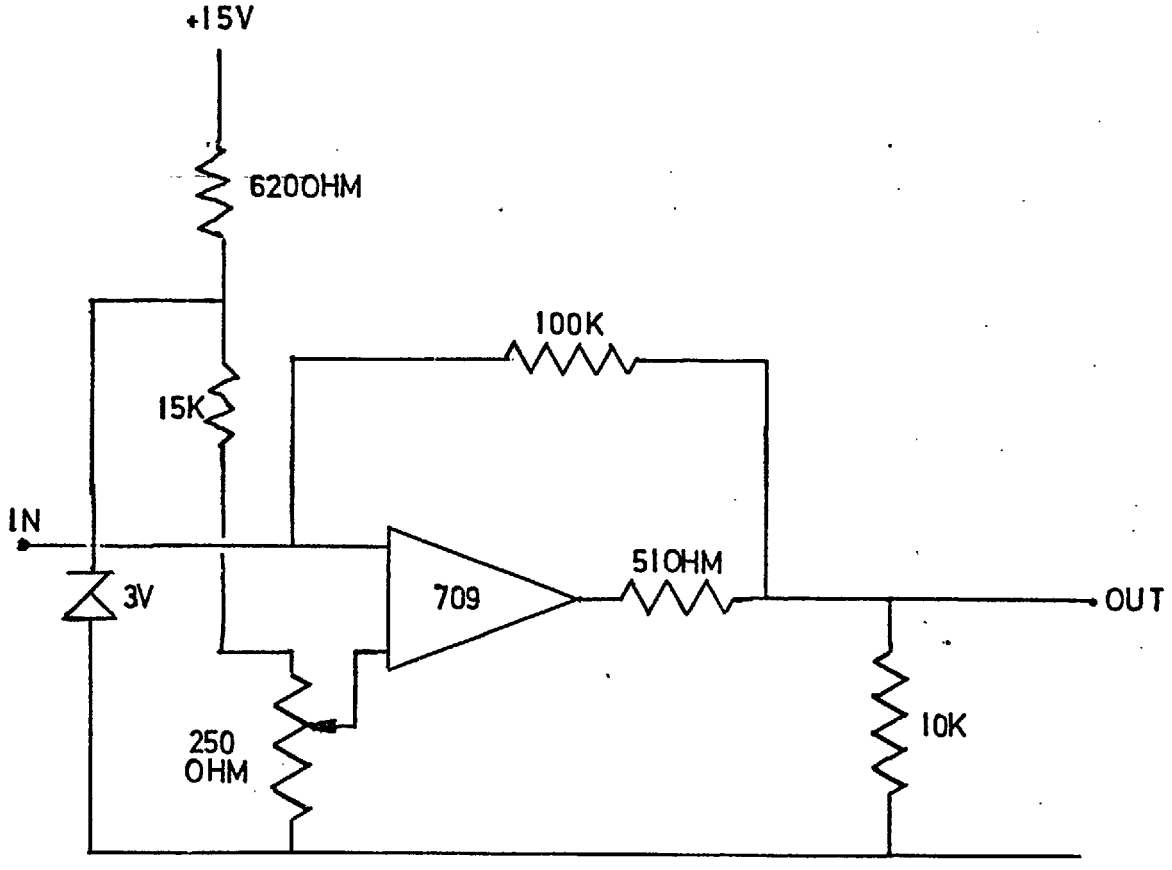

Fig. (4.10) STRAIN GAUGE OFFSET COMPENSATING CIRCUIT

CORRECTION:

The photo-cell system shown in this figure was discontinued; also the capstan device was replaced by a handling arm.

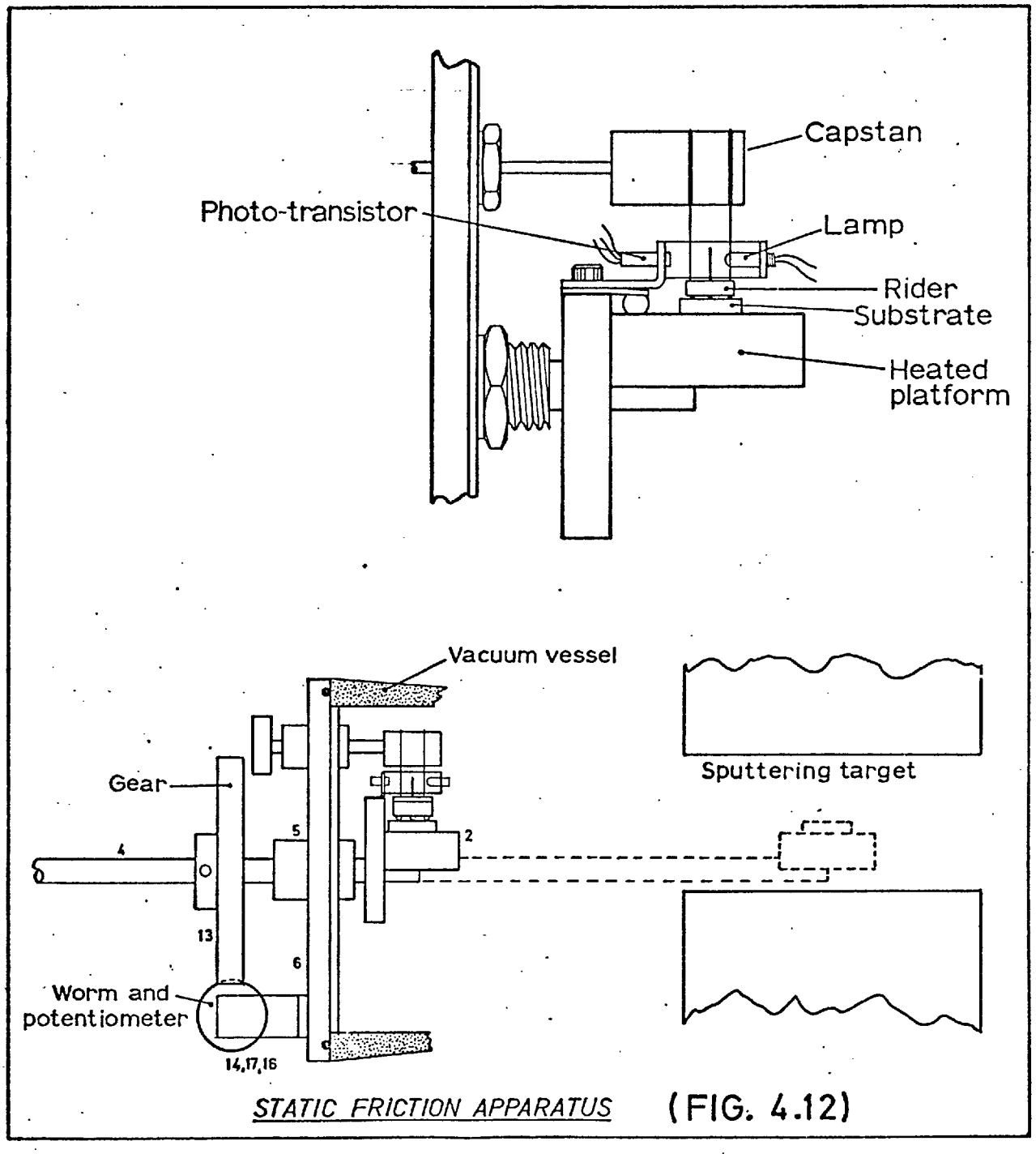

STATIC FRICTION APPARATUS (FIG. 4.12)

exactly, the output voltage for zero appled strain being referred to as the offset voltage. In most cases the offset voltage is small compared with the signal due to an applied strain but where very small strains are to be measured, techniques must be applied to remove the effect of the offset. In this work some very small forces were encountered while measuring the friction of molybdenum disulphide and it was necessary to build a differential D.C. amplifier, constructed in such a manner as to subtract a fixed D.C. potential from the output of the strain gauge. This was achieved using the circuit of fig. (4.10).

(4.4) Static Friction Apparatus.

The principle of this apparatus is that a coating is sputtered onto the substrate, which is then retracted from the sputtering environment and allowed to cool; a rider is now lowered onto the substrate, making contact with it through three spherical feet. The table on which the substrate is mounted is now tilted slowly until the rider slips; the angle of tilt is accurately measured and knowing the geometry of the rider, the mean shear strength of the three contacts can be calculated. Once a measurement has been made, the rider is removed and the substrate returned for the deposition of a further layer of film. In this manner thickness effects upon friction can be studied.

The apparatus is shown schematically in fig. (4.12); the substrate is in the form of a disc 1" in diameter and 1 mm. thick, one surface being highly polished. The substrate lies in a recess in the top of the table (2), which can be heated if required; the table is attached to the end of a long shaft (4), which can be either rotated or moved back and forth through a vacuum seal (5) in the centre of plate (6). The rider (shown in

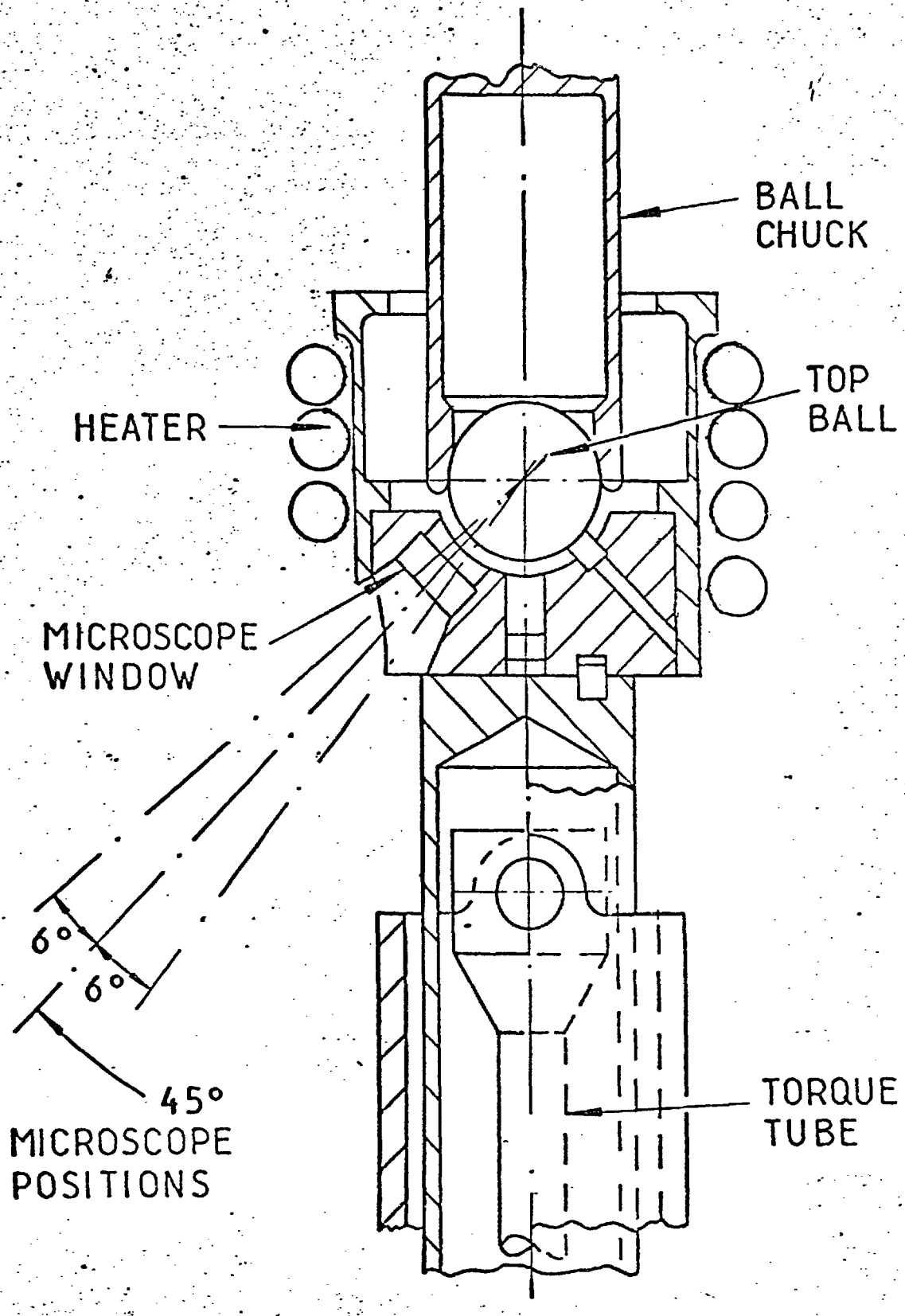

FIG. (4.13) BALL ON PEG MACHINE.

fig. 4.12) consists of three 3/16" balls firmly set on the vertices of an equilateral triangle into a stainless steel holder. The upper surface of the holder is fitted with a stiff wire loop by which it may be handled on or off the substrate; annular weights may be attached to the rider if required. A handling arm (7) projects from the plate (6) and is capable of holding the rider clear of the substrate during sputtering and then lowering it into position once the table has been retracted. Once the friction measurement has been made the handling arm can then remove the rider once again.

The position of the stop (12) is set so that the table can be accurately aligned horizontally before the rider is placed on it; once this has been done, the gear wheel (13) is locked onto the shaft (4) by a clutching mechanism and this is slowly and smoothly turned through the worm (14) by operating the knob (15) manually. A multi-turn potentiometer (17) is fitted to shaft (16) and the potential divided across this is calibrated directly in degrees and displayed on a digital voltmeter. The accuracy is estimated to be $\mp$ 0.1°.

Electrodes fitted to plate (6) enable the rider to be sputter-cleaned prior to use; the substrate can of course be cleaned by the usual sputtering techniques. Plate (6) is designed to seal onto one of the 6" side arms of the sputtering chamber.

(4.5) Description of the Ball and Tri-plane Friction and Wear Apparatus.

This apparatus was kindly made available by Professor Cameron of Imperial College, having been designed by members of his group. Fig. (4.13) shows the schematic layout.

Fig. (4.15) COMPACTING DIE (MILD STEEL)

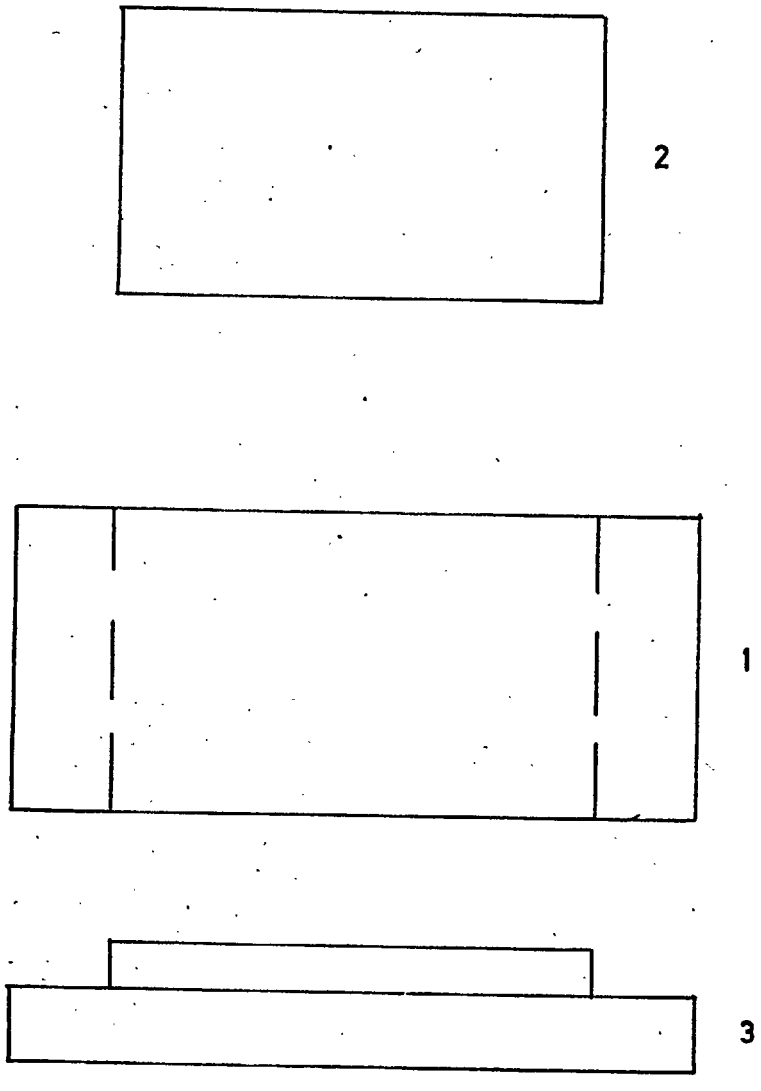

For the purposes of the present work, films were sputtered onto 1" diameter EN31 steel balls and these were inserted into a collet which was then clamped; the collet was attached to a spindle which could be rotated at various speeds. The ball fitted into a cup, from the inside of which three flat-ended pegs, also of EN31 (actually roller bearings presented end-on), projected so as to make three point contacts. The ball was then loaded against the pegs, forming three Hertzian contacts, and the collet rotated. The pegs were so positioned in the cup as to make three wear tracks of slightly different radius on the ball and their axes were inclined in a manner which made the contact load the same at each. The cup assembly was fitted with strain gauges to measure the torque acting on it and thus, knowing the loading, the coefficient of friction could be determined. A thermo-couple was also mounted in the cup to measure any temperature rise due to friction.

(4.6) Target Fabrication Techniques.

(4.6.1) Molybdenum Disulphide.

Commercial molybdenum disulphide powder (Murex grade AA) was used for target construction. A compacting die was constructed as detalied in fig. (4.15); a quantity of powder was evenly distributed in the chamber formed by the cylinder (1) and the end-plug (3), the piston (2) was inserted and the die compressed in a hydraulic press to an overall load of 120 Tons, which is equivalent to 6 Tons/sq." pressure on the powder. The end plug was then carefully removed from the cylinder and the piston pushed in until the compact was ejected. Compacts formed in this manner have strengths which are quite adequate for handling purposes but certainly not adequate for use as targets, where the thermal stress quickly causes

them to disintegrate. In order to enhance their strength, the compacts were sintered in vacuum for one hour at 1,100°C. During this process, some sulphur was liberated but this was judged not to be excessive and was apparently derived from a thin superficial layer, this depleted layer could be scraped off prior to target mounting.

Since the target backing plate is composed of Dural, a material of high thermal expansion coefficient, targets were bonded to thin copper discs using conductive epoxy and then the copper disc was bonded to the backing plate in the same manner.

Molybdenum disulphide targets made in this manner performed superbly and were used in the sputtering system at powers of up to 500 Watt; this power level could quite probably have been raised still further. Due to some porosity, targets required outgassing in vacuum for about one hour before sputtering; the sputter-cleaning operation then removed most of the remaining absorbed contaminants.

(4.6.2) Gold.

Gold targets were constructed from sheets of gold measuring 5" x 5" x 0.05", obtainable from Johnson Mathey Ltd. The sheets were simply machined into 5" diameter discs and then bonded to the Dural backing plate with conductive epoxy.

(4.6.3) Chromic Oxide.

These were prepared by plasma-spraying chromic oxide powder directly onto the roughened backing plate. The technique for performing this opera-

tion has been reported elsewhere[38]. The estimated thickness of these coatings is 0.005".

(4.7) Substrate Preparation Techniques.

Steel substrates were obtained initially with a surface-ground finish. The substrates were lapped using grade 400 silicon carbide paper (Seal Brand) on a plate glass backing and using white spirit as a lubricant. The paper was then changed to grade 600 and a silky finish obtained. Subsequently the surfaces were polished using 3 micron diamond on a cloth wheel and white spirit as a lubricant, applying considerable manual pressure. A final finish was given using 1 micron diamond in the same manner, but with less applied pressure.

Substrates were cleaned initially using a soft brush and a hot solution of Decon liquid detergent. They were then given a 10 minute ultrasonic clean in hot Decon solution, a long rinse in hot tap water and a further 5 minute ultrasonic clean in distilled water. Substrates were then dried with lens tissue and finally ultrasonically cleaned in Freon.

The 2" diameter disc substrates used in the dynamic friction apparatus of fig. (4.8) were placed on the substrate table of the sputtering system and clamped firmly in place to ensure good thermal conduction to the substrate table and to allow correct positioning. A sputter etching operation was next performed upon them, using the shutter as the anode with a spacing of 3 cm. and an applied D.C. voltage of 1,200 V. The argon pressure was 4×10^{-2} Torr. and the normal duration was 4 minutes. It was found that if the voltage or the time were allowed to exceed these stated values, the finish of the prepared surface would be impaired due

to etching.

The 1" disc substrates, used with the static friction apparatus were placed in the recess of the table and positioned in the sputtering system with the shutter approximately 3 cm. above. The sputter etch cycle described above was then initiated, with the negative potential applied to the shaft (4) of fig. (4.12). In general shorter times were used for fear of contaminating the target, since in this case the plasma is poorly confined.

Tungsten carbide discs were also used in conjunction with the static friction apparatus and these were prepared differently from the steel specimens in view of their extreme hardness (Moh scale 9).

Tungsten carbide discs were received with an 'as sintered' finish with rough and uneven surfaces. Initially the discs were polished with 40 micron diamond paste on a cast iron wheel for many hours, the operation being automatic with four discs lapped at a time. The polishing proceeded using a copper wheel and diamond paste grades 10, 3 and 1 micron respectively. Preparation from this point was identical for all substrates and as detailed above.

(4.8) Sputter Deposition Techniques.

Although some early work was done using D.C. diode sputtering, the results obtained were not considered to be of sufficient quality or significance to warrant reporting them, since in general the adhesion of the D.C. diode sputtered films was found to be inadequate for friction work. The results reported in this section pertain exclusively to films

produced by R.F. diode and bias techniques. In all cases it was found to be desirable to apply a magnetic field to the system for containment purposes and this was achieved using horizontally mounted Helmholtz coils, which gave a magnetic flux density of 0.018 Tesla.

(4.8.1) The Sputtering of Molybdenum Disulphide.

Two basic techniques were evolved for sputtering these films:

(1) High adhesion technique.

(2) High yield and diffusivity technique.

In the case of the first technique, the parameters were adjusted to give conditions most favorable to producing films of high strength and adhesion; thus the pressure was reduced as far as possible (to approximately 2×10^{-3} Torr.), the inter-electrode spacing was minimized (typically to 3 cm.) and the R.F. power input was maximized (to 450 Watt, the upper limit here being determined by the level considered safe for the target). From the discussion of chapter 3, it is apparent that such a course of action should lead to the required objective.

High yield and diffusivity (that is departure of sputtered particles from rectilinear propogation) will result if the pressure is raised. If diffusivity is a prime concern, the interelectrode spacing is increased to about 10 cm., while for high yield this is held at 3 cm. The pressure for each operation is in both cases 15×10^{-3} Torr.

(4.8.2) The Sputtering of Gold.

In the development of techniques for production of gold films, adhesion was a major problem. The sputtering parameters were therefore

accordingly constrained and those found to be effective were as follows:

Argon pressure 1 to 5×10^{-3} Torr.

R.F. power 600 Watt.

Interelectrode spacing 5 cm.

Bias voltage -100 V.

In early work on gold films some problems were encountered with uneven thickness distribution due to the effect of bias field upon the edge of the substrate (see 3.5). A guard ring was therefore placed around the substrate during deposition and this corrected the problem.

(4.8.3) The Sputtering of Chromic Oxide.

Since this material is electrically reasonably conductive in the sputtered form, it is possible to employ D.C. biasing. Adhesion was found to be a major problem and the parameters used for successful deposition were the same as those used for gold, except that the applied power was kept to 400 Watt to avoid damage to the target.

(4.9) Techniques for Film Evaluation.

The techniques used in conjunction with the friction evaluation have been largely elucidated in our discussion of the apparatus construction. Further discussion of these can properly be left to the next chapter.

We shall consider in this concluding section a number of special techniques used to explore film properties.

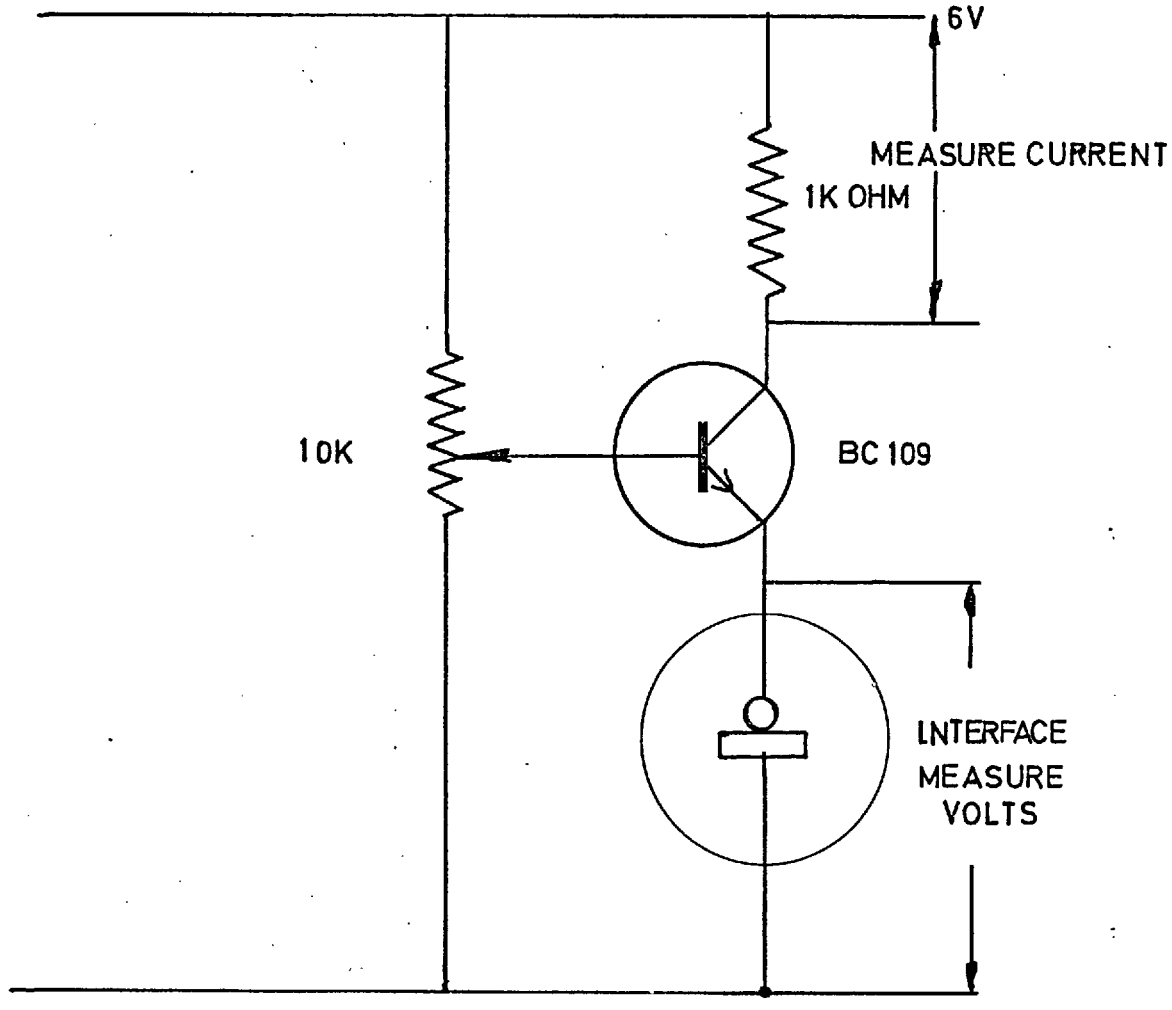

FIG. (4.16) CONTACT RESISTANCE MEASURING SYSTEM

(4.9.1) Film Thickness Determination.

Two techniques were used which were found to give excellent reliability. In the first of these, weighed microscope cover-slips were coated and then re-weighed, knowing the density of the film material, the thickness could be accurately determined and in view of the small size of the cover-slips, a number of them could be coated simultaneously in order to explore variations of thickness at different points on the substrate table. The disadvantage of this method and indeed all methods using insulating substrates, is that if D.C. bias is applied, the bias voltage does not immediately appear on the substrate which acquires a potential determined by the ratio of the numbers of arriving charged particles of opposite sign. Probably this difficulty is only significant for very thin films.

The second technique was employed with molybdenum disulphide and involved the removal of a small patch of film, using concentrated nitric acid. A Talysurf scan of the patch then gives a double step for thickness estimation; the substrate, EN58 steel, is not affected by the acid.

(4.9.2) Electrical Resistance of Spherical Contact with Films.

In an attempt to confirm the nature of the dependence of contact area upon load, some contact resistance measurements were made with molybdenum disulphide films. A voltage was applies across the interface and this was maintained at a constant low value in order to reduce the effects of heating and field emission[39][40]; the circuit of fig. (4.16) assisted with this but gross variations had to be handled manually using R_1. The variation of current as a function of the load applied was measured, using the apparatus of fig. (4.8) to provide the mechanical interface.

CHAPTER 5 --- PRESENTATION AND DISCUSSION OF RESULTS

(5.1) The Dependence of Deposition Rate and Other Factors Upon Sputtering Parameters.

The intention of this section is to convey an appreciation of the consequences of varying the major sputtering parameters within the range of operation which has been used in this programme. Except for the data concerning the diffusivity of deposition, which were obtained with the apparatus of (4.2.1), the results of the following three sub-sections were obtained using an M.R.C. model SM 8620 R.F. sputtering module. A platinum target was used, having a diameter of 5"; the inter-electrode spacing was 6 cm. and the sputtering gas was argon.

(5.1.1) The Effect of D.C. Offset Potential on Deposition Rate.

The offset potential is of primary significance in determining the energy of bombarding ions, since the mobility of these is far too low for them to be affected by the R.F. component of the applied field. Increasing bombardment energy produces initially a higher sputtering yield and a higher ejection energy of sputtered species and this results in an increased deposition rate, as seen in fig. (5.1). As the bombardment energy continues to rise, a stage is reached where the momentum exchange with surface atoms of the target becomes decreasingly efficient as more and more ions become implanted, liberating the greater proportion of their energy within the bulk material. This process has the eventual consequence of producing a decline in the deposition rate with increasing energy but such an effect is only encountered with ion beam systems and need not concern us here.

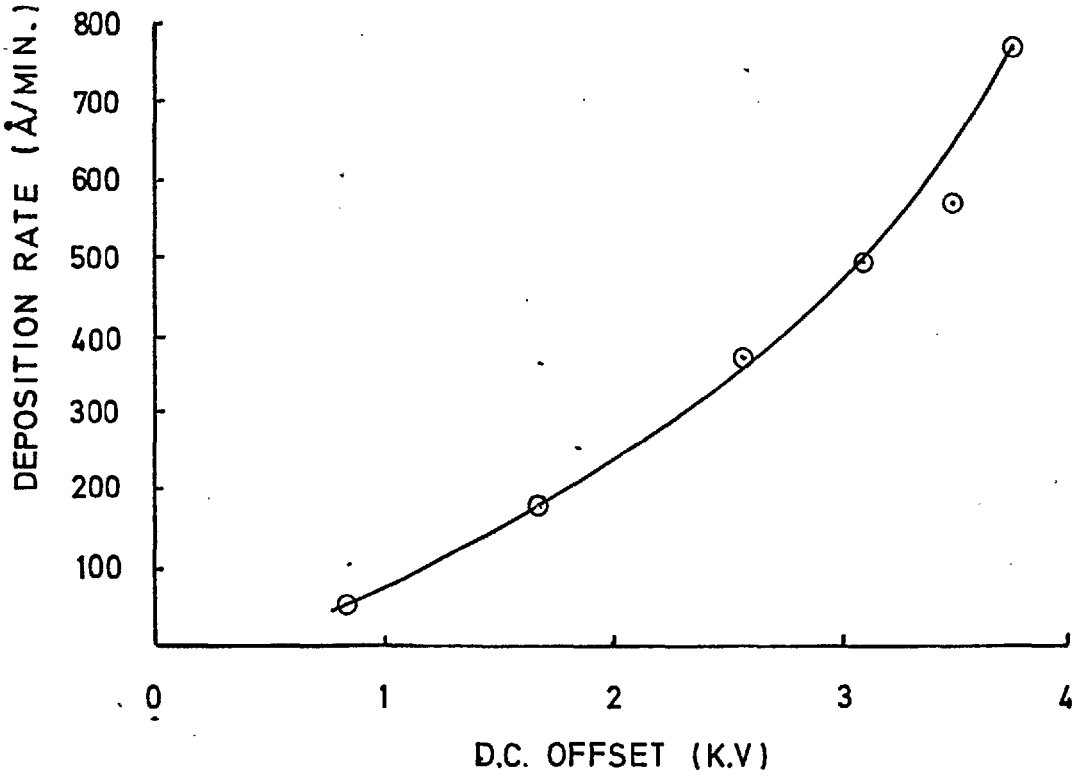

Fig. (5.1) Dependence of deposition rate on D.C. offset potential.

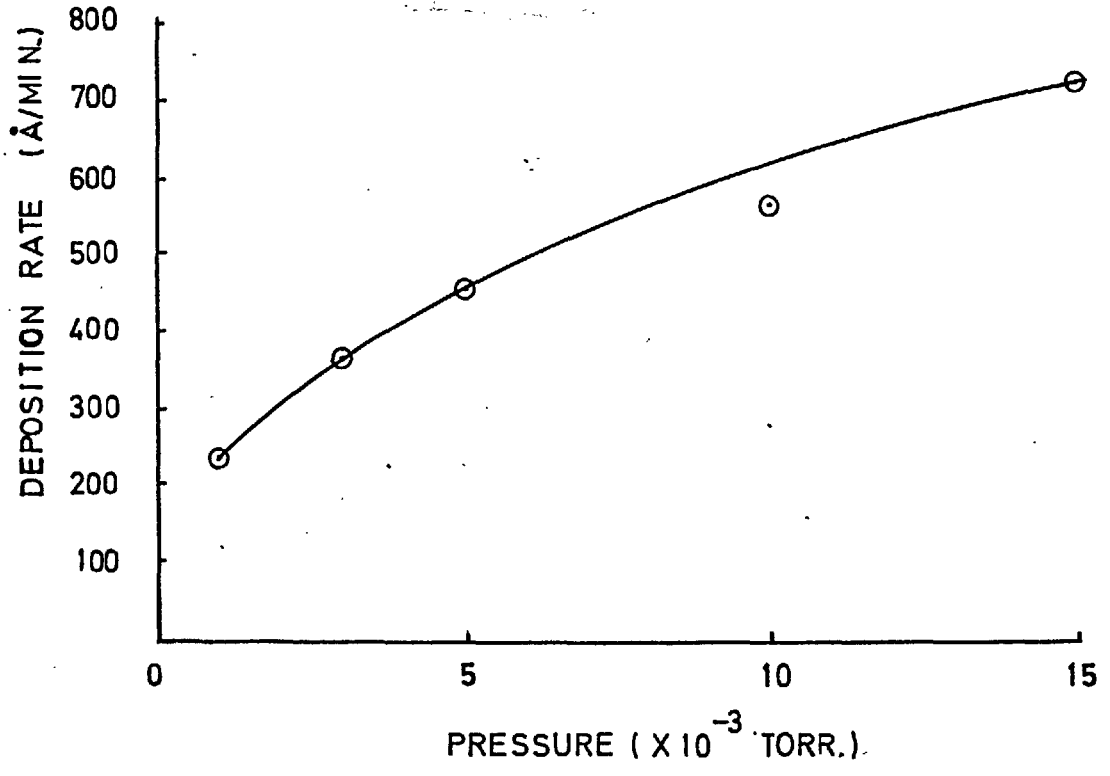

Fig. (5.2) Dependence of deposition rate on pressure.

Film thickness distribution of MoS_2 on a 1" diameter cylinder, with argon pressure as a parameter.

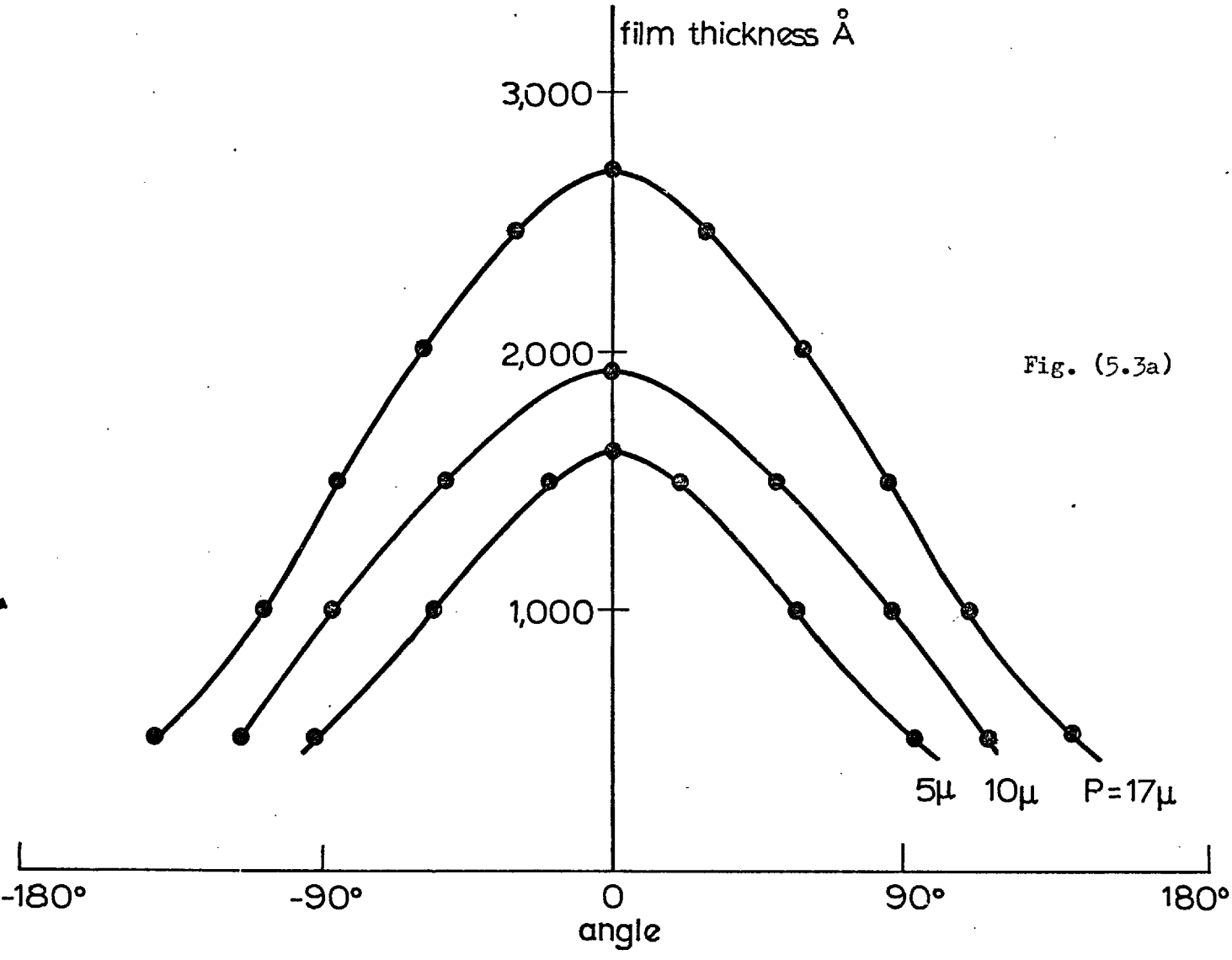

Fig. (5.3a)

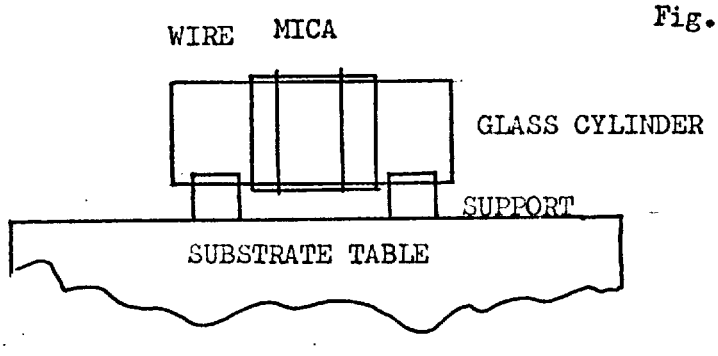

Fig. (5.3b)

(5.1.2) The Effect of Pressure on Deposition and Diffusivity.

We have already remarked that the sputtering pressure can have a pronounced effect on the deposition rate and that while increasing the pressure results in the production of greater numbers of ions to bombard the target, these will suffer more collisions as the pressure is raised and in consequence their momentum will be reduced. We thus have two counteracting mechanisms affecting the deposition rate; we see the result of this in fig. (5.2) where a saturation condition is being approached for higher pressures.

Sputtered particles, ejected from the target, will be increasingly liable to collision before reaching the substrate as the pressure is raised. We have seen in chapter (3) that this will cause the angular distribution of sputtered material to increase and that in certain circumstances such an effect can be utilized to advantage in the coating of substrates of irregular shape. Fig. (5.3a) shows the dependence of angular distribution on pressure, where the substrate used was a very thin sheet of mica, bent into a 1" diameter cylinder around a glass former as shown in fig. (5.3b); film thickness was estimated by an interferometric method.

In fig. (5.3a), if we take the results for a pressure of 17×10^{-3} Torr. as a standard and normalize the curves for 10 and 5×10^{-3} Torr. so as to give equal deposition for all pressures at $\theta = 0^{\circ}$ (i.e. for planes parallel to the target), we obtain a more accurate picture of the diffusion effect. For example, when the pressure is increased from 5 to 17×10^{-3} Torr., the deposition rate is doubled for $\theta = 90^{\circ}$ (i.e. for planes perpendicular to the target). The normalized results are shown in fig. (5.3c)

Fig. (5.3c) Normalized Angular Deposition Distribution

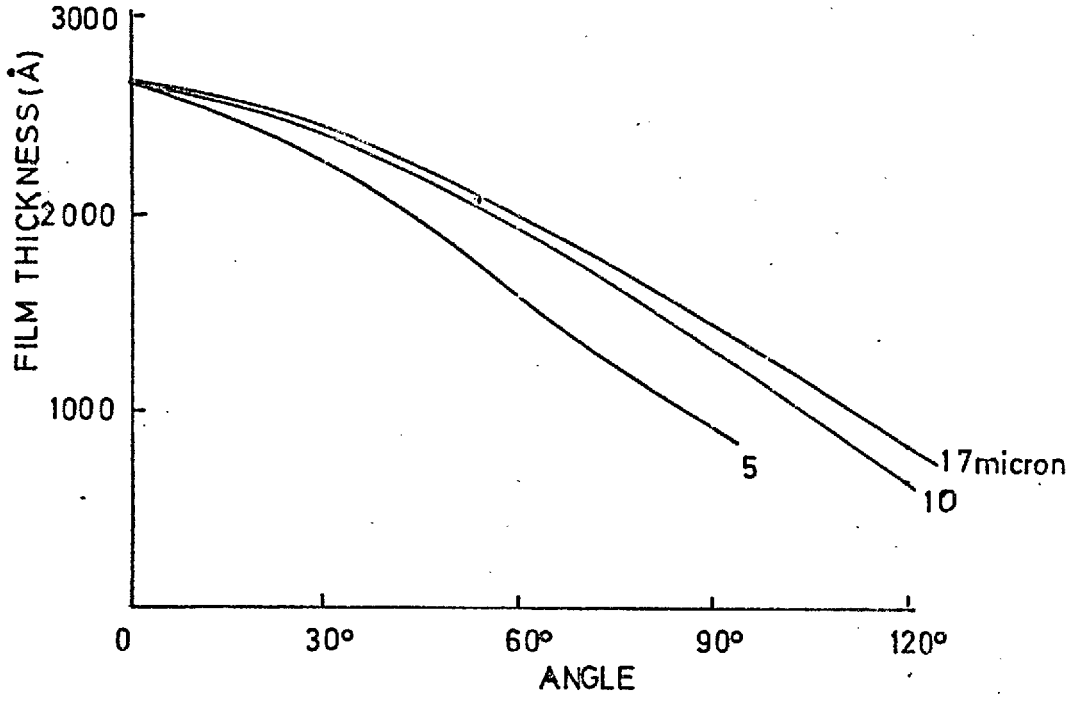

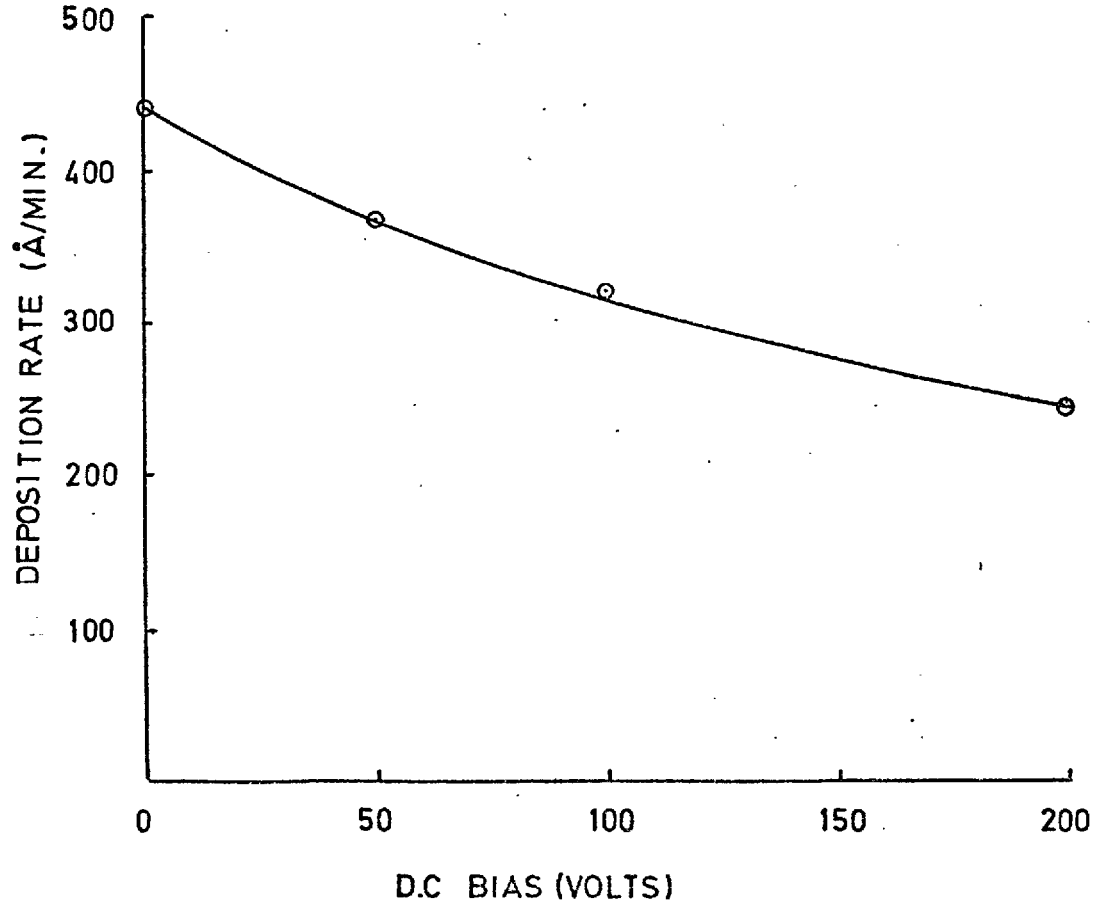

Fig. (5.4) Dependence of Deposition Rate on D.C. Bias Potential

Pressure = x 10^{-3} Torr. Target Power = Watt

Fig. (5.5a) X-Ray Spectrum from a 30 KV. Electron Microprobe Examination of a 9,000 A MoS_2 Film on an EN 58A Substrate.

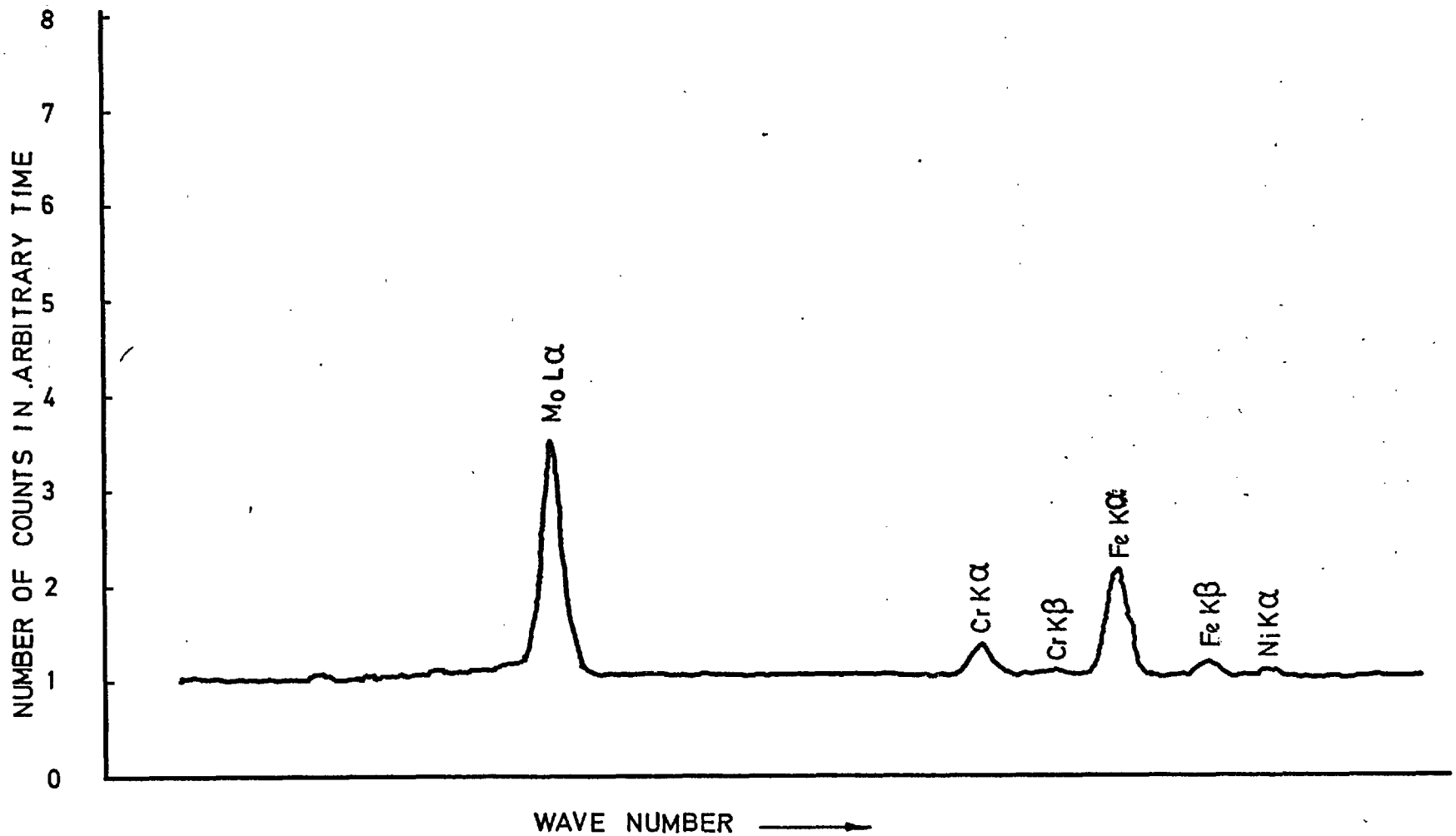

Fig. (5.5b) X-Ray Spectrum from a 30 KV. Electron Microprobe Examination of EN 58A Substrate.

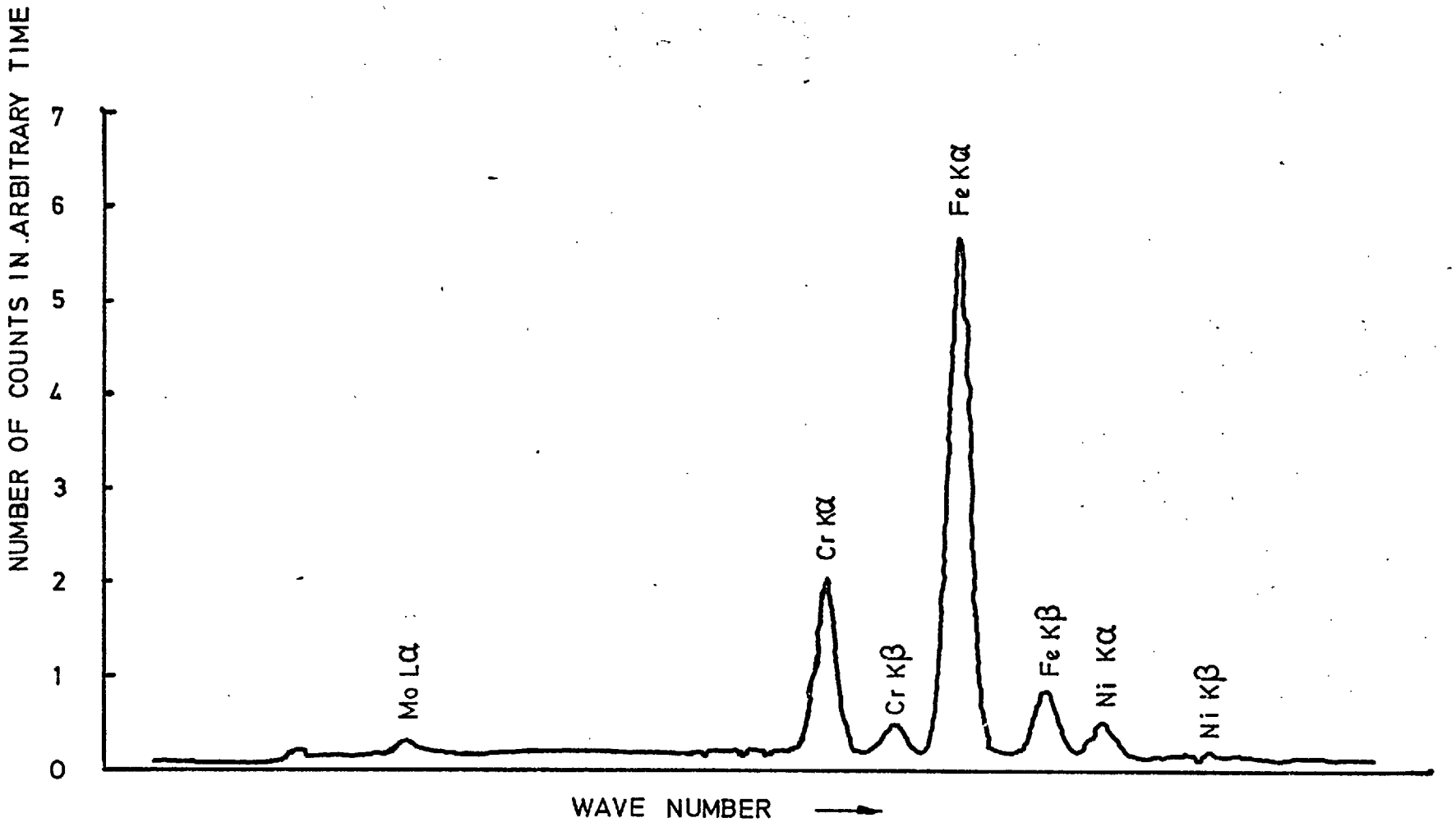

(5.1.3) The Effect of Bias Potential upon Deposition.

In this programme, films of gold and chromic oxide were deposited under bias conditions and it is therefore important to have an appreciation of the extent to which bias voltage affects the deposition rate. In fig. (5.4), the dependence is shown and we see that there is a gradual decrease in the deposition as the bias is increased. This situation is only to be expected, since a major result of applying bias is the back-sputtering of loosely adhering material from the substrate and obviously this effect will become more pronounced as the bias voltage increases.

(5.2) General Observations on the Properties of Sputtered Films.

(5.2.1) Molybdenum Disulphide.

An early concern in our work with molybdenum disulphide was that the films should be stoichiometric; films were consequently subjected to electron microprobe analysis, the technique being to scan first a sample of sputtered material and then a sample of pure molybdenite. X-ray counts were then taken corresponding to the Mo:S ratio present in each specimen and it was determined that this ratio was 1:1.7 for the sputtered material. This result was judged to be acceptable in view of the inherent inaccuracy of the method for quantitative measurement.

Some electron microprobe results (taken with a beam energy of 30 K.V.) for a 9,000 Angstrom film of MoS_2 on an EN 58A substrate are shown in fig. (5.5a), while those for an uncoated region of the substrate are shown in fig. (5.5b). In fig. (5.5a) we see a strong resonse for molybdenum and small but significant peaks due to iron, chromium and nickel; the constituents of the substrate. In fig. (5.5b) we see the position reversed, with

Plate (5.1) Electron diffraction by a sputtered gold film, showing preferential orientation.

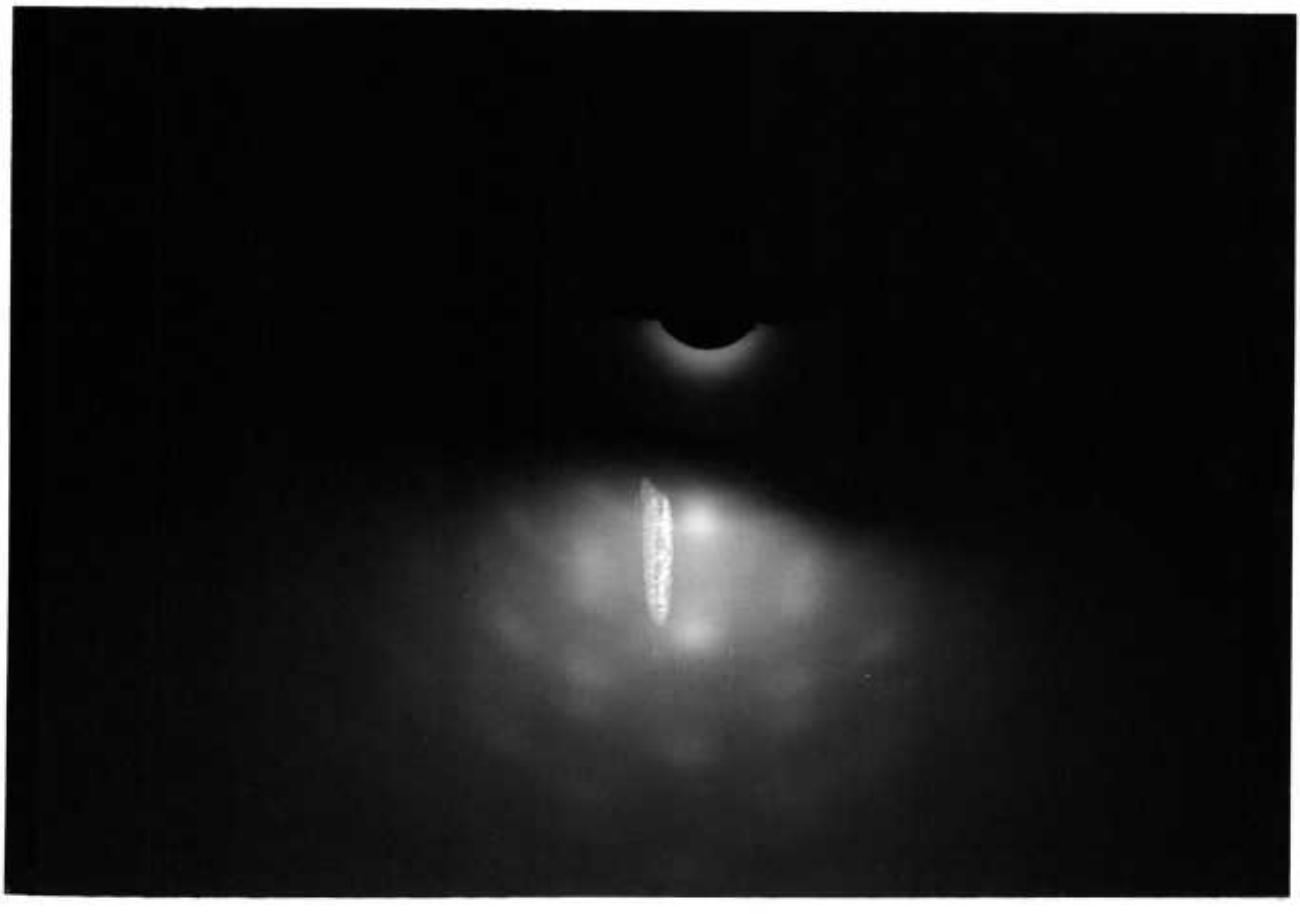

a strong substrate response and a small peak due to stray deposition of MoS_2. These results are interesting in that they give an indication of the resistance of the film to penetration by an electron beam and this was found to be greater than expected.

Transmission electron micrographs, obtained by replication from sputtered MoS_2 films, were quite featureless with no grain boundaries apparent; this was taken to indicate that the grain size of these films was too small to be resolved in the microscope and this would indicate a size of less than 50 Angstrom, which is in keeping with the estimate of Spalvins[32]. High energy reflection electron diffraction showed that films were randomly oriented polycrystalline, as seen in plate (5.4a).

The results of friction tests upon MoS_2 will be fully discussed later in this chapter; it is however appropriate to mention here that these yield friction coefficients in the range 0.05 to 0.01. Since this is the order of magnitude that we should expect for this material, these results lend weight to the view that the crystal structure is unchanged after sputtering.

(5.2.2) Gold.

In a later section we shall show that sputtered gold films, while capable of yielding friction coefficients of less than 0.1, do not show good durability in sliding friction and although this can partly be explained in terms of the tendency of metal films to form alloys with the rider material (see (2.14.2)), there is a probability that the strength of the sputtered gold may be low. This view is supported in plate (5.1) which shows the result of a reflection electron diffraction examination of a sputtered gold film, deposited on EN 58A steel, the contrast is unfortunately rather poor but a high degree of crystallinity is evident and the crystallites

appear to be oriented; it is not possible to accept that this could be the result of epitaxy, since the substrate is randomly oriented polycrystalline. Apparently the deposition conditions favour oriented growth and this effect is frequently encountered[41].

The physical appearance of these films is similar to that produced by electroplating; that is to say, the surface is highly reflective and free from flaws. The adhesion appears to be excellent, provided the precautions outlined in (4.8.2) are observed.

(5.2.3) Chromic Oxide.

This material exhibited very good wear resistance but the friction was rather high (approximately 0.6). Sputtered coatings appear to be amorphous since no structure is apparent from electron diffraction examination. The colour of these films is a brownish green and according to some observations by Holland[42] on evaporated films, the departure from the anticipated deep bottle-green is due to the presence of lower oxides. An attempt was made to sputter the material in the presence of oxygen in order to compensate for any deficiency but although partial pressures of oxygen of up to 33% were used, no change was observed in the colour of the films. Since the wear characteristics were already regarded as being very good, this line of approach was not pursued further.

Adhesion was a considerable problem in the early films and it was noted that exposure to solvents could result in these penetrating pinholes in the film and invading large areas of the interface between film and substrate. With the introduction of an applied bias to the sputtering process, this problem was eliminated and the adhesion was excellent.

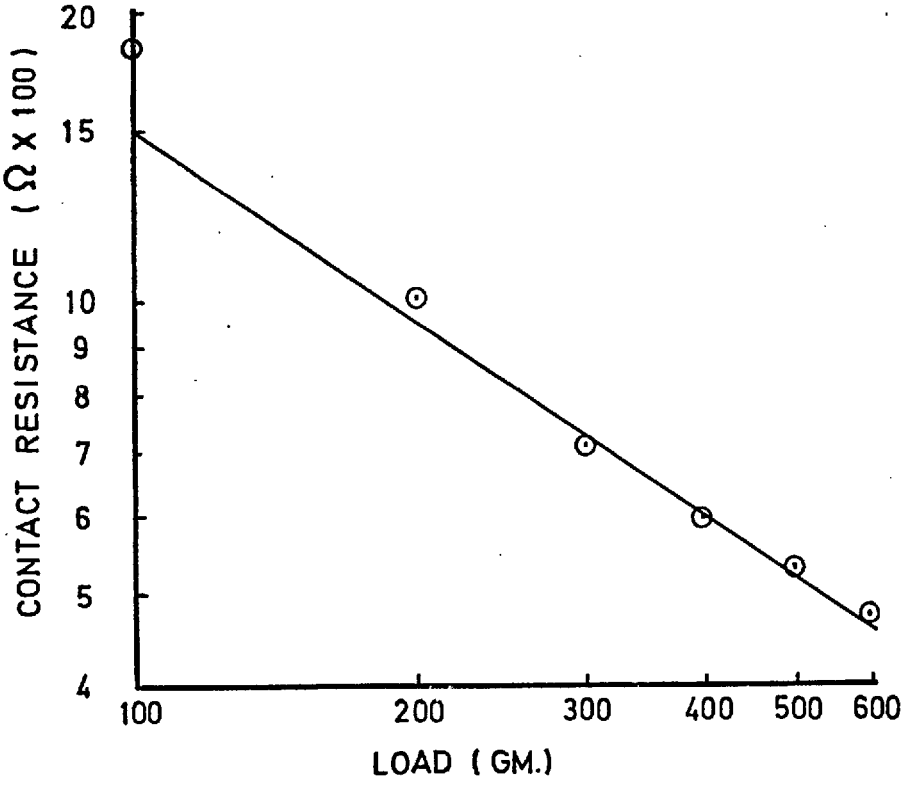

Fig. (5.6) Contact resistance plotted against load for a 3/16" steel rider indenting a flat steel surface coated with a 10,000 A MoS_2 film.

(5.3) Electrical Resistance Measurements.

In order to determine the nature of the dependence of contact area upon load the sphere-on-flat configuration used in this programme, measurements were made of the variation of contact resistance with load and these were performed using the apparatus designed for dynamic testing (see 4.9.2). It was found that MoS_2 coatings, which had a resistivity $\sim 10^3$ ohm cm. greatly assisted in these measurements since the high contact resistance enabled reasonably high voltages to be applied ($\sim$500 mV.) without the fear of Joule heating due to high current. Electronically MoS_2 is a semiconductor exhibiting both p and n-type behaviour according to the circumstances of preparation[43]; the intrinsic band-gap is large ($\sim$4eV) and this implies that the pressure dependence of conductivity will be insignificant, since the conductivity is principally extrinsic.

The conductivity of MoS_2 is highly suseptible to variation due to the presence of impurities, thus with the lubricant grade material used in these experiments it was found that the resistance varied considerably for each new contact made. Nevertheless, for each contact the functional dependence of contact resistance upon load obeyed the predicted -2/3 power law with reasonable accuracy (assuming resistance proportional to real contact area) and the mean of a series of ten readings is shown in fig. (5.6). For each set of load readings taken, a new ball was fitted to the friction head and a new point was chosen on the film; the results of fig. (5.6) were taken for a film of 10,000 Angstrom thickness.

(5.4) The measurement of Static Friction and its Dependence on Film Thickness.

These experiments, carried out with the apparatus described in (4.4), were originally conceived in order to explore the dependence of friction

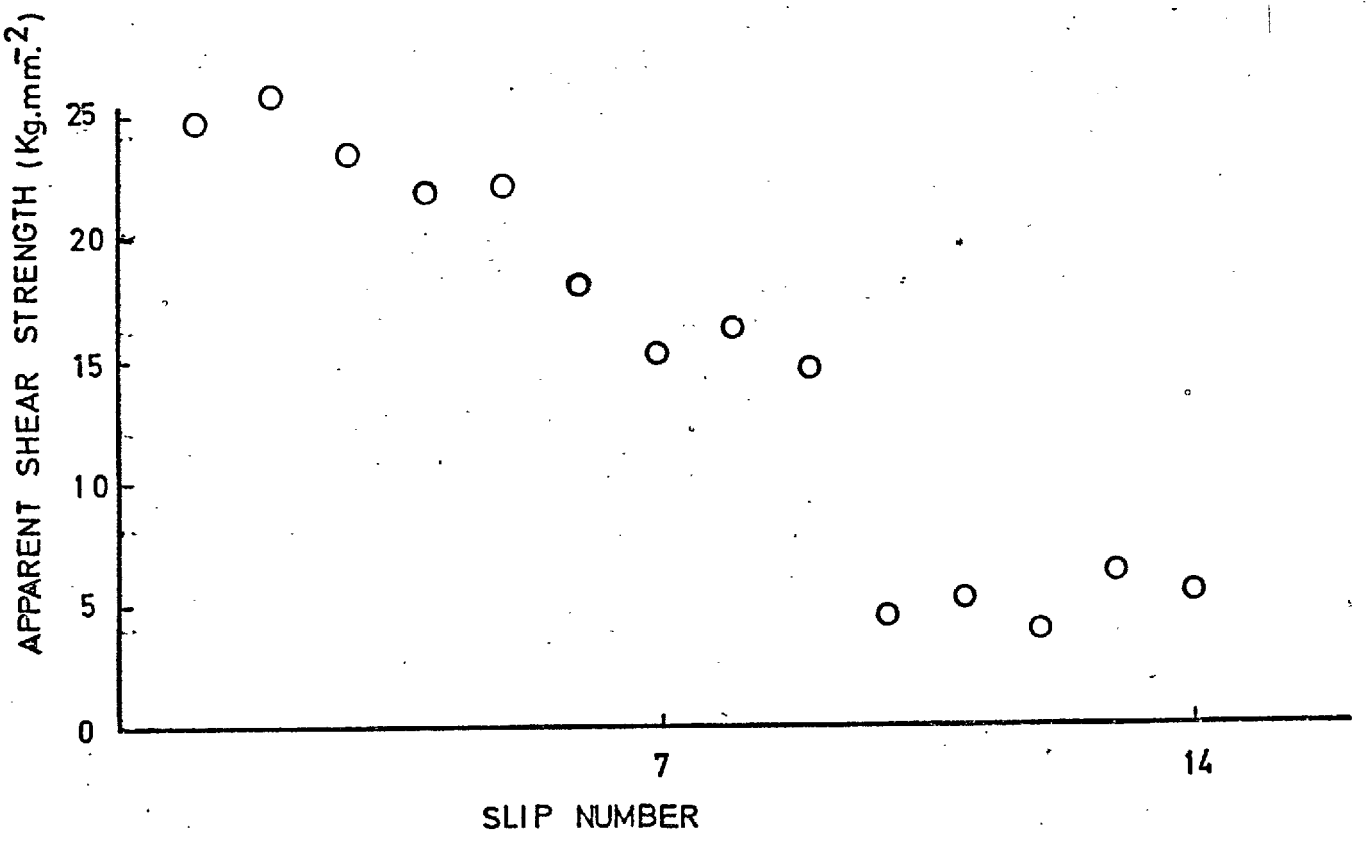

Fig. (5.7) The variation of apparent shear strength of sputtered MoS_2 with slip-number.

on film thickness for films up to 1,000 Angstrom thick; the relevant theory is considered in (2.11.2). Since the rider used made contact with the film covered surface at three points, the load at each would in general vary as the table was tilted prior to sliding. To simplify matters, the rider was placed on the surface so that two of the contacts lay on a line parallel to the axis of tilting, equalizing the reaction at each. In addition the two equal contacts were arranged to be below the third contact during tilt and this was found to reduce the tendency for the rider to slew round prior to complete slipping. The mechanics of this contact are considered in Appendix (2), where an expression relating the shear strength of the film material to the other parameters is derived.

(5.4.1) Static Friction of Molybdenum Disulphide.

Initial static experiments utilized this material since it was of primary interest to the programme and because the ratio of its modulus to that of the substrate material (tungsten carbide) is small, a fact which it was hoped would demonstrate micro-elastic effects to best advantage.

Films of molybdenum disulphide between 100 Angstrom (nominal) and 1,000 Angstrom were deposited onto tungsten carbide. In all cases the friction was found to be high for the first few slips of the rider but subsequently reducing rapidly to a constant value. Fig. (5.7) shows the results obtained for a film 1,000 Angstrom thick; the apparent shear strength is plotted against the slip-number and the value is seen to fall from 26 $Kg.mm.^{-2}$ to 4 $Kg.mm.^{-2}$ From these results it may be concluded that MoS_2 is not intrinally a lubricant in its sputtered form, but requires crystallographic orientation before it will operate satisfactorily. We can presume that the sputtered material has a reasonably high compressive strength, in view of

Fig. (5.8)

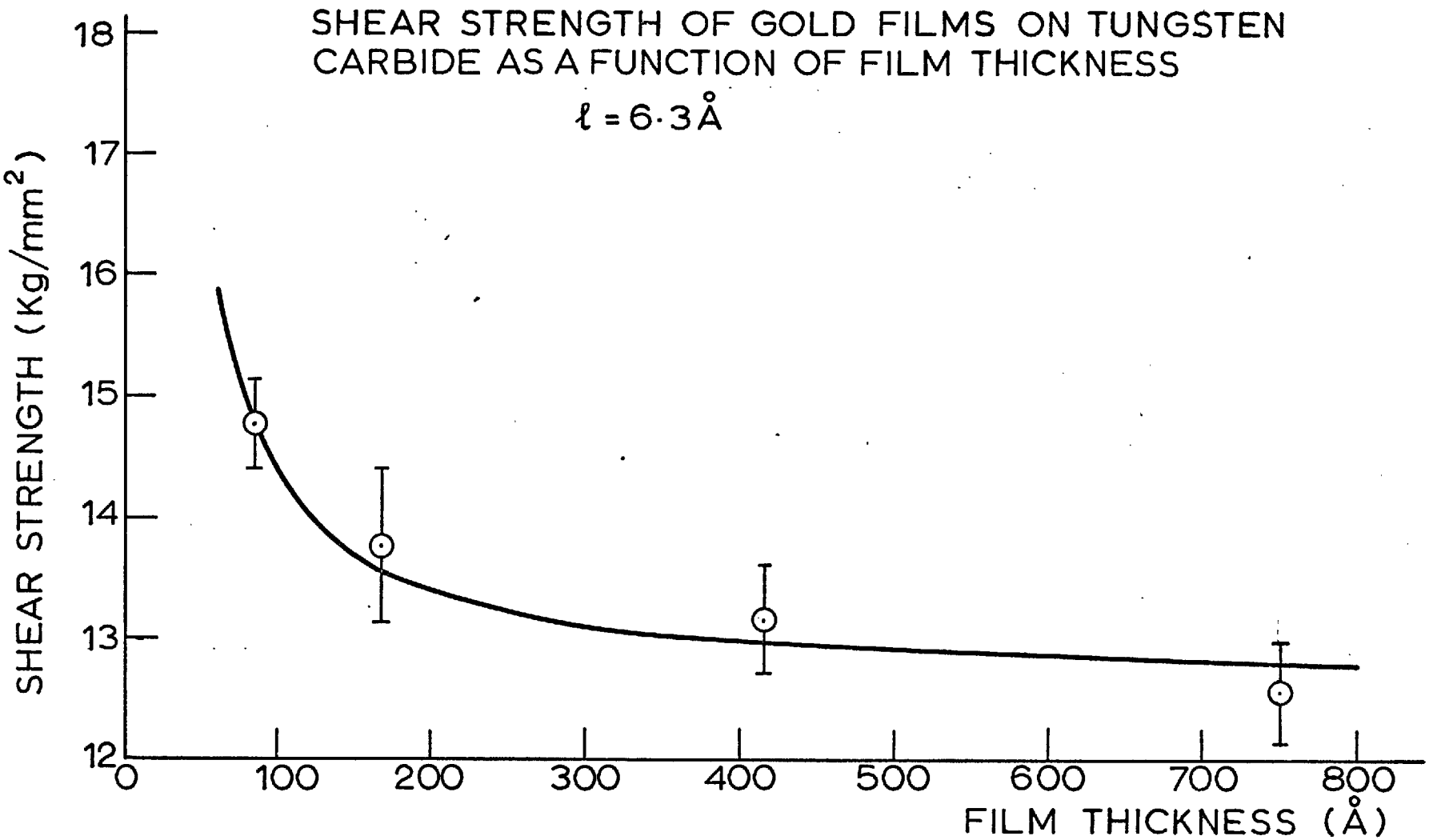
SHEAR STRENGTH OF GOLD FILMS ON TUNGSTEN CARBIDE AS A FUNCTION OF FILM THICKNESS
ℓ = 6·3 Å
SHEAR STRENGTH (Kg/mm²)
18
17
16
15
14
13
12
0
100
200
300
400
500
600
700
800
FILM THICKNESS (Å)

the the value we have obtained for the maximum shear strength and this would be in keeping with the observed small grain size.

It was decided to discontinue attempts to explore possible micro-elastic effects with this material since the orientation effects made such measurements unreliable.

(5.4.2) The Static Friction of Gold.

Successive layers of gold were deposited onto the highly polished tungsten carbide substrate and a series of six static friction measurements made for each thickness. The thickness in each case was known by extrapolation from the sputtering time, knowing that the deposition rate was 8.3 Angstrom per second. The rotary vacuum pump was switched off during friction measurements in order to reduce vibration.

Fig. (5.8) shows the mean of the six readings for each thickness plotted against the thickness; the spread indicated gives twice the standard deviation of the readings.

The expression:

$$T = \frac{C}{1 - (2\ell/h)\tanh(h/2\ell)}$$

where C is a proportionality constant and T is the apparent shear strength of the film, is taken from equation (2.26); this was expanded as a polynomial and the values of C and ℓ required to give a least squares fit with the data of fig. (5.8). The resulting curve is plotted in the figure and yields a value of 6.3 Angstrom for ℓ.

The apparent shear strength resulting from static friction measurements of tungsten carbide upon itself, prior to deposition, gave a mean value of 20.5 $Kgm.mm.^{-2}$, with a standard deviation of 0.5 $Kg.mm.^{-2}$

The results here could indeed be interpreted as being due to a transfered stiffness from the substrate to the film but the obtained for ℓ is very much smaller than those obtained by Finkin[27], who found values for ℓ of several hundred Angstroms. It seems that this present determination is much more in keeping with results obtained from X-ray examination of local lattice distortions[44] and with the predictions of Mindlin[45]. It is very interesting that the apparent shear strength of tungsten carbide is not very different from that found for the thickest gold film ($20.5 Kg.mm.^{-2}$ for WC and $12.5 Kg.mm.^{-2}$ for Au.); while the figure for gold is in keeping with experience, that for tungsten carbide is obviously too low and we must accept the probability that, despite the fact that the entire experiment was carried out in vacuum $\sim 10^{-6}$ Torr., contamination must have been present on the carbide surface. Such effects would not be expected to influence the micro-elastic mechanism, provided that the sputtering process produces the anticipated high strength bonding between film and substrate.

The thinnest films examined here were 68 Angstrom thick and this value will obviously be small compared with the size of the surface irregularities, for which a C.L.A. value of 200 Angstrom is reasonable; it is therefore appropriate to question whether this situation could affect the properties we are trying to measure. Films of the thickness under consideration have been shown to have a negligible effect in determining contact area; thus, provided we can guarantee a continuous coating of gold on the substrate, we can be confident that when we measure the angle of slip of the rider we are

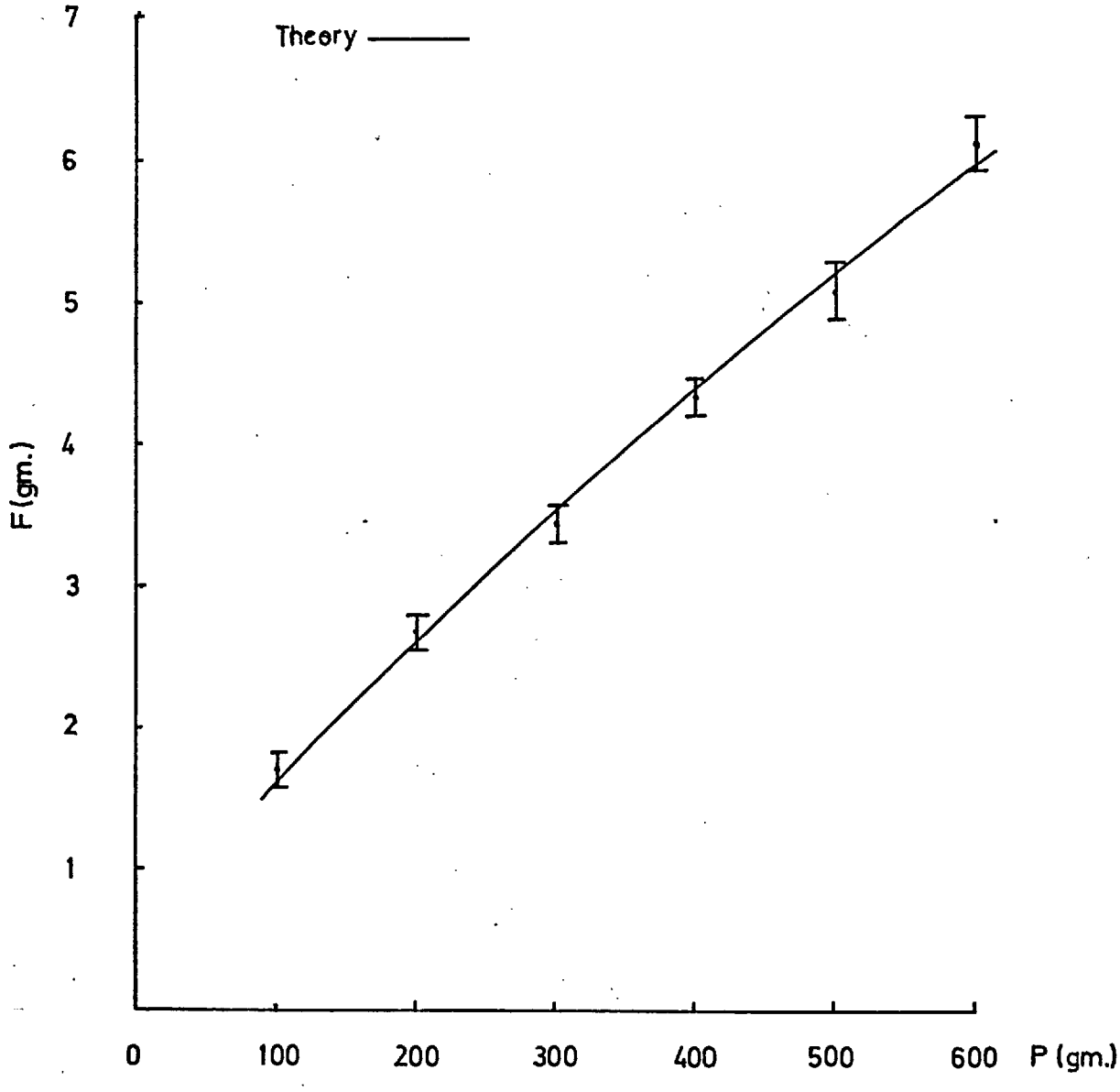

Fig. (5.9) Friction Force Plotted Against Load for a 9,000 A MoS_2 Film.

indeed testing the shear strength of the film. The fact that the shear strength is not seen to rise as the film becomes thicker gives confidence that our assumption regarding contact area is correct. Obviously as the thickness further increases the apparent shear strength will eventually be seen to rise.

(5.5) Dynamic Friction Experiments with Molybdenum Disulphide Films

The apparatus described in (4.3) was used for this work, which was carried out in vacuum at 10^{-6} Torr. The running speed was 60 RPM. (equivalent to 0.14 $m.sec.^{-1}$) and the applied loads were in the range 0 to 600 gm. The high adhesion sputtering schedule of (4.8.1) was employed.

(5.5.1) The Dependence of Friction Force on Applied Load.

A series of experiments were carried out in order to determine the dependence of friction on applied load under dynamic conditions. Films of thickness 9,000 Angstrom were prepared, placed in the friction apparatus and operated under cyclic loading with increments of 100 gm., the load being maintained at each value for 200 cycles. A series of results were obtained for increasing and for decreasing load in the range 0 to 600 gm. The load cycle was repeated four times for each specimen. The friction was observed to be very low and the spread of the results small; the dependence of friction force F on the load P was found to be nearly linear, with a tendency for the coefficient to decrease with load, giving $f = 0.017$ at $P = 100$ gm. and $f = 0.010$ for $P = 600$ gm. Fig. (5.9) shows the dependence where the theoretical curve shows the prediction of equation(2.22) is seen to give good functional agreement with $B^* = 2.97 \times 10^{-3}$ and $Ck = 5.85 \times 10^{-2}$ in the units appropriate to fig. (5.9).

---

*The values for B and Ck were found from a least squares fit of equation (2.22) to the data of fig. (5.9).

PLATE (5.2) ETCHED MoS_2 WEAR TRACK

140 MICRON

Fig. (5.10) A series of 'Talysurf' scans across the track of Plate (5.2)
(indicated lines of scan are approximate only)

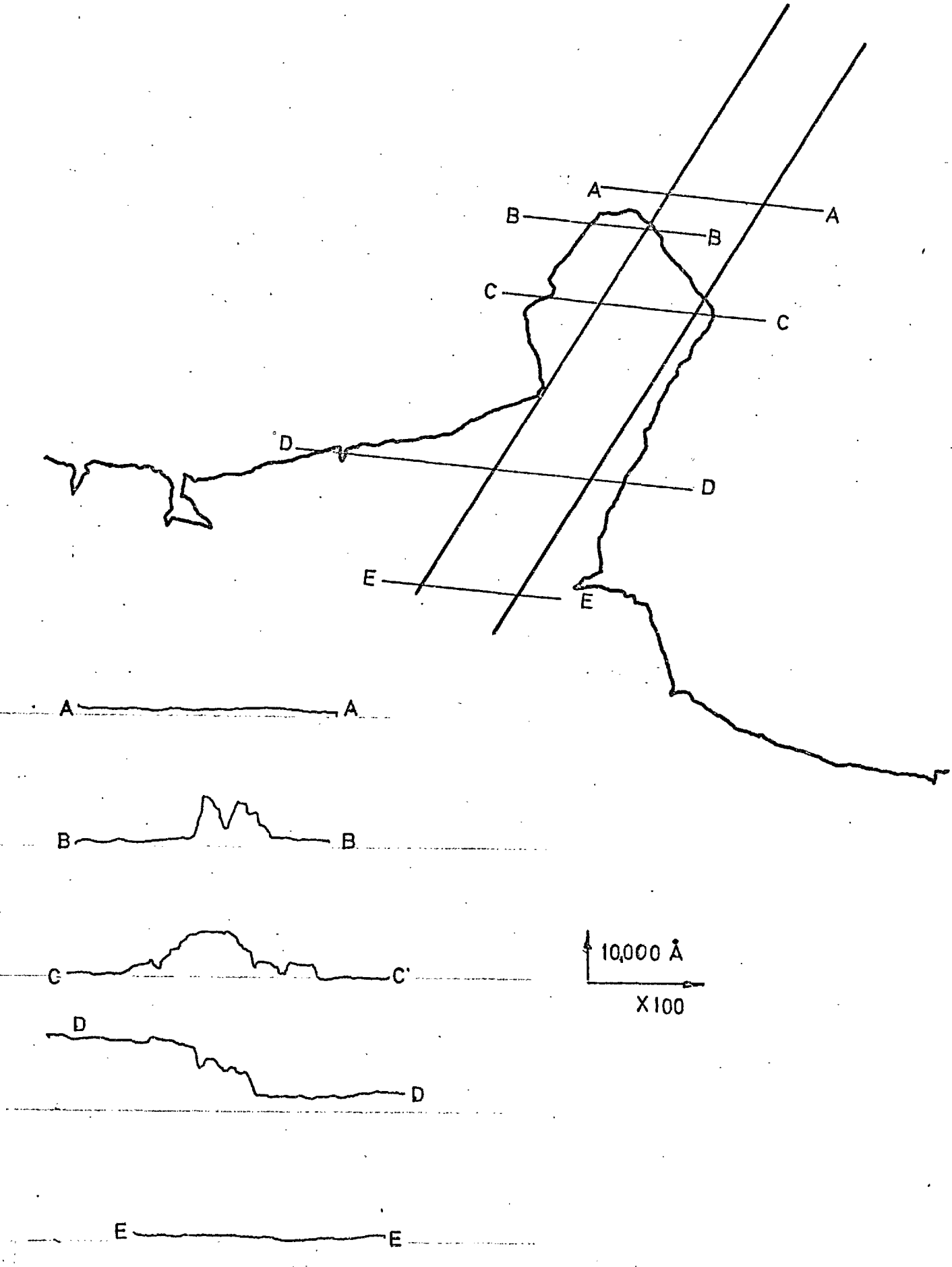

Experiments were carried out for a range of film thicknesses between 1,000 Angstrom and 12,000 Angstrom and no significant variation was found in the form of the dependence of F on P.

(5.5.2) Analysis of Wear Tracks.

The wear track of a specimen which had been subjected to the friction test schedule described in the preceeding section was analysed in the optical microscope. A small portion of track was etched with concentrated nitric acid in order to remove the MoS_2 and plate (5.2) shows the appearance of the track as it runs from the intact film into the region which has been etched. The MoS_2 on the track is etched with much greater difficulty than the surrounding film and as a result a 'causeway' of undissolved film is seen to run out for some distance into the etched region. A reasonable explanation for this effect is that the track itself has undergone orientation and that as a result a surface is presented which is much less chemically active than the non-oriented material. A series of 'Talysurf' scans were taken across the region seen in plate (5.2) and these are shown in fig. (5.10); the figure also indicates the approximate points along the track from which these were taken.

From the 'Talysurf' results we see that the instrument was not able to resolve the score marks seen in the track, nor was it possible to detect any wear at this magnification (approximately 10^4X). The bulk of the film material has therefore remained in place and there is no evidence of any gross plastic deformation. Score marks are however plainly visible on the exposed substrate, indicating that there have been some plastic incidents during the test schedule on a microscopic level but whether these have arisen from irregularities on the rider or are the result of temporarily

Plate (5.3) MoS_2 wear track showing detail of score lines

40 MICRON

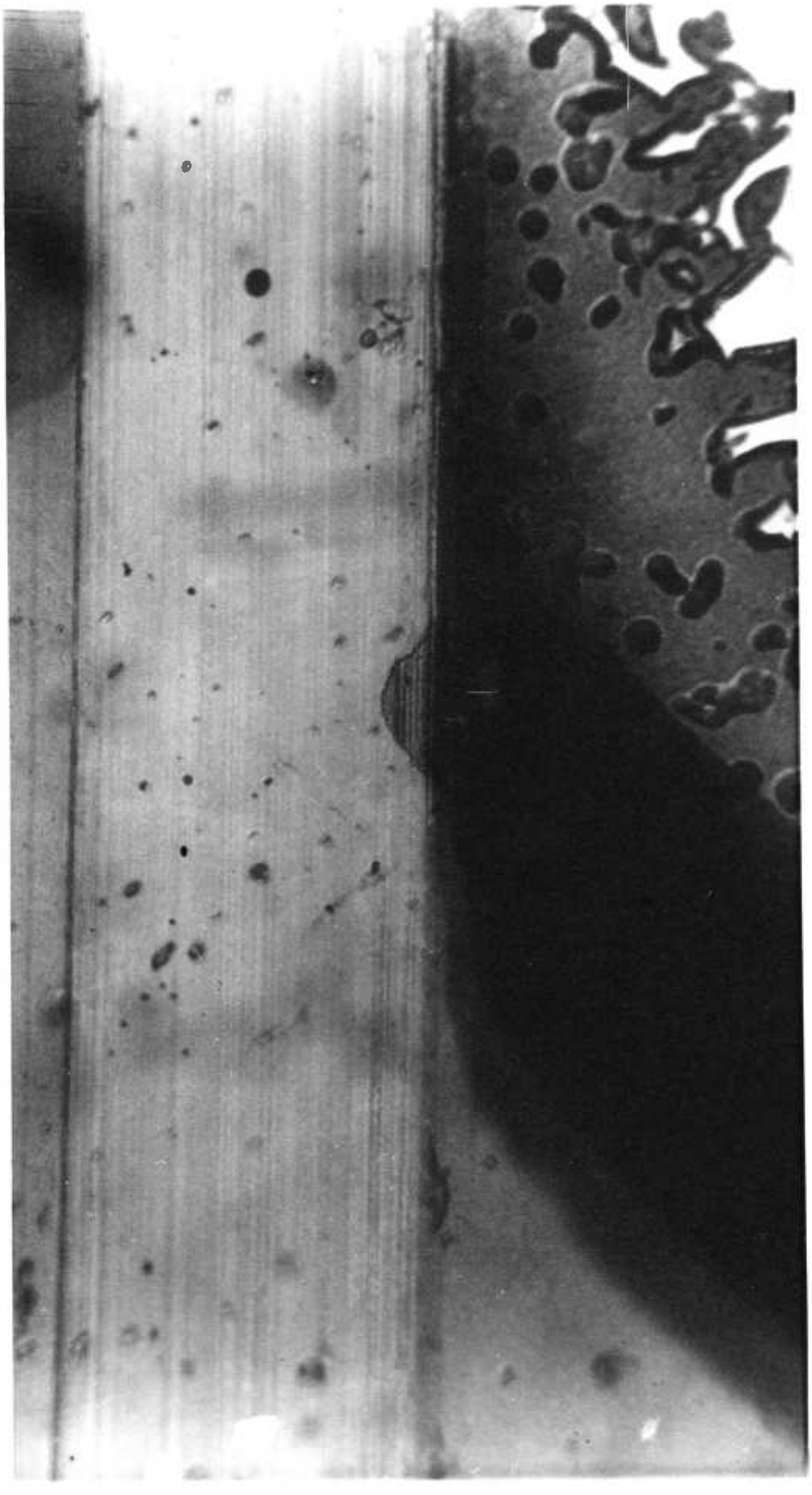

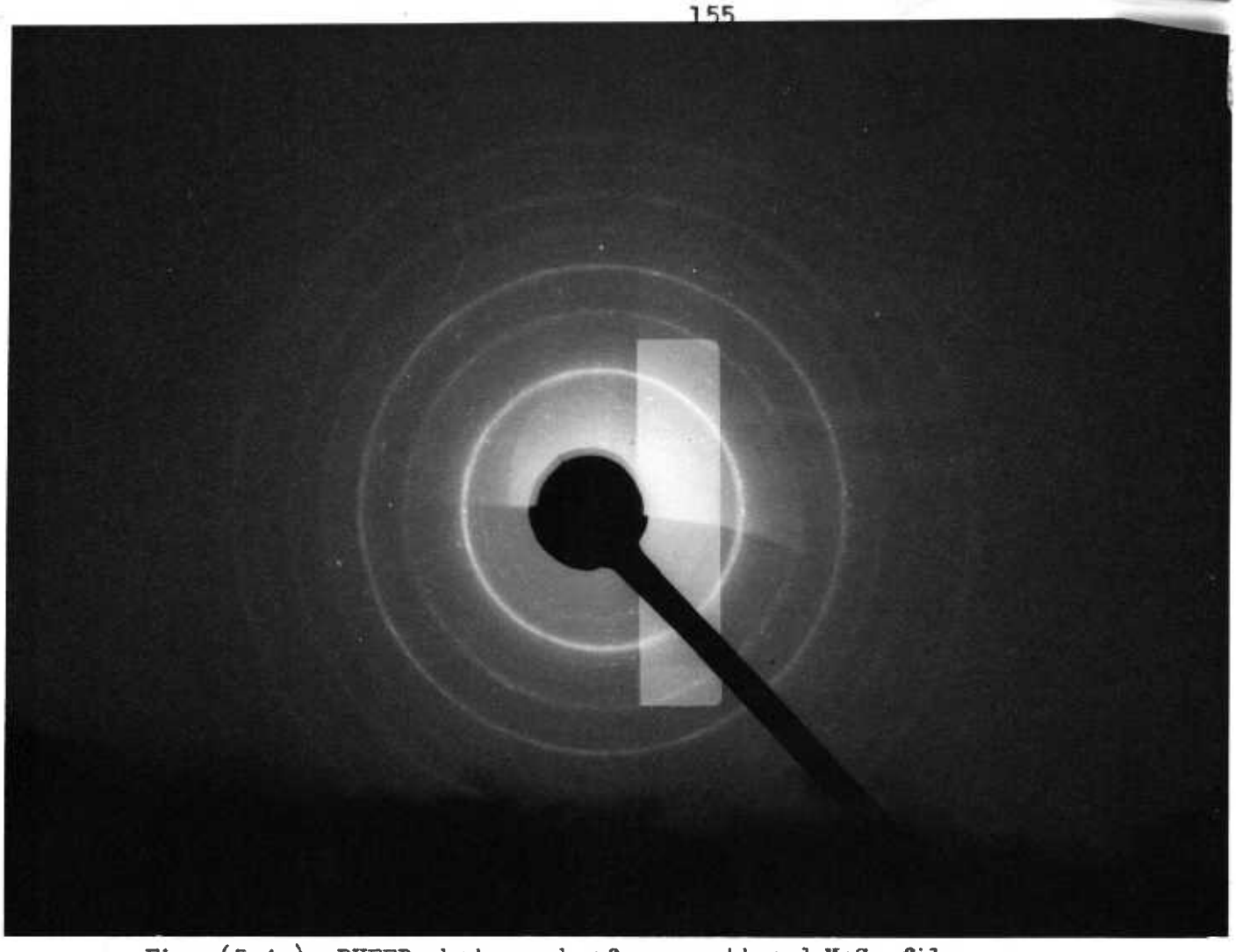

Fig. (5.4a) RHEED photograph of as-sputtered MoS_2 film.

Fig. (5.4b) RHEED photograph of wear track on same film.

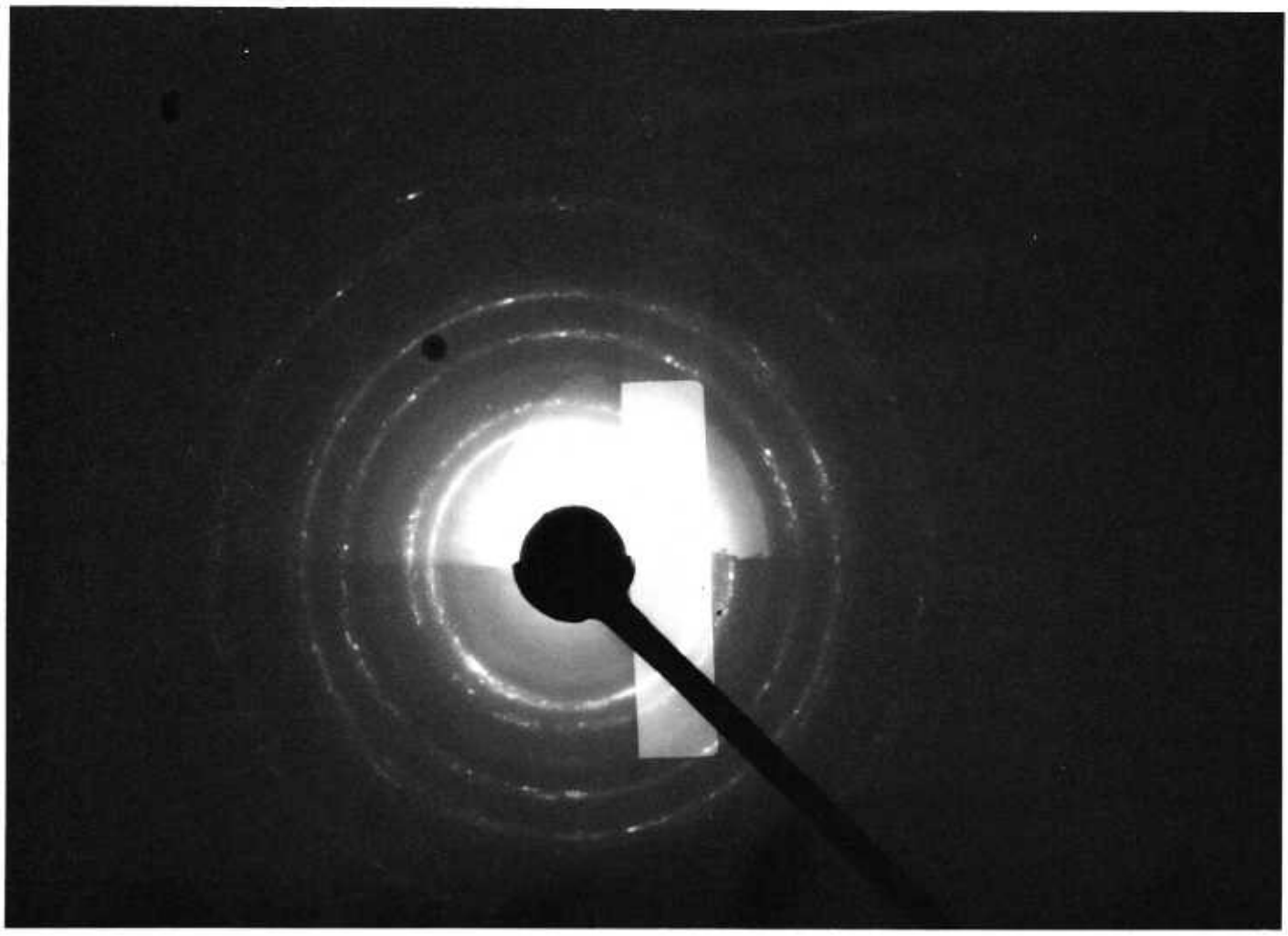

Plate (5.5) Stereoscan of contact zone on 3/16" ball.

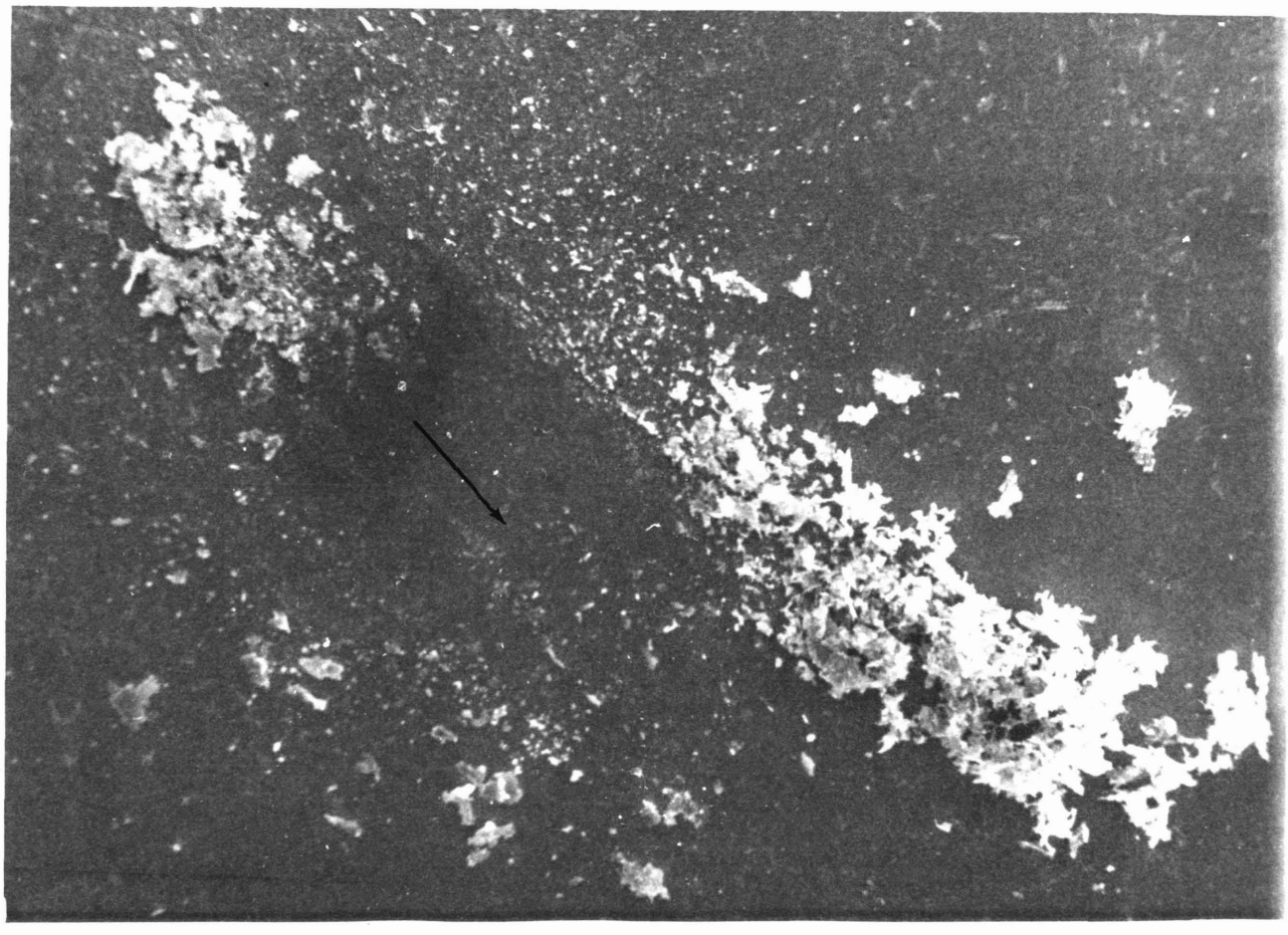

140 MICRON

entrapped wear debris is uncertain; we can however be sure that these have been impressed on the substrate through the film. Plate (5.3) shows the unetched wear track at greater magnification and here the score lines are more plainly visible.

It should be mentioned here that it is unfortunately not possible to relate the width of wear tracks obtained in the present apparatus to the Hertzian contact diameter; tracks are always observed to have a width greater than this, the reason being that the compliance of the friction arm allows some lateral movement as the friction force varies and naturally this widens the track.

We have already seen that there is evidence of orientation of MoS_2 during sliding; this is confirmed in plates (5.4a and b) where high energy reflection electron diffraction photographs have been taken from the as-sputtered film and the wear track respectively. The diffraction rings from material in the wear track show a very pronounced granular structure, indicating that orientation has taken place, while those from the untouched film are characteristic of a randomly oriented polycrystalline structure.

In plate (5.5) the contact spot on a 3/16" 440C stainless steel ball is shown in a scanning electron micrograph. This specimen had been run for 2×10^4 cycles under dynamic test and the direction of sliding is indicated by the arrow. The contact region appears to have a somewhat elliptical shape and this is consistent with the discussion of (2.13) in which the wear of films was considered. Since the contact surface of the ball is facing upwards during operation, any wear debris can be expected to collect

Plate (5.6) Stereoscan of wear debris (MoS_2) on 3/16" rider.

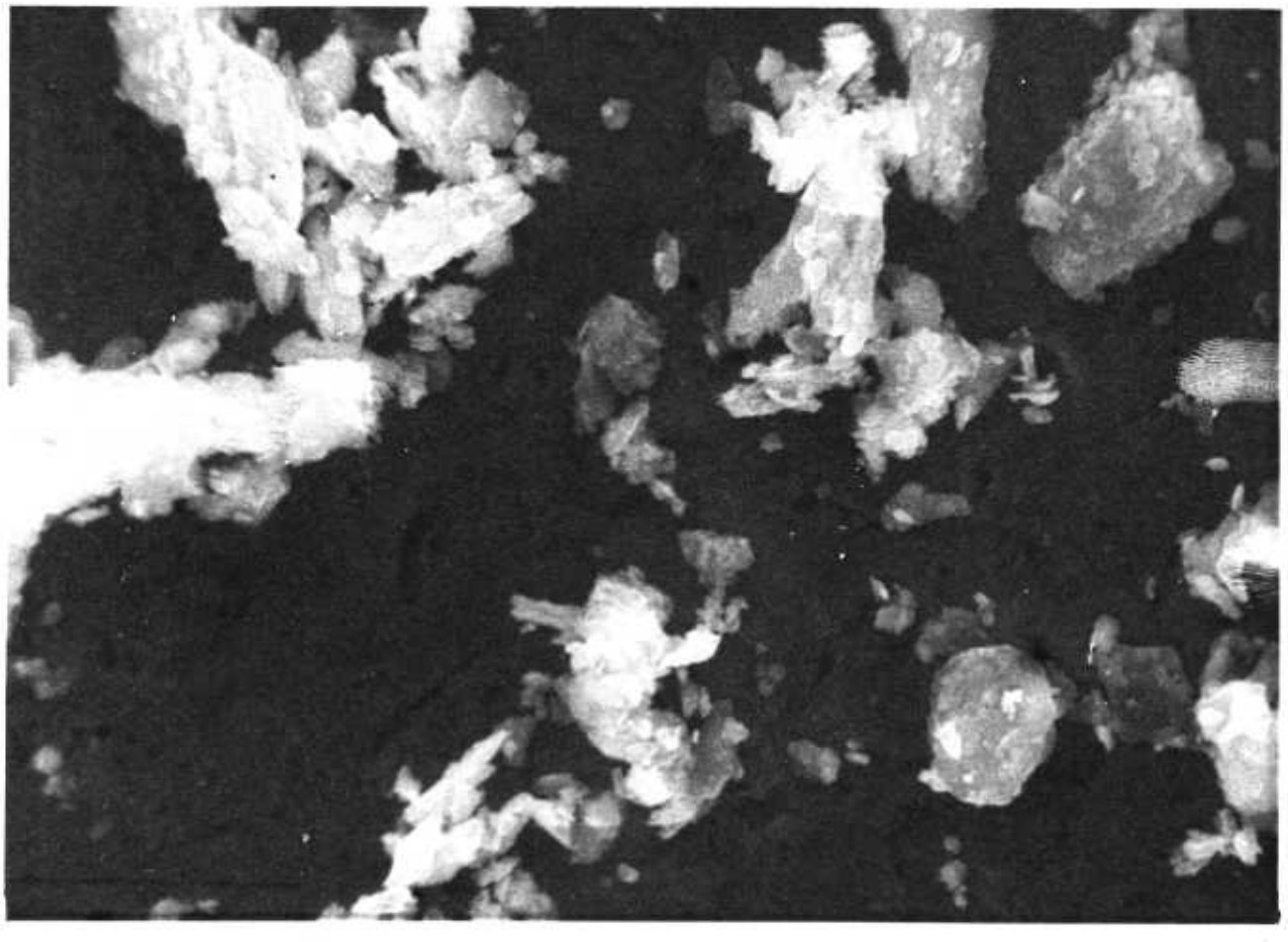

3.5 MICRON

here and these are revealed in plate (5.5), while plate (5.6) shows these in detail at higher magnification. The large size and apparent integrity of many of these particles is of great interest; fragments of up to 5 micron are seen here and the formation of particles of this size would not be in keeping with the observed wear behaviour of these films if it were a frequently occuring phenomenon, since these fragments appear to be complete patches of film which have been plucked off. We can suggest that these occurences are not typical and probably result from regions of film suffering from impaired adhesion.

(5.6) The Wear Characteristics of Molybdenum Disulphide Films.

The apparatus used for the dynamic friction experiments was found to be inadequate for the measurement of wear life of our films, since the maximum driving speed was still insufficient to take the majority of films to failure in the time available. The work of Spalvins[32] has shown that sputtered MoS_2 films can exhibit wear lives exceeding 10^6 cycles under conditions similar to those of our dynamic experiments.

Two alternative approaches were used; in the first, samples were sent for independent analysis in a 'Falex' test and in the second the ball and tri-plane system, discussed in (4.5) was employed.

(5.6.1) Falex Tests on Sputtered MoS_2 Films.

In the 'Falex' test a cylindrical pin of 0.25" diameter is compressed between a pair of 'V-jaws' and the load is increased linearly until failure occurs. The results of this test, kindly undertaken for us by Dr. D.J. Grieve of I.C.I. Cassel Heat Treatment Service, are included in a letter which is

PO Box 216 Kynoch Works
Witton Birmingham 6
England

Telephone 021-356 6265
Telex BM 33-231
Cables Genkem Birmingham

Fig. (5.11)

Imperial Chemical Industries Limited

Cassel Heat Treatment Service

Department of Electrical Engineering
Imperial College of Science and Technology
Exhibition Road
LONDON S W 7

Your ref	Our ref	Tel ext	Date
	DJG/LD/760	2030	6 Jul 72

Dear Mr Leveson

TRIBOLOGY TREATMENTS

We have tested some of the specimens you sent us, unfortunately you only sent 7 jaws and 7 test pins and as it requires two jaws to test each pin, we have only been able to do 3 tests. The results of these are as follows ;-

JAWS	PINS	TIME TO FAILURE	FAIL LOAD
2000Å coat	2000 Å coat	17 seconds	340 Kg
6000Å coat	2000 Å coat	40 seconds	710 Kg
6000Å coat	2000 Å coat	35 seconds	690 Kg

These tests were run without lubricant, with a pre load of 200 Kg, linearly increasing during the test. Under such conditions untreated steel specimens last about 5-10 seconds and reach a load of about 300 Kg, whereas specimens treated by one of our tribology processes, Tufftride, Sulfinuz, Noskuff or SULF BT would last upward of 50 seconds to give a fail load which is often well in excess of 1000 Kg.

The coefficient of friction was very low initially, but rose rapidly and catastrophically towards the end of each test showing that the film was being destroyed and the failed testpieces show considerable scuffing.

We hope these results are useful to you, if you would like to send us the rest of the testpieces we will be pleased to test them.

For your interest we enclose a leaflet describing our most recent tribology treatment, the Sulf BT Process.

Yours faithfully

D. J. Grieve

D J Grieve
Engineer

Enc 1

THE QUEEN'S AWARD TO INDUSTRY 1968

reproduced here as fig. (5.11). In these tests, the pins were coated with a 2000 Angstrom film and the jaws with 2000 and 6000 Angstrom films. The samples were assessed relative to some commercial anti-scuff chemical treatments which are normally applied to surfaces which run together in the presence of a hydrodynamic lubricant. The thickness of these coatings is measured in hundreds of microns and they are not intended to exhibit particularly low friction. Against this background, the performance of our sputtered films is seen to be most impressive; the sputtered films are two orders of magnitude thinner than the treated layers and yet the best sputtered film survived for 40 seconds to a terminal load of 710 Kg. as compared to 'upward of 50 seconds' with a failure load 'in excess of 1000 Kg.' in the case of the treated surfaces. The MoS_2 showed 'very low friction' until failure occured.

While this was never considered to be a very realistic comparison and the two processes are intended for completely different applications, it does show the excellent durability of sputtered films.

(5.6.2) Ball and Tri-Plane Wear Measurements.

The apparatus used was that described in (4.5). It was decided to determine the dependence of wear life on film thickness using this apparatus in normal atmospheric environment; films of thickness between 15,000 and 1,250 Angstrom were deposited onto EN 31 steel balls, 1" in diameter. The high diffusivity sputtering schedule of (4.8.1) was used in order to compensate for the curvature of the balls.

The rotation speed of the ball was chosen to be 888 RPM. which was equivalent to a mean linear speed of 1.0 $m.sec.^{-1}$ (the three pegs are set

Fig. (5.12)

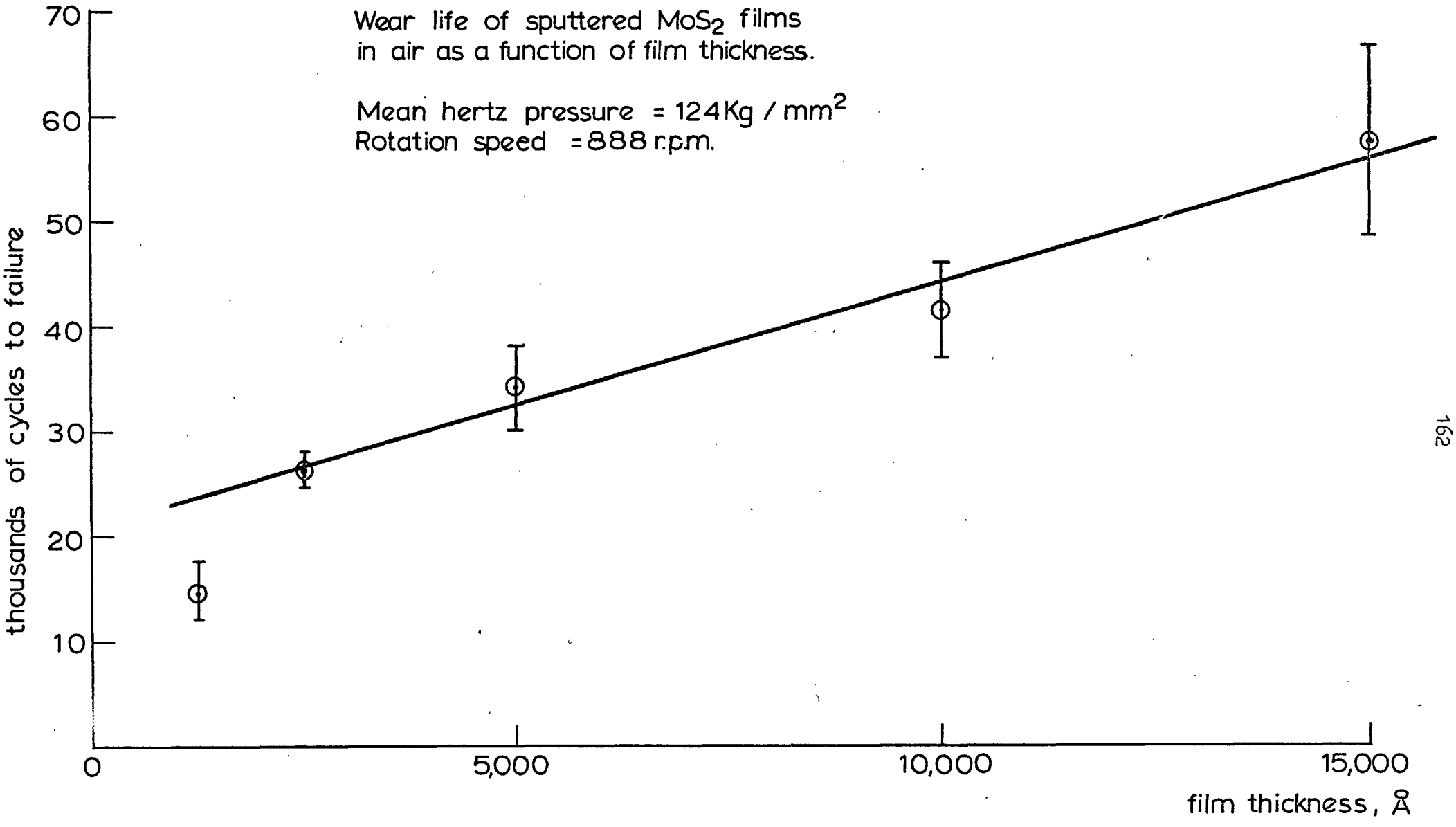
Wear life of sputtered MoS_2 films
in air as a function of film thickness.
Mean hertz pressure = 124 Kg / mm²
Rotation speed = 888 r.p.m.
thousands of cycles to failure
70
60
50
40
30
20
10
0
5,000
10,000
15,000
film thickness, Å

on slightly different radii) and the mean Hertzian pressure was 124 Kg.mm.$^{-2}$ Four balls were prepared for each thickness value. During the tests, the friction coefficient rapidly stabilized to approximately 0.02 and failure was judged from the sudden rise in friction which invariably attended it. Failed specimens exhibited obvious film breakdown with scuffing evident on both surfaces.

Fig. (5.12) shows the results with the number of cycles required to produce failure plotted against the film thickness. Above 2,500 Angstrom the dependence appears to be reasonably linear but below this thickness the wear life falls more rapidly than the linear prediction; nevertheless, if we calculate the wear coefficients at 1,250, 2,500 and 15,000 Angstrom using equation (2.33), we find values of 0.96×10^{-10}, 1.0×10^{-10} and 2.8×10^{-10} respectively and thus we see that the thinner films have better wear properties. This is in keeping with the fact, discussed in (3.6), that thinner films are stronger. We can thus explain the behaviour of fig. (5.12) in terms of an initial layer of high strength material, whose strength varies with thickness and which gives way at approximately 2,500 Angstroms thickness to material of lower strength and homogeneous composition, which would explain the observed linearity.

Since this study was carried out in air, we must remember that there may be formation of molybdenum oxide at hot spots in the interface and this could cause the performance of these films to deteriorate[46].

If we apply equation(2.33) to some results of Spalvins[32][47], who used loads of 200 gm. in conjunction with a 3/16" ball and plane system and found wear lives of 10^6 cycles for films 2,000 Angstrom thick, we arrive at a wear coefficient of 4×10^{-11} which is a slight improvement from our results

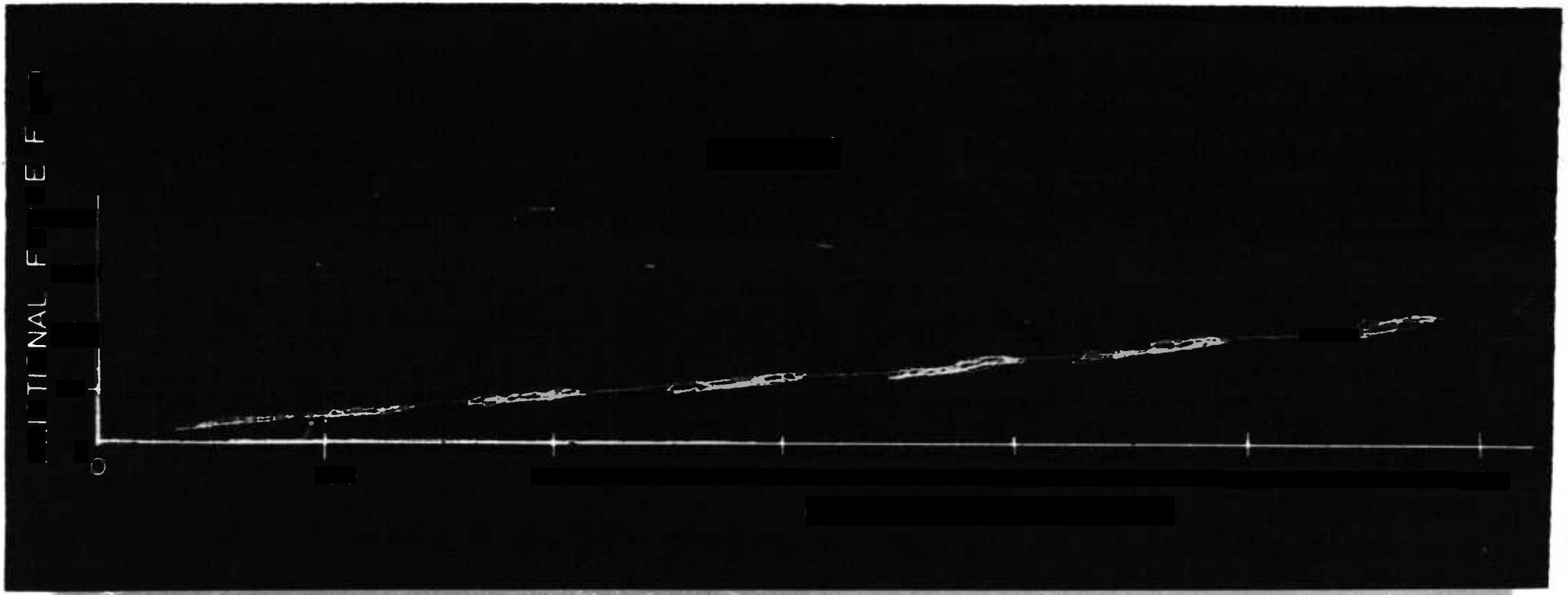

Fig. (5.13) Variation of friction force with normal load for a 250 A gold film.

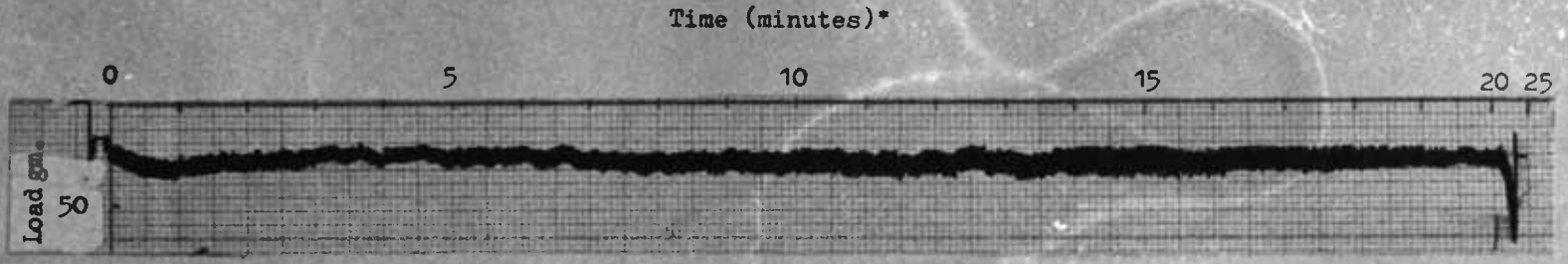

Fig. (5.14) Variation of friction force with time for a 2,500 A gold film under a load of 120 gm. at a rotation speed of 34 RPM.

*Note: Time scale changes from 20 to 25 min.

and could possibly be explained in terms of film oxidation.

(5.7) The Dynamic Friction of Gold Films in Sliding Contact.

Gold films in the thickness range between 125 and 10,000 Angstrom were deposited onto EN 58A steel substrates by the bias technique discussed in (4.8.2). The dynamic testing procedures were the same as those employed with molybdenum disulphide.

Two distinct classes of friction behaviour were observed, dependent on the thickness of the film. For the thicker range of films, i.e. those thicker than ~3,000 Angstrom, a very chaotic friction behaviour was found, with large variations between apparently identical specimens. In this regime, friction coefficients were found to be high, frequently approaching unity; no consistent functional dependence of friction on load could be discerned and even the same specimen would yield results varying unpredictably with time.

Examination of wear tracks showed that in many cases the films broke down after only a few tens of cycles and there was excessive pick-up of film material on the rider.

For films less than ~3,000 Angstrom and down to ~200 Angstrom, the behaviour became much more predictable with lower values for the friction coefficient and a very repeatably linear dependence of friction force upon load. This class of behaviour was most marked in the thickness range 1,000 - 200 Angstrom and fig. (5.13) shows a typical output from the X-Y plotter for a film of 250 Angstrom thickness. The load was continuously varied between 0 and 600 gm. and for a given load, the variation of friction force with

Plate (5.7) Wear track on a gold film.

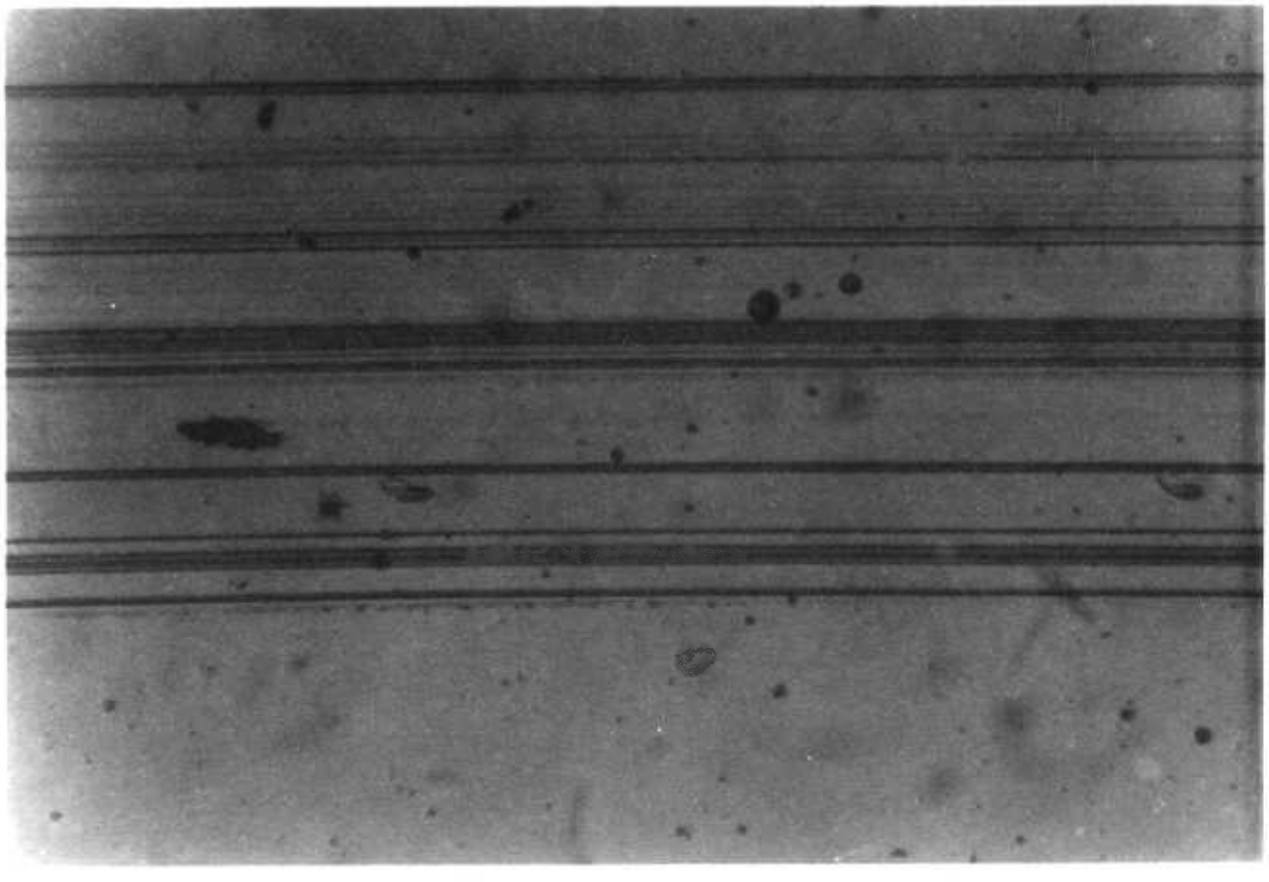

40 MICRON

small superimposed load fluctuations (due to 'run-out' in the disc) followed the general curve, demonstrating that there was no angular variation of friction properties. Fig. (5.13) was produced over approximately 20 cycles; no general variation was observed between the form of the curve produced for increasing and decreasing loads. Plate (5.7) shows a typical wear track for a 1,500 Angstrom film.

Films below 125 Angstrom (nominal thickness) exhibited virtually instantaneous breakdown and the results of these were of little significance to a dynamic test.

A wear test was conducted for a 2,500 Angstrom film, with a load of 120 gm. applied. The friction rose rapidly initially but stabilized at a value for f of approximately 0.26, remaining at this value for 780 cycles after which a sudden increase of friction occured. Fig. (5.14) reproduces the variation of friction during the test.

In explaining our results for gold, it is useful to recall the work of Takagi and Lui[21] who examined the dependence of friction on thickness for electroplated gold films under conditions of constant load. These workers found that the lowest friction arose from the thinnest films (the minimum thickness examined was 2,000 Angstrom) and that the material of the rider had a profound effect on the friction. In (2.14.2) we discussed the implications of alloying between film and rider materials, it is evident that pick-up of film material is very important in gold/steel systems.

The large spread in results obtained for thick gold films can be explained in terms of a continual and unstable exchange of film material

between substrate and rider and with a large scale transfer taking place we might expect this material to become displaced from the region of active friction, resulting in the rapid failure observed for thick films. As films become thinner, the quantity of material available for transfer reduces and a measure of stability is reached.

The very smooth and repeatable results seen in fig. (13) are not easy to explain; the linear dependence of friction force on load has three explanations:

(1) There is total Hertzian contact and the shear strength dependence on ~~load~~ PRESSURE is in direct proportion; this would give $F \propto P$.

(2) There is asperity contact and the asperities are deforming in a predominantly plastic fashion.

(3) There is asperity contact and the asperities are deforming in a predominantly elastic fashion.

Bridgman[9] found that the pressure dependence of shear strength for gold was insignificant below 200 $Kg.mm.^{-2}$, as the pressures of our experiment are well below this value, explanation (1) seems unlikely. The values of friction coefficient are ~0.1 and this value at an applied load of 600 gm. implies that the shear strength of gold should be 5.7 $Kg.mm.^{-2}$ in total contact, far lower than the value that we would expect, particularly as the film is likely to be in a work-hardened condition. We can however explain the low value if we assume there is asperity contact, i.e. the real contact area is less than the Hertzian.

Fig. (5.15)

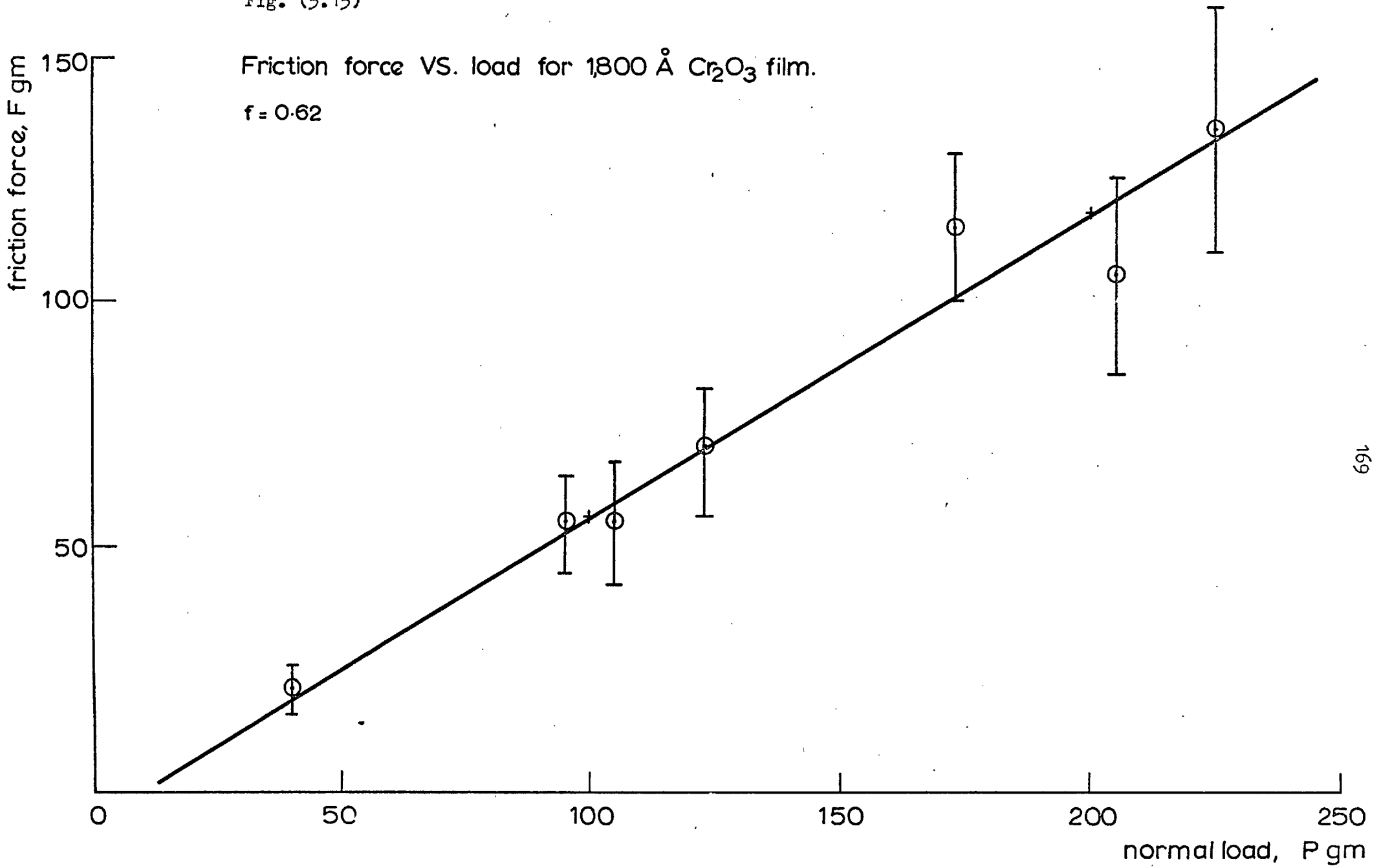
Friction force VS. load for 1,800 Å Cr_2O_3 film.
f = 0·62
friction force, F gm
150
100
50
0
50
100
150
200
250
normal load, P gm

Plate (5.8) wear track on a chromic oxide film.

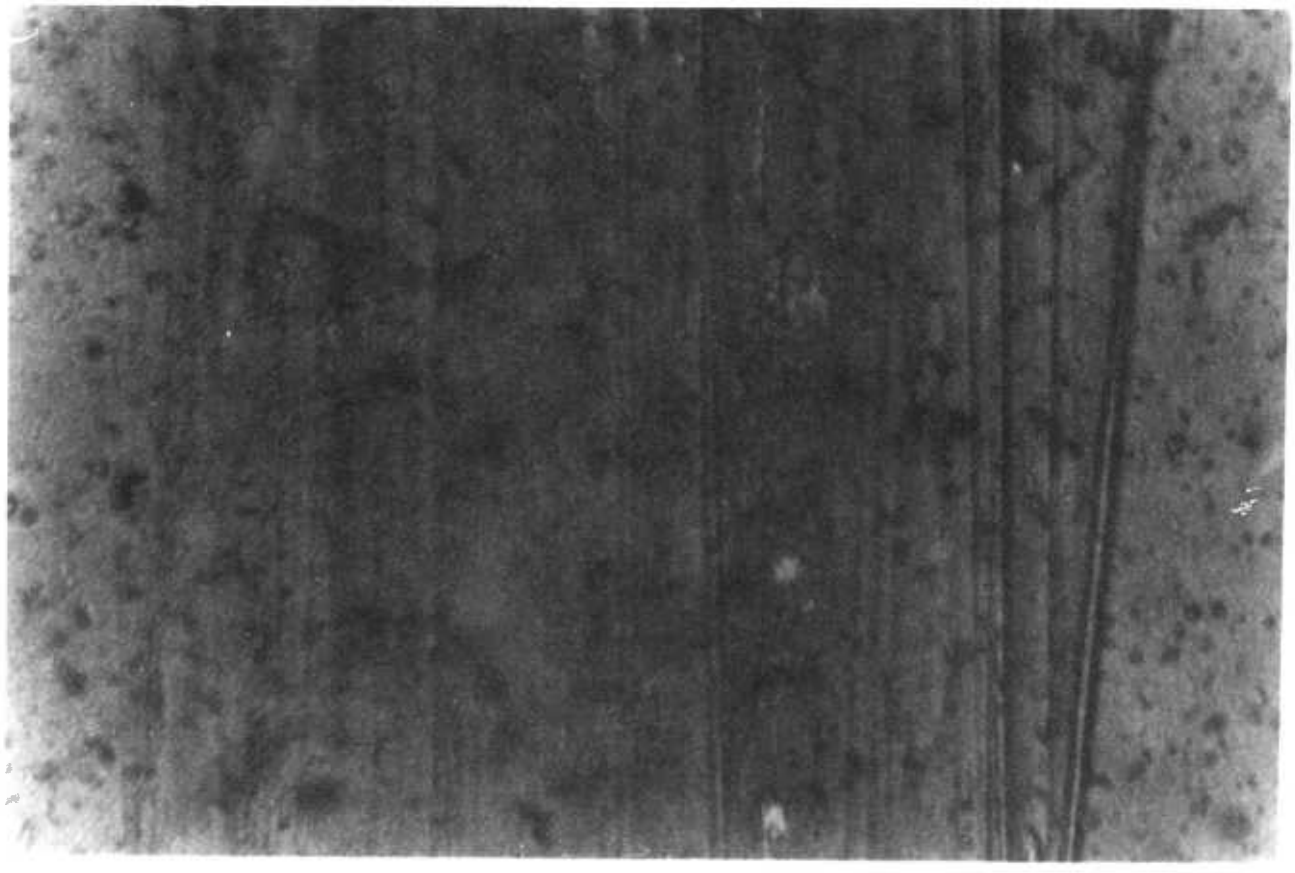

40 MICRON

Because there is a continual shearing process taking place between what is effectively two gold surfaces and also because material transfer is continually taking place, the instantaneous contact is likely to be very rough by the standards of the original surfaces. The excellent linearity seen in fig. (5.13) seems rather unlikely to have resulted from elastic asperity contact since insufficient contact points exist for the statistical process required to effect such a consistently linear dependence of real contact area on load. It is probable that explanation (2) is correct.

(5.8) The Friction of Chromic Oxide Films.

First attempts to explore the friction of this material employed a 440C rider sliding against the film as in the previous dynamic experiments; it was found that the friction behaviour was very erratic and that all the wear appeared to take place in the steel. Chromic oxide has an excellent record as a wear resistant coating when sliding against itself and consequently films of approximately 1,000 Angstrom each were deposited onto both rider and disc. The friction force was found to vary considerably for a given load but the dependence of its mean value on applied load was reasonably linear, as shown in fig. (5.15). If we examine the resulting wear tracks, these are seen to consist of a number of individual tracks parallel to each other and this is an unfortunate consequence of the apparatus design, where the lateral compliance of the friction arm has allowed the contact point to move radially as the friction force was varied; plate (5.8) shows the situation in a sample which has operated for over 1,000 cycles. The friction of chromic oxide is always high and our results yield a value of 0.62 for the coefficient.

The dynamic test which we have applied here is obviously not at all

suitable for evaluating this material, since the real conditions in which chromic oxide would be used in an engineering mechanism are in no way being simulated; however the fact that the film survived this very severe test for over 1,000 cycles without penetration demonstrates its durability and the probability that the asperity contact is largely elastic.

CHAPTER 6 --- CONCLUSIONS AND SUGGESTIONS FOR FUTURE WORK

It has been shown that in certain circumstances applicable to thin film lubrication, elastic processes can predominate in determining the real contact area. Assuming elastic contact, the effect on this of film thickness and other parameters has been examined, with particular reference to spherical contact; as a consequence, numerical criteria have been established from which the role of a given film in dictating contact area may be specified.

These results have enabled us to make an initial step in the quantitative understanding of the mechanics of hard protective coatings.

The consequences of the dependence of shear strength on pressure have been examined in the context of friction phenomena and we have proposed that this effect, when applied at the asperity level, gives an elastic counterpart to the plastic effect of work hardening in dictating the location of the frictional shear-plane.

A linear wear equation has been applied to sputtered films and we have attempted to obtain an expression in which the wear results for different contact conditions can be compared; thus it was possible to relate the results obtained by Spalvins[32] for the wear of sputtered molybdenum disulphide films in ultra high vacuum to some results obtained in this programme for similar films operating in air and reasonable agreement was found for the value of the wear coefficient.

It has been demonstrated that orientation plays a powerful role in the lubricating efficiency of sputtered molybdenum disulphide films and

that prior to orientation the material is in fact a very poor lubricant. From this result it is possible to conclude that the compressive strength of the sputtered material is reasonably high and this is in keeping with the observed fine grain structure. We propose that the excellent wear performance of sputtered molybdenum disulphide is a direct consequence of the properties mentioned above; a thin oriented layer appears on the surface of the film and on the counter-surface, giving a low interaction energy and quite probably a reversible shearing process. The high strength of the underlying unoriented material ensures elastic support and provides a reservoir of material for orientation as wear proceeds.

Contact resistance measurements, supported by determinations of the variation of friction with load and microscopic examination have led us to conclude that the load support behaviour of molybdenum disulphide films is predominantly elastic and this is also in keeping with our theoretical predictions. It was found that the effect of varying shear strength with load had to be accounted for in order to explain the friction/load dependence.

In the regime of very thin film friction, we have established the credibility of micro-elastic effects as one of the mechanisms responsible for the increase in friction with decreasing film thickness. We cannot say with certainty that we are observing micro-elastic effects because we have not discounted the possibility of micro-plastic strengthening; tensile strengthening has been observed in films at thicknesses of 1,000 Angstrom[30] and we might speculate that if these effects are important in friction, the observed decay constant of 6.3 Angstrom is surprisingly low. Micro-elastic stiffening undoubtedly occurs, the only question has always concerned the magnitude of the decay constant and the value found in this programme appears to be very realistic.

It is well accepted that soft metal films are unsuitable in systems involving sliding friction and to this extent our dynamic tests on sputtered gold films were not of particular engineering significance. Such films are of value in conditions of rolling contact and particularly for vacuum lubrication; here our observations are of value since the wear mechanism occuring in rolling friction will be principally involved with differential slip between the surfaces and consequently the films which perform best in sliding contact are likely to give the best performance here also. Thus our results indicate a nominal thickness for gold films of the order of 1,000 Angstrom. The results obtained pertaining to the role of films in determining contact area are also of interest when applied to the rolling case, since we have seen that if the film is thick enough for a significant proportion of the elastic strain energy to reside within it, the hysteresis loss will contain a component characteristic of the film and if this is a soft metal such a loss could be high.

It was unfortunately not possible to carry out a very thorough examination of chromic oxide films, since more specialized equipment would have been required than was available. From the small amount of information that has been obtained, it appears that sputtered films of this material may have important applications in such areas as coating low clearance air bearings and precision cutting edges.

SUGGESTIONS FOR FUTURE WORK

A considerable handicap in the development of a theoretical approach to the performance of thin film systems has been the absence of an analytical solution to the problem of an elastic sphere indenting an elastic film, bonded to an elastic substrate. This problem is very complex and its solution requires a highly specialized knowledge of continuum mechanics; once a solution has been obtained it should not only be possible to treat a wider variety of friction problems but the mechanics of the interaction of wear particles with hard protective coatings will be more ammenable to treatment.

This programme has been restricted to considering only the contact geometry of a sphere sliding on a plane. We have observed that for gold and chromic oxide such evaluation does not demonstrate the materials to best advantage; it would be of great interest to examine chromic oxide under conditions of lower contact stress and gold and molybdenum disulphide in rolling friction. The predictions we have made regarding the wear and hysteresis effects encountered in rolling contact could then be examined.

A problem encountered with the design of the dynamic apparatus used in this work was that lateral compliance in the friction arm caused the radius of the track to vary slightly with friction force. An improved design is desirable, with the flexibility to examine the friction of various geometries. A possible solution would involve mounting the friction arm so that its axis of rotation is the same as that of the specimen disc; in this manner, radial movement would be virtually eliminated.

Finally it should be observed that we have mainly been concerned with

the fundamental aspects of friction in films; we believe that a stage has been reached where future work should concentrate more heavily on possible applications and any equipment designed should endeavour to simulate the performance of the film in realistic situations.

APPENDIX (1)

The two-dimensional field equations, derived in reference (48) are

$$\frac{\partial}{\partial x}\left(\psi - \ell^2 \nabla^2 \psi\right) = -2(1-\nu)\ell^2 \frac{\partial}{\partial y} \nabla^2 \phi \qquad (1)$$

$$\frac{\partial}{\partial y}\left(\psi - \ell^2 \nabla^2 \psi\right) = +2(1-\nu)\ell^2 \frac{\partial}{\partial x} \nabla^2 \phi \qquad (2)$$

where ϕ is a stress function describing the classical field and describes the couple stress field. ℓ is a constant associated with couple stress having the dimensions of length and being defined by $\ell = \sqrt{B/G}$, where G is the shear modulus. ν is Poisson's ratio.

The stress functions, $\phi(x,y)$ and $\psi(x,y)$ are defined by

$$\tau_{xy} = -\frac{\partial^2 \phi}{\partial x \partial y} - \frac{\partial^2 \psi}{\partial y^2} \qquad \tau_{yx} = -\frac{\partial^2 \phi}{\partial x \partial y} + \frac{\partial^2 \psi}{\partial x^2} \qquad (3)$$

$$\mu_x = \frac{\partial \psi}{\partial x} \qquad \mu_y = \frac{\partial \psi}{\partial y} \qquad (4)$$

The condition that $\tau_{xy} = \tau_{yx}$, which is always obeyed in classical elasticity is no longer true here and in the extreme case we can have $\tau_{xy} = -\tau_{yx}$, resulting in no net deformation and an apparent shear modulus of infinity.

We will now solve an actual problem and for simplicity take the case of a plane interface between a rigid material and one with a shear modulus of G. Fig. (A1.1) shows the situation, with a unit

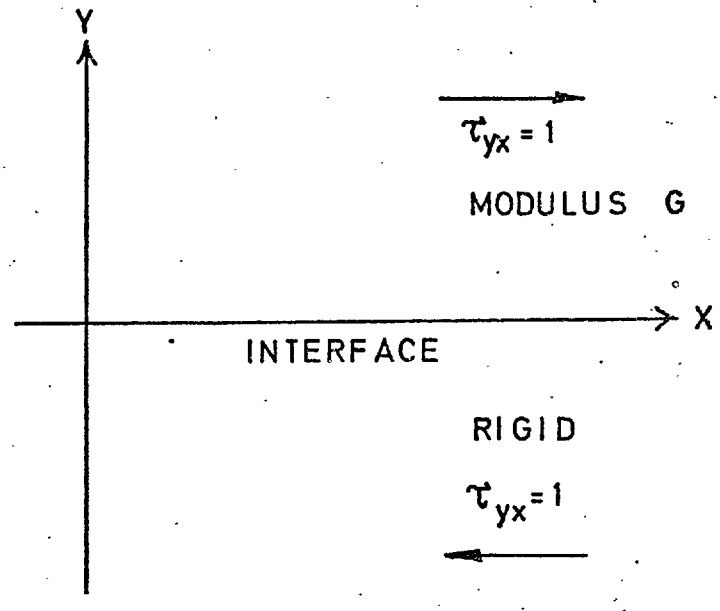

Fig. (A1.1)

shear stress applied parallel to the interface. Equilibrium requires that this shall remain constant throughout the system and hence τ_{yx} can not be changed by couple stress. τ_{xy} will however be changed and subject to the boundary conditions

$$\tau_{xy} = -\tau_{yx} = -1 \text{ at } y = 0$$

$$\tau_{xy} = \tau_{yx} = 1 \text{ at } y = \infty$$

Since this is a case of pure shear, we can assume that the normal stresses are zero. We now have adequate material to solve the problem.

Successive differentiation of equations (1) and (2) yields

$$\nabla^4 \phi = 0 \qquad \nabla^2 \psi - \ell^2 \nabla^4 \psi = 0 \tag{5}$$

The first of equations (5) is familiar to classical elasticity and its solutions for specific stress fields are well known[13]. For the case of pure shear this is simply $\phi = A_1 xy$, where A_1 is a constant. If this solution is substituted into equations (1) and (2), these reduce to

$$\psi - \ell^2 \nabla^2 \psi = C_1 \quad \text{(a constant)} \tag{6}$$

or $$\psi' - \ell^2 \nabla^2 \psi' = 0 \tag{7}$$

where the solution of ψ is the sum of a constant and the general solution. Since we require a solution for ψ which will modify τ_{xy} at the interface and decay as y increases to zero, we consider the

solution

$$\psi = C_1 + B_1 \exp(- y/\ell)$$

which satisfies the equation.

Inserting these solutions for ϕ and ψ into equations (3) we have, after applying the boundary conditions;

$$\tau_{xy} = 1 - 2 \exp(- y/\ell) \quad \text{and} \quad \tau_{yx} = 1$$

Shear strain is defined by $\gamma_{xy} = (\tau_{xy} + \tau_{yx})/2G$.

In this case $\gamma_{xy} = \left\{1 - \exp(- y/\ell)\right\} /G$.

The apparent shear modulus is therefore $G_{app.} = G/\{1 - \exp(- y/\ell)\}$.

It is not difficult to extend the problem just discussed to the case of an elastic film between two rigid half planes. This is solved in reference (49) and the result gives:

$$G_{app.} = \frac{G}{1 - \frac{2\ell}{y} \tanh(y/2\ell)} = \frac{G}{1 - \frac{2\ell}{h} \tanh(h/2\ell)}$$

where h is the film thickness.

APPENDIX (2)

The three balls fitted to the rider to form the contacts lie on a circle of radius r; the height of the centre of gravity of the rider above the contact plane is h and the rider weight is w. The three reactions are denoted by R_1, R_2 and R_3 (where $R_1 = R_2$) and the three forces of friction associated with these are F_1, F_2 and F_3 ($F_1 = F_2$). Thus, from Fig. (A2.1) we see that:

$$2R_1 + R_3 = w \cos \theta \tag{1}$$

$$2F_1 + F_3 = w \sin \theta \tag{2}$$

and taking moments about the centre of gravity:

$$R_1 - R_3 = h/r \ (2F_1 + F_3) \tag{3}$$

hence from these equations we have the reactions:

$$R_1 = w/3 \ (h/r \sin \theta + \cos \theta) = R_2 \tag{4}$$

$$R_3 = w/3 \ (\cos \theta - 2h/r \sin \theta) \tag{5}$$

If we assume Hertzian contact, the total contact area will be:

$$A = k(2R_1^{2/3} + R_3^{2/3}) \tag{6}$$

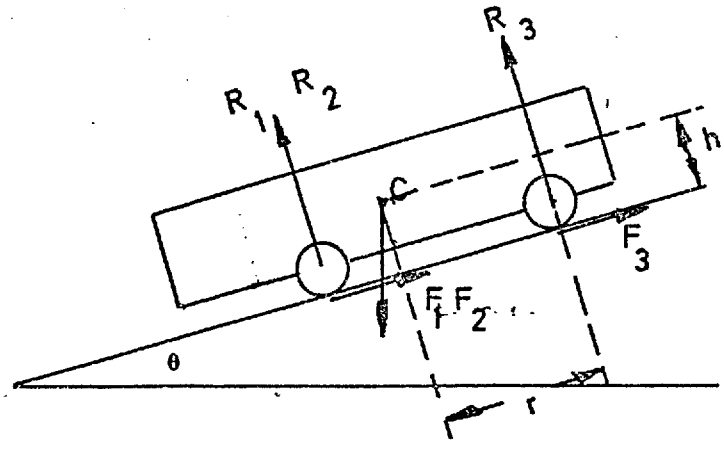

Fig. (A2.1) Detail of forces acting on rider

where k is the proportionality constant for the Hertzian contact of a $^{3}/_{16}$" tungsten carbide sphere on a tungsten carbide flat and R_1 and R_3 are found from eqs. (4) and (5).

If slip occurs at a critical angle θ_s then we can write an expression for the shear strength of the film material, T:

$$T = 2F_1 + F_3/A = w \sin \theta_s / k(2R_1^{2/3} + R_3^{2/3}) \qquad (7)$$

Thus knowing θ_s we can determine the shear strength of the film material under the conditions of the experiment. Due to the variation of the reaction with load, it would not be meaningful to speak of a friction coefficient in this context, since this is expected to vary with load.

REFERENCES

1.

2. J.F. Archard, Proc. Roy. Soc., 243A,190 (1957)

3. H. Hertz, Journal fur die reine und angewandte Mathematic, 92, 156 (1881)

4. J.A. Greenwood and J.B.P. Williamson, Proc. Roy. Soc., 295A,300 (1966)

5. H. Block, Proc. Roy. Soc., 212A, 480 (1952)

6. E.F. Finkin, Jnl. Lub. Tech., 91, 551 (1969)

7. V.M. Alexandrov, V.A. Babeshko and V.W. Kucherov, Jnl. App. Math. and Mech., 30, 148 (1966)

8. F.P. Bowden and D. Tabor, Friction and Lubrication of Solids, Oxford University Press (1954)

9. P.W. Bridgman, Proc. Am. Acad. Arts and Sci. , 71, 387 (1937)

10. C. Dayson, A.S.L.E. Trans., 14, 105 (1971)

11. J.F. Archard, Proc. Roy. Soc., 238A, 515 (1957)

12. I.V. Kragelski, Friction and Wear, Butterworths, (1965)

13. S. Timoshenko and J.N. Goodier, Theory of Elasticity, McGraw Hill (1951)

14. P.K. Gupta and J.A. Walowit, To be published.

15. V.M. Alexandrov, Jnl. App. Math. and Mech.,27, 1164 (1963)

16. V.M. Alexandrov and I.I. Vorovich, Jnl. App. Math. and Mech., 28, 425 (1964)

17. E.F. Finkin, Jnl. Lub. Tech., 92, 274 (1970)

18. R.C. Bowers and W.A. Zisman, Jnl. App. Phys., 39, 5385 (1968)

19. W. Schroeder and D.A. Webster, Jnl. App. Mech., 16, 289 (1949)

20. E.F. Finkin, Jnl. Lub. Tech., To be published.

21. R. Takagi and T. Lui, A.S.L.E. Trans., 10, 115 (1967)

22. J.A. Greenwood and J.H. Tripp, Jnl. App. Mech., 34, 153 (1967)

23. M. El Refaie and J. Halling, I. Mech. Eng. Trib. Conv., p116 (1969)

24. J. Boyd and B.P. Robertson, Trans. Am. Soc. Mech. Engrs., 67, 51 (1945)

REFERENCES

25. L.M. Berry, Private Communication to E.F. Finkin

26. B.J. Briscoe and D. Tabor, Faraday Soc. Special Disc., In press (1972)

27. E.F. Finkin, Wear, 15, 231 (1972)

28. W.E. Campbell, Trans. A.S.M.E., 61, 633 (1939)

29. N. Gane and J.M. Cox, Phil. Mag., 22, 881 (1970)

30. D.W. Paschley, Proc. Roy. Soc., 255A, 218 (1960)

32. T. Spalvins, NASA TMX-52819 (1970)

33. R.V. Stuart and G.K. Wehner, Trans. 9th. Symp. Am. Vac. Soc., p160 (1962)

34. C.K. Layton and D.S. Campbell, Jnl. Mat. Sci., 1, 367 (1966)

35. L.B. Loeb, Fundamental Processes of Electrical Discharges in Gasses, Chapman and Hall, (1939)

36. J.C. Anderson, Private Communication.

37. M. Crosset, S. Rigo and G.Amsel, App. Phys. Letters, 19, 33 (1971)

38. R.T. Smyth and D. Downer, 7th. Intl. Metal Spraying Conf., London, (1973)

39. R. Holm, Electrical Contacts, Springer, Berlin (1958)

40. R. Leveson, Imperial College internal report (1969)

41. J.F. Pocza, A. Barna and P.B. Barna, Jnl. Vac. Sci. and Tech., 6, 472 (1969)

42. L. Holland, Vacuum Deposition of Thin Films, Chapman and Hall (1956)

43. J.A. Wilson and A.D. Yoffe, Adv. in Phys., 18, 193 (1969)

44. L.H. Germer and A.U. McRae and C.D. Hartman, Jnl. App. Phys.,32, 2432 (1961)

45. R.D. Mindlin, Private communication.

46. E.R. Braithwaite, Solid Lubricants and Surfaces, Pergamon Press (1964)

47. T. Spalvins, Private communication.

REFERENCES

48. R.D. Mindlin, Office of Naval Research, Proj. No. 064-388 Rep. No. 49

49. M.A. Sadowsky, Y.C. Hsu and M.A. Hussain, Tech. Report of Benet RandD Laboratories, Watervliet Arsenal, Watervliet, N.Y., U.S.A., AD 424879